TECHNISCHE UNIVERSITÄT MÜNCHEN

Fakultät Chemie

Lehrstuhl für Biotechnologie

The Proteostasis System in Nematodes and Baker´s Yeast

Katharina Papsdorf

Vollständiger Abdruck der von der Fakultät für Chemie der Technischen Universität München zur Erlangung des akademischen Grades eines

Doktors der Naturwissenschaften (Dr. rer. nat.)

genehmigten Dissertation.

Vorsitzender: Univ.-Prof. Dr. J. Buchner

Prüfer der Dissertation: 1. Priv.-Doz. Dr. K. Richter

2. Univ.-Prof. Dr. M. Feige

Die Dissertation wurde am 17.04.2015 bei der Technischen Universität München eingereicht und durch die Fakultät für Chemie am 25.08.2015 angenommen.

Für meine Eltern

Publications

Part of this work is published or is currently in the process of being published. The equal contribution of authors is indicated with a star (*).

- **Papsdorf, K.***, Kaiser, C. J. O.*, Drazic, A., Grötzinger, S. W., Haeßner, C., Eisenreich, W., & Richter, K. (2015). Polyglutamine Toxitcy in Yeast Induces Metabolic Alterations and Mitochondrial Defects. *BMC Genomics, submitted*
- **Papsdorf, K.**, & Richter, K. (2014). Protein folding, misfolding and quality control: the role of molecular chaperones. *Essays in Biochemistry*, *56*, 53–68. doi:10.1042/bse0560053
- **Papsdorf, K**., Sacherl, J., & Richter, K. (2014). The balanced regulation of Hsc70 by DNJ-13 and UNC-23 is required for muscle functionality. *The Journal of Biological Chemistry*, *289*(36), 25250–61. doi:10.1074/jbc.M114.565234
- Kaiser, C. J. O., Grötzinger, S. W., Eckl, J. M., **Papsdorf, K.**, Jordan, S., & Richter, K. (2013). A network of genes connects polyglutamine toxicity to ploidy control in yeast. *Nature communications*, 4, 1571. doi:10.1038/ncomms2575
- Haslbeck, V., Eckl, J. M., Kaiser, C. J. O., **Papsdorf, K.**, Hessling, M., & Richter, K. (2013). Chaperone-interacting TPR proteins in Caenorhabditis elegans. *Journal of molecular biology*, 425(16), 2922–39. doi:10.1016/j.jmb.2013.05.019
- Sun, L., Edelmann, F. T., Kaiser, C. J. O**., Papsdorf, K.**, Gaiser, A. M., & Richter, K. (2012). The lid domain of Caenorhabditis elegans Hsc70 influences ATP turnover, cofactor binding and protein folding activity. *PloS One*, *7*(3), e33980. doi:10.1371/journal.pone.0033980

.

Content

Publications 6

Content 8

1. Summary 11

2. Introduction 13

2.1 Chaperones and the Cellular Proteostasis System 13

2.2 The Protein Folding Challenge 13

2.3 Degradation and Maintenance 14

2.4 Assisted Protein Folding in the Cell 15

2.5 Hsc70 and its Cofactors 17

2.5.1 Hsc70 in *C. elegans* 20

2.5.2 The Muscular System of *C. elegans* 20

2.5.3 Modulating Hsc70 Activity as a Therapeutic Target 21

2.6 Diseases of the Proteostasis Network 22

2.6.1 Polyglutamine Diseases 25

2.6.2 Polyglutamine Toxicity in Yeast 26

2.6.3 The Poliovirus Precursor VP0 28

3. Aim of the Work 30

3.1 Studying the Hsc70 System in Relation to Muscular Deficiencies in Nematodes 30

3.2 Analyzing the Underling Mechanism of Polyglutamine Induced Toxicity 30

4. Material and Methods 32

4.1 Material 32

4.1.1 Reagents 32

4.1.2 Buffers 34

4.1.3 Media 38

4.1.4 Amino Acid dropout-mix 40

4.1.5 Enzymes and Kits 40
4.1.6 Fluorophores 41
4.1.7 Antibodies 42
4.1.8 Strains and Organisms 42
4.1.9 Plasmids 43
4.1.10 Oligonucleotides 45
4.1.11 Equipment 47
Computer Programs and Databases 50
4.2 Methods 50
4.2.1 E. coli 50
4.2.2 S. cerevisiae 51
4.2.3 C. elegans 57
4.2.4 Imaging 59
4.2.5 Molecular Biology 60
4.2.6 Protein Purification and Analysis 61
4.2.7 Statistical Analysis 68
4.2.8 Data Acquisition 68
5. Results 69
5.1 The Balanced Regulation of Hsc70 by UNC-23 and DNJ-13 is Required for Muscle Functionality 69
5.1.1 UNC-23 Contains a Disordered N-terminal Domain with PXXP Motifs 69
5.1.2 UNC-23 Mutated Nematodes Show Severe Muscular Deficiencies 72
5.1.3 Muscular Expression Pattern of UNC-23 and CeHsc70 73
5.1.4 UNC-23 Binds to Hsc70 with its BAG-domain 76
5.1.5 Hsp40s Cooperate with UNC-23 78
5.1.6 Knock-down of DNJ-13 Rescues UNC-23 Induced Motility Phenotype 80
5.2 Modulating the Nematode Hsc70 System 83

5.3 Polyglutamine Toxicity in Yeast Induces Metabolic Alterations and Mitochondrial Defects 86

5.3.1 Toxic and Non-Toxic PolyQ Stretches Alter the Phosphate Balance in Yeast 86

5.3.2 Polyphosphate Levels are Elevated in Q56-YFP Expressing Yeasts..... 90

5.3.3 Expression Changes in Toxic Q56-YFP Show a Specific Up-regulated Response 92

5.3.4 Iron-homeostasis is Affected in Q56-YFP Expressing Yeasts..... 95

5.3.5 Regulator Activity is Activated by Polyglutamine Constructs 96

5.3.6 Q56-YFP Reduces Mitochondrial Carbon Source Utilization..... 101

5.3.7 Q56-YFP Intoxication Results in Decreased Cox4p Levels 104

5.3.8 Polyglutamine Constructs Are Processed via Autophagy..... 105

5.4 Investigating Similarities between Aggregation Systems 109

5.4.1 Polyploidy Rescues Toxicity in other Systems 109

5.4.2 Poliovirus Precursor VP0 Induces Polyphosphate Production 111

5.4.3 Poliovirus Precursor Does Not Interfere with Septin Ring Assembly but Reduces Cox4 Levels..... 112

6. Discussion 114

6.1 The Balanced Regulation of Hsc70 by UNC-23 and DNJ-13 is Required For Muscle Functionality 114

6.2 Modulator Screen of the Hsc70/DNJ-12/BAG-1 System..... 116

6.3 Polyglutamine Toxicity in Yeast Induces Metabolic Alterations and Mitochondrial Defects 118

6.4 The Cellular Response to VP0 Aggregates 121

7. References..... 123

8. Abbreviations..... 138

9. Danksagung..... 140

10. Eidesstattliche Erklärung..... 142

1. Summary

The proteostasis system is a complex network of proteins regulating the homeostasis of the cellular proteome. Diverse protein classes ensure proteostasis by promoting folding and degradation of client proteins. Chaperones are part of this network as they assist *de novo* folding, in aggregation prevention and refolding of damaged proteins. In this work the chaperone Hsc70 was investigated regarding its effect on muscular proteostasis in *Caenorhabditis elegans* and the failure of cellular proteostasis examined after expression of toxic polyglutamine stretches in *Saccharomyces cerevisiae*.

The molecular chaperone Hsc70 folds non-native proteins together with Hsp40 proteins and Nucleotide Exchange Factors. BAG-domain containing proteins are Nucleotide Exchange Factors for Hsc70 and facilitate nucleotide exchange and client release. In *C. elegans* two BAG-domain containing proteins were identified, one of them being UNC-23, whose mutation induces severe motility dysfunctions. Using reporter strains the full-length UNC-23 was found to localize specifically to the muscular attachment sites, in contrast to C-terminal fragments of UNC-23. Instead these fragments performed all Hsc70 related functions, such as ATPase stimulation and regulation of folding activity, albeit with lower affinity than BAG-1, the second BAG protein of *C. elegans*. Interestingly, overexpression of CFP-Hsc70 induced muscular defects in wild-type nematodes that phenocopy the knockout of its cofactor UNC-23. Strikingly, the motility dysfunction in the *unc-23* mutated strain were cured specifically by down-regulation of the antagonistic Hsc70-cochaperone DNJ-13, implying that the severe phenotype is caused by misregulation of the Hsc70 cycle. These findings point out that the balanced action of UNC-23 and DNJ-13 with respect to Hsc70's activity is crucial for the contribution of Hsc70 to muscle functionality.

Given that Hsc70 is a central regulatory protein a modulator screen based on Hsc70s ATPase activity was executed. As Hsp40 proteins and Nucleotide Exchange Factors transfer specificity to the Hsc70 system, the screen was performed in presence of DNJ-12 and BAG-1. Three activating compounds were found to stimulate Hsc70 ATPase activity in presence of the cochaperones.

Diseases of the proteostasis network occur if protein aggregation is augmented during chronic stress or aging. Protein aggregation and its pathological effects are the major cause

of several neurodegenerative diseases. In Huntington´s disease an elongated polyglutamine stretch within the protein Huntingtin leads to increased aggregation propensity. This induces defects culminating in cell death. Nevertheless the connection between aggregation and toxicity remains to be established. To uncover cellular pathways relevant for intoxication genome-wide studies in a yeast model system were applied. Mitochondrial genes were found as suppressors of toxicity pointing to a challenged mitochondrial system. Microarray analysis was employed to decipher the transcriptional response upon polyglutamine intoxication, which exposed an up-regulation of genes involved in sulfur and iron metabolism. Indeed, *in vivo* iron concentrations were detected to be misbalanced and a reduction in the activity of the prominent Fe-S cluster containing protein aconitase was observed. As in other yeast strains with impaired mitochondria, non-fermentable growth was not possible after intoxication with the polyglutamine protein. NMR-based metabolic analyses revealed that mitochondrial metabolism was reduced, leading to accumulation of metabolic intermediates in polyglutamine-intoxicated cells. These data show that damages to the mitochondrial system occur in polyglutamine intoxicated yeast cells and suggest an intricate connection between polyglutamine-induced toxicity, mitochondrial functionality and iron homeostasis in this model system. Additionally the aggregation system consisting of the viral precursor protein VP0 was analyzed in *S. cerevisiae*. Ploidy changes were found and polyphosphate was enriched in VP0 intoxicated yeast. Alterations in the mitochondrial respiratory chain complex subunit Cox4 were detectable. Hence related mechanisms are induced by polyQ and VP0 intoxicated cells. These systems provide a powerful chance to decipher aggregation specific mechanism leading to cellular toxicity.

2. Introduction

2.1 Chaperones and the Cellular Proteostasis System

All cellular functions are performed by proteins. The folding state and thereby the functionality as well as the concentration of all cellular proteins, commonly called proteome, has to be controlled constantly. This is essential to preserve cellular functions and guarantee cell survival. The balance is regulated by the protein homeostasis (proteostasis) network consisting of molecular chaperones, the protein degradation machinery and signaling pathways to control these functions (Morimoto & Cuervo, 2014).

Cells are confronted with a range of external and internal stressors and persistently have to adapt to these conditions. If the network gets misbalanced during aging or in protein misfolding diseases deleterious effects for the survival of the cell emerge. Stresses such as heat or radiation can induce the accumulation of aggregates. Proteins usually obtain their correct fold during *de novo* folding and their folding status is controlled throughout their whole life. Damaged and unfolded proteins have to be dealt with by the proteostasis system and refolded, degraded or held in a folding competent state to continually safeguard the folding state of the cellular proteome (Papsdorf & Richter, 2014).

2.2 The Protein Folding Challenge

Proteins are cellular components, which need the correct three-dimensional conformation to fulfill their assigned tasks. Anfinsen showed in the early 70ies that an isolated protein can fold spontaneously without cellular components. He postulated that the correct folding of a protein is determined by its amino acid sequence (Anfinsen, 1972). These findings raised the question of how native proteins fold correctly. The optimal fold of a protein represents a thermodynamic energy minimum in a funnel-like energy landscape (Hartl *et al*, 2011). Various parameters define the optimal conformation of a protein such as Van-der-Waals interaction, hydrogen bond formations, electrostatic interactions, backbone angle preferences and chain entropy (Kiefhaber *et al*, 1991). Passing all possibilities of peptide bond rotations in a 150 amino acid protein would take 10^{24} years. The Levinthal paradoxon describes the phenomenon of obtaining the correct fold on a reasonable time scale in milliseconds (Honig *et al*, 1976). In order to reach the optimal fold faster folding

pathways with partially structured states were postulated. These folding pathways have been analyzed in the last decades and the majority of the cellular proteins were found not to fold spontaneously (Dill *et al*, 2012). A native protein is a metastable, flexible form, which can form intermediates while finding the optimal structure (Figure 1). Obtaining the optimal folding state in the crowded cellular environment is challenging task, as proteins tend to aggregate due to macromolecular crowding (Ellis & Minton, 2006). Most proteins are trapped in local energy minima during the folding process and cannot overcome the energy barriers in order to find the optimal global minimum. Alternative routes are taken by a partially folded protein, which could lead to a misfolded state (Dill *et al*, 2012). Thereby protein aggregates can be formed. A protein aggregate is an association of more than one protein in its non-native fold (Hipp *et al*, 2014). Components of the proteostasis network assist cellular proteins en route to its correct fold. Chaperones are the most important folding helpers in the cellular environment, with three central purposes: Aggregation prevention, refolding of misstructured proteins and disentangling of specific protein aggregates.

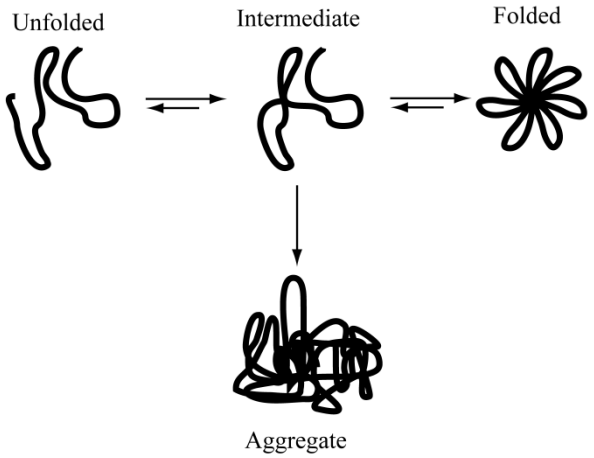

Figure 1 Model of protein aggregation as a result of protein instability. An unfolded protein obtains its native fold via folding intermediates. This intermediate can aggregate if the cellular requirements for a correct folding are not given (Papsdorf & Richter, 2014).

2.3 Degradation and Maintenance

Cellular proteostasis is guaranteed by a tightly regulated protein turnover and an efficient clearance of misfolded proteins. Therefore misfolded proteins are marked with the signal marker ubiquitin to be subsequently degraded by the proteasome. This so called ubiquitin proteasome system (UPS) consists of more than 600 proteins in human cells (Varshavsky,

2012). The proteasome degrades its ubiquitinated targets in the nucleus and in the cytosol. Endoplasmatic proteins, which are targeted for degradation, have to be relocated to the cytosol and processed subsequently (Hiller *et al*, 1996). For degradation of bulky protein aggregates or organelles the cell uses a different degradation method termed autophagy. Thereby components of the autophagy system form a preliminary structure named phagophore surrounding the affected target. Subsequent fusion with lysosomes in mammalian cells or the vacuole in yeast leads to degradation. For the clearance of non-functional organelles specific autophagy degradation pathways exist with specialized protein subsets as seen in mitophagy. To facilitate aggregate clearance misfolded proteins concentrate in the cellular environment in intracellular quality control compartments (INQ), cytosolic quality control bodies (Q-bodies) or insoluble protein deposits (IPODS) in yeast and in mammalian cells (Kaganovich *et al*, 2008; Miller *et al*, 2015). A regulated protein turnover ensures clearance of non-functional proteins, which are potentially toxic to the cell, evaluates the folding status of proteins constantly and thereby is essential for cellular proteostasis (Hipp *et al*, 2014).

2.4 Assisted Protein Folding in the Cell

The concept of assisted protein folding is strongly conserved in all kingdoms of life (Preissler & Deuerling, 2012). In eukaryotes assisted *de novo* folding of proteins happens at different points during synthesis (Figure 2). The proteins which coordinate this folding are termed chaperones and classified according to their molecular weight as Heat-shock Protein 70 (Hsc70), Heat-shock Protein Hsp90 and the small Heat-shock Proteins (sHsps). The newly synthesized peptide chain emerges from the ribosome and is immediately in contact with chaperones. The nascent chain associated complex (NAC) provides a shield for the nascent chain (Wang *et al*, 1995). Additionally ribosomal located Hsc70 (RAC) and its cofactors assist co-translational folding (Willmund *et al*, 2013). Moreover cytosolic located Hsc70 is involved in *de novo* folding of proteins after release from the ribosome and, additionally, in the folding process of misstructured proteins. Its chaperone machinery acts in an ATP-dependent manner and nucleotide hydrolysis is coupled to conformational changes within the chaperone. But many chaperones, including Hsc70, do not function on theirown but a plethora of cochaperones regulate their functions (Figure 2). A cochaperone is defined as a non-client binding partner participating in the function of the chaperone and conferring specificity to the chaperone system (Caplan, 2003). They can modulate the

folding cycles and direct the system to cellular localizations (Young *et al*, 2003). The large multi subunit chaperonin TRiC/CCT consists of a folding chamber assisting *de novo* folding of a specific subset of proteins mostly, cytoskeletal clients. Substrates of TRiC are cytoskeletal proteins as actin and tubulin, but in general TRiC only appears to fold 5-10 % of the eukaryotic proteins (Yam *et al*, 2008). Conformational changes in the chaperonin, triggered by ATP hydrolysis initiate the closing of a folding chamber (Douglas *et al*, 2011). If aggregation of proteins occurs despite these diverse mechanisms and the protein is not able to be folded into the functional state other helpers have to be activated.

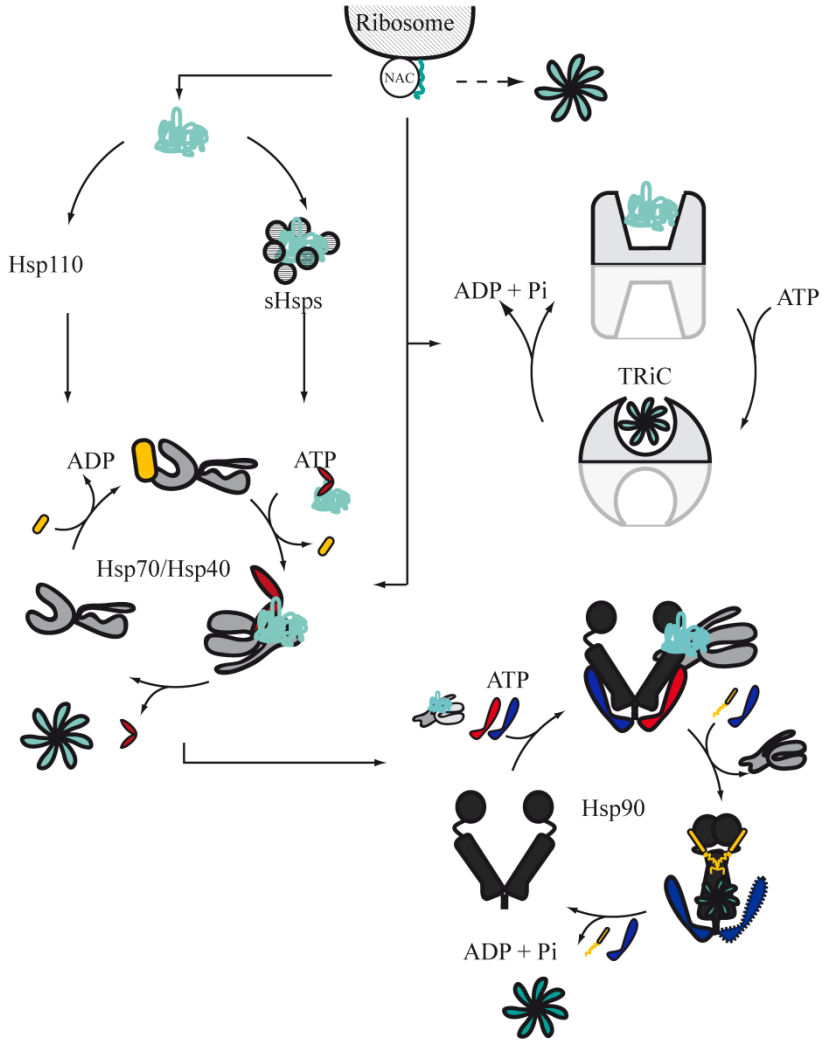

Figure 2 The cellular proteostasis system controlling folding of cytosolic proteins (green). Here the chaperones of the proteostasis network are summarized. Shown are the ribosome-associated chaperones of the nascent chain associated complex (NAC) and the cytosolic chaperones TRiC, Hsc70, Hsp90, Hsp110, sHsps, which control protein homeostasis in the cytosol. Several pathways are described, which help the misfolded, aggregated or freshly synthesized protein (green) to obtain the native fold. The "holdases" Hsp110 and the sHsps stabilize client proteins (green) to prevent aggregation. Afterwards they can transfer their client to the Hsc70 system, where the protein is actively folded. For the Hsc70 system (middle grey) cofactors can alter its cycle. Hsp40 proteins (red) present the client to the chaperone and facilitate ATP hydrolysis. Nucleotide exchange factors (NEF, yellow) subsequently trigger nucleotide release. If the substrate is not folded correctly it can be transferred to the Hsp90 system (dark grey) by TPR containing cofactors such as Sti1 (red). Other cofactors such as Aha1 (blue) accelerate the ATPase cycle. p23 is shown in yellow. TRiC/CCT (lightest grey) acts on the folding of newly synthesized clients by providing a folding chamber (Papsdorf & Richter, 2014).

Chaperones can be subdivided into the subclasses ‘foldases’ and ‘holdases’. Foldases hydrolyze ATP to provoke allosteric movements inducing conformational changes in substrate proteins. Small heat-shock proteins (sHsps) or Hsp110 are holdases which bind the misfolded aggregation prone protein to prevent further irreversible aggregation (Figure 2). Subsequently, the substrate is transferred to Hsc70, where it is folded (Richter *et al*, 2010; Oh *et al*, 1999). Among the described chaperones Hsp90 may have a special role as it is not thought to interact with unfolded or aggregating proteins, but is required to stabilize folded, metastable proteins or intermediates (Papsdorf & Richter, 2014). The subset of specific clients includes steroid hormone receptors, kinases and transcription factors (Taipale *et al*, 2014, 2012). Also for Hsp90 cofactors are present, which control the nucleotide hydrolysis reaction and the conformational states during the ATPase cycle (Figure 2). Beyond ATPase control these proteins are central for the correct folding and stability of defined Hsp90 client proteins. p23 and Sti1/Hop are known to be supportive during the activation of steroid hormone receptors (Smith *et al*, 1993; Johnson *et al*, 1994). Heat-shock proteins, or chaperones, were originally identified as being overexpressed in response to proteotoxic challenges, but are also found in the cytosol of unstressed cell. Some chaperones like Hsp90 and Hsp70 are up-regulated upon heat stress to cope with the increasing amount of destabilized proteins (Gasch *et al*, 2000; Guhathakurta *et al*, 2002; Bardwell & Craig, 1988). Hence chaperones do not only fold clients but also stabilize different conformational states of proteins, affect protein-protein interaction and buffer the many mutations present in the proteome (Morimoto & Cuervo, 2014; Rutherford & Lindquist, 1998).

2.5 Hsc70 and its Cofactors

The Hsc70 family is an essential protein system and conserved through all kingdoms of life. Hsc70 was first identified in *E. coli* and named DnaK (Tilly *et al*, 1983). In eukaryotes the constitutive form Hsc70, the heat-shock inducible form Hsp70 as well as organelle specific forms such as BiP exist. Hsc70 assists in *de novo* protein folding, refolding of aggregated and misfolded proteins, membrane translocation of proteins and activity control of regulatory proteins (Mayer & Bukau, 2005). It possesses a nucleotide binding domain (NBD), a substrate binding domain (SBD) and a flexible C-terminal lid, which covers the SBD. During protein folding Hsc70 shuffles between two states, an ADP bound state with

low substrate affinity and an ATP bound state possessing high substrate affinity. The chaperone cycle is regulated by two classes of cofactors the Hsp40/J-proteins and the Nucleotide Exchange Factors (NEF, Figure 3). Hsp40 proteins bind the substrate via the C-terminal domain and hold it in a folding competent state, thereby fulfilling a holdase function. Eventually they present the substrate to Hsc70 by docking to Hsc70´s SBD with their J-domain. ATP hydrolysis is the rate limiting step during the cycle, which is accelerated by the addition of Hsp40 proteins. NBD and SBD of Hsc70 communicate with an allosteric mechanism by docking and undocking to each other (Zhuravleva *et al*, 2012). Conformational rearrangements in the SBD and the C-terminal lid trigger substrate folding. Nucleotide binding to Hsc70 is very tight, with dissociation constants in the nanomolar range (Arakawa *et al*, 2011). Dissociation of the nucleotide is thus facilitated by NEFs, which interfere with the nucleotide binding groove in the NBD. Subsequent substrate release is triggered by ATP binding and Hsc70 is able to reenter the cycle (Montgomery *et al*, 1999).

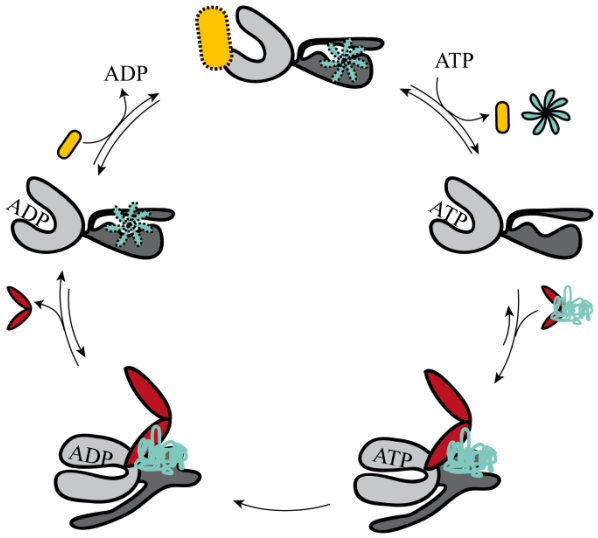

Figure 3 Model of the function of Hsp70 (grey) together with its cofactors. The client protein (green) is presented to Hsc70 by Hsp40 (red). The client is folded after initially binding to the open conformation of Hsc70. ATP hydrolysis, which is triggered by Hsp40 (red), results in conformational changes which help the client to adopt the native fold. Nucleotide exchange factors (yellow) facilitate the following ADP release and Hsc70 is able to reenter the cycle. Subsequently the client is released (adapted from Sun et al., 2012).

Modifying the ATPase cycle is not the only function of these cofactors. *In vivo* they are present in substochiometric amounts compared to Hsc70 to facilitate an optimal folding efficiency (Kampinga & Craig, 2010). Interestingly higher amount of cochaperones tend to

inhibit the *in vitro* luciferase folding capacity (Kampinga & Craig, 2010). Diversity of Hsc70 functions could be achieved through multiple copies of the Hsc70 gene but in eukaryotes only few cytoplasmic isoforms exist (Mayer & Bukau, 2005). Instead the cell provides a great number of Hsp40 proteins, which are differentially regulated, tissue specific and possess a diversity of domain compositions. A common feature all Hsp40 proteins share is the N-terminal J-domain. Some target Hsc70 to specific cellular compartments and others confer substrate specificity to the chaperone. Multiple J-proteins can function with a single Hsc70 (Kampinga & Craig, 2010). Alongside Hsp40 proteins, NEFs provide additional variability to the Hsc70 system. Although in a smaller diversity NEFs modulate the chaperone activity and likewise direct Hsc70 to cellular locations. Four large classes of NEFs are found in eukaryotes: Hsp110, BAG-domain containing proteins, Sil1/HspB1-like proteins and the mitochondrial located GrpE-like proteins. Hsp110 proteins resemble Hsc70 in sequence and domain composition. They are able to prevent aggregation of client proteins but fail to actively fold these. They act as a NEF for Hsc70 by embracing the NBD of Hsc70, inducing opening and the release of bound ADP from Hsp70 (Polier *et al*, 2008). GrpE and HspBP1 trigger nucleotide release by interacting with Hsc70´s SBD (Höhfeld & Jentsch, 1997). The BAG-domain containing proteins all possess an 85 amino acid helix bundle BAG-domain, which interacts with Hsc70s NBD (Takayama & Reed, 2001). Outside this BAG-domain other domains and regulatory elements such as ubiquitin like domains can be found in the different BAG-proteins (Doong *et al*, 2002). It is now clear that these eukaryotic Hsc70s strongly depend on their NEFs *in vivo* as temperature sensitivity or lethality are induced by their knockout (Bracher & Verghese, 2015). Another group of cochaperones are the TPR-domain containing proteins, which bind with the TPR domain to the EEVD motif at the very C-terminus of Hsc70 and the MEEVD motif in Hsp90 thereby connecting both systems (Haslbeck *et al*, 2013). Cofactors like the TPR protein Hop facilitate substrate transfer between Hsp90 and Hsc70 and promote substrate folding (Chen & Smith, 1998). Other TPR proteins including CHIP encourage substrate degradation instead, as they function as ubiquitin ligases. The longer a misfolded protein stays under surveillance of an Hsc70/CHIP complex the higher is the tendency to be marked for subsequent degradation (Höhfeld *et al*, 2001; Kettern *et al*, 2010). The Hsc70 system represents a central position in the proteostasis network fine-tuned by different cofactors and thereby used for a diversity of cellular events.

2.5.1 Hsc70 in *C. elegans*

Most of the studies on Hsc70 and its molecular behavior have been performed on the bacterial homolog DnaK. Nevertheless addressing *in vivo* relevance in connection with isolated protein assays provides a great platform to understand how molecular processes influence a multicellular organism. *C. elegans* offers the great opportunity to combine these features, as it contains muscular, intestinal, epithelial and neuronal tissues and its chaperone systems are in current focus of research (Sun *et al*, 2012; Guisbert *et al*, 2013). Additionally it is easily genetically manipulable, fast to cultivate and translucent. The mammalian Hsc70 system consists of multiple cytosolic Hsc70 isoforms and additional stress inducible forms. In *C. elegans* only one cytosolic (F26D10.3) and three inducible forms exist. Nematode Hsc70 is present in most tissues and knock-down via RNAi leads to enhanced aggregation and growth arrest in early larval stages (Kamath *et al*, 2003; Nollen *et al*, 2004; Guisbert *et al*, 2013). Overall 33 J-proteins have been found in *C. elegans* with three cytosolic J-proteins: DNJ-12, DNJ-13 and DNJ-19 (Mayer & Bukau, 2005). Compared to the nematode system the mammalian system is more complex consisting of 44 J-proteins and 6 BAG proteins. In *C. elegans* two cytosolic BAG proteins were found using the HMMER algorithm: BAG-1 and UNC-23 (Eddy, 2009; Papsdorf *et al*, 2014). BAG1 contains an N-terminal ubiquitin like domain besides its C-terminal BAG-domain. Its interaction with Hsc70 has been shown for mammalian and nematode systems. Further UBX2, a protein related to the ubiquitin system, was shown to connect with BAG-1 in yeast two-hybrid studies (Sun *et al*, 2012; Takayama *et al*, 1997; Li *et al*, 2004). Its knockout did not lead to any phenotype in *C. elegans* contrary to *unc-23* (Waterston *et al*, 1980). Here strong muscular defect arise, which induced the further dissection of the muscular Hsc70 system in this thesis.

2.5.2 The Muscular System of *C. elegans*

C. elegans contains two different types of muscular structures: The somatic striated body wall muscles and the non-striated muscles in the pharynx, the intestine and the reproductive system. The striated body wall muscles were investigated in the last decades into detail with their structure and the components being observable via light microscopy without requiring any staining procedure. Here the typical striature and the dense bodies, which connect the muscle to the cuticula are visible in differential interference contrast microscopy (DIC microscopy). Knockout of most of the Hsc70 cochaperones in *C. elegans*

does not lead to muscular phenotypes (Frumkin *et al*, 2014). *Unc-23* has been identified based on motility defects, a head-bent phenotype and a disordered muscular striature by Sydney Brenner in 1980 (Waterston *et al*, 1980). Later on it was identified as a BAG-domain containing protein, which represents a possible homolog of human Bag2 (Rahmani, 2002; Meissner *et al*, 2009). So far this protein remains the only Hsc70 cofactor in the wider family related to a severe muscular phenotype. Nevertheless Hsp90 is also closely related to muscular functionality. Its role in muscular maintenance is directed to specific muscular structures by the TPR protein UNC-45 (Gaiser *et al*, 2011). Its down-regulation causes defects in the body wall muscles of the nematode and together with its cofactors Aha1, Sti1 and p23 it is crucial for correct myosin assembly in *C. elegans* (Frumkin *et al*, 2014). These two examples indicate the need of the nematode muscular components to be chaperoned, as they constantly experience sheer stress and contraction strain.

2.5.3 Modulating Hsc70 Activity as a Therapeutic Target

Hsc70 is an essential protein involved in a great diversity of cellular processes. Its function has been shown to be involved in cancer, neurodegenerative diseases, infection and allograft rejection (Meimaridou *et al*, 2009; Broadley & Hartl, 2009; Mosser & Morimoto, 2004). Inhibiting its activity is a large intervention to almost all cellular processes and is thought to be potentially beneficial for several therapeutic approaches. It has been shown that a high level of Hsc70 in cancer cells correlates with an adverse outcome in breast cancer, colon cancer and leukemia (Rohde *et al*, 2005; Ciocca & Calderwood, 2005). Besides this an impact of Hsc70 regulation in neurodegenerative disease models including Huntington's disease (HD) has been discussed. Mutated huntingtin causes HD in humans due to extended polyglutamine stretches which lead to increased aggregation propensity. Overexpression of Hsc70 together with Hsp40 can prevent huntingtin aggregation and the chaperone system alternates inclusion body formation (Muchowski *et al*, 2000; Rujano *et al*, 2007). Overexpression of Hsc70 is beneficial under some circumstances but has little or no effect in other disease models (Evans *et al*, 2010; Hansson *et al*, 2003). Nevertheless modifying such an abundant protein with connections to a diversity of cellular processes is of great interest. Still it is under debate and has to be carefully evaluated whether targeting specific Hsc70 complexes, the ATPase activity or other functions performed by Hsc70 should be aimed at.

Several modifying compounds have been detected with distinct binding sites on Hsc70 representing a wide range of chemical classes (Evans *et al*, 2010). Specific peptides interacting solely with the bacterial DnaK have been shown to exhibit antibiotic functions, while not effecting mammalian cells (Otvos *et al*, 2000). The allosteric communication between SBD and NBD in DnaK is targeted by thiopene-2 carboxamide, which also possess antibiotic functions (Cellitti *et al*, 2009). Spergualin-like compounds have been shown to interact with the EEVD motif of Hsc70 and have been used to avoid allograft rejection (Evans *et al*, 2010; Nadler *et al*, 1998). Besides this, fatty acids such as sulfoglucolipides were able to bind the NBD of Hsc70 (Mamelak *et al*, 2001). ATP mimicking substances bind the NBD and are found to inhibit carcinoma cell growth (Williamson *et al*, 2009). Some of the listed Hsp70 modifying compounds were found to directly change Hsc70 activity, whereas others alter cochaperone binding. Dihydropyrimidines were found to inhibit the stimulation in ATPase activity of yeast Hsc70 by Hsp40 *in vitro* (Evans *et al*, 2010; Fewell *et al*, 2004). Alterations in ATPase and refolding assays for bacterial DnaK in presence of DnaJ can be additionally observed for this compound group (Chang *et al*, 2008; Wisén & Gestwicki, 2008). *In vivo* models showed that stimulation by this compound led to enhanced aggregation of tau, a protein involved in Alzheimer's disease (Jinwal *et al*, 2009). Organelle specific Hsc70 isoforms can be targeted by phenylethynesulfonamide (PES) which interact specifically with the C-terminus of human heat-shock inducible Hsp70 and not with the mitochondrial, endoplasmatic or the constitutively expressed isoforms of Hsc70. PES inhibited the cofactor complex assembly of Hsp70 and some BAG proteins. Selective toxicity to tumor cell lines was shown but the exact mechanism remains unknown to date (Leu *et al*, 2009). The promising rhodacyanine derivate MKT-077 targets specifically mitochondrial Hsc70 near the ATP binding site (Wadhwa *et al*, 2000). It was found to inhibit cancer cell line proliferation (Koya *et al*, 1996). Genetic and biochemical investigation support the idea of Hsc70 being a potential drug target (Evans *et al*, 2010). Modifying Hsc70 compounds for an application in humans is of great pharmaceutical interest and could possibly change the outcome of diverse diseases.

2.6 Diseases of the Proteostasis Network

Protein quality control mechanism in the proteostasis network prevent the proteome from being challenged by the accumulation of misfolded proteins (Morimoto & Cuervo, 2014).

The regulation of the proteostasis network happens at multiple stages and extends beyond the single cell level to a tissue wide regulation (Gidalevitz *et al*, 2011). It folds proteins and targets their degradation if aggregation occurs during stress (Figure 4A). As long as the system is balanced the cell can overcome acute stresses such as metal ion exposure or elevated temperatures. The performance of the proteostasis network has been shown to decline with age or the expression of aggregating proteins (Morimoto & Cuervo, 2009; Hipp *et al*, 2014). Numerous diseases arise from constitutively expressed metastable proteins, which fail to adopt their native conformational state and subsequently aggregate. Toxic aggregate species are formed which attack the proteostasis regulatory mechanisms once the system shifts out of balance during chronic stress (Figure 4B). These diseases are commonly termed proteopathies. The proteins evoking proteopathies are diverse including α-synuclein in the Parkinson's disease (PD) or the Aβ peptide in Alzheimer's (Chiti & Dobson, 2006). The mutated regulators of the proteostasis network such as the ubiquitin ligase parkin cause early-onset PD and mutations in HSPA5 cochaperone SIL1 lead to the Marinesco-Sjörgen syndrome (Hipp *et al*, 2014). Intra or extracellular protein deposits are common characteristics among these diseases including neurodegeneration, cancer, metabolic and immunological diseases (Morimoto *et al*, 2011). Nevertheless, it remains to be investigated how many other diseases have underlying mechanisms in deficiencies in proteostasis.

The toxicity of aggregating proteins can be explained by two different scenarios: Loss of function or gain of function mechanisms. Thereby cystic fibrosis represents a loss of function phenotype. Due to mutations in the cystic fibrosis transmembrane receptor (CFTR) a correct folding is hindered and transportation of the intact protein to the cellular surface fails. Cystic fibrosis occurs if the ion channel cannot fulfill its tasks at the cellular surface, namely to pump chloride ions into the extracellular space. In this context cochaperone expression of Hsp90 and Hsc70 was shown to alter mutant CFTR maturation (Höhfeld *et al*, 2001). This indicates that a sophisticated balance between chaperones is needed to correctly decide between folding and degradation of substrate proteins (Youker *et al*, 2004).

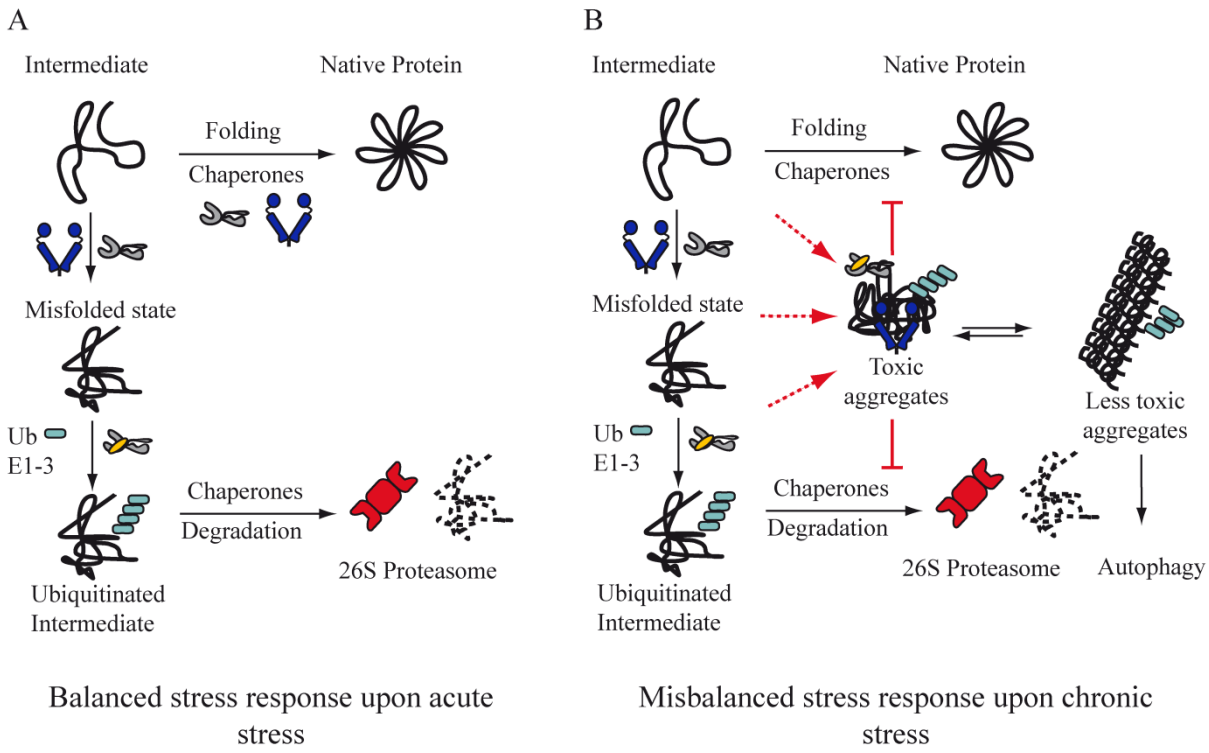

Figure 4 Balance and misbalance of the proteostasis network. A: Homeostasis. The capacity of the proteostasis network is sufficient to ensure client protein folding by chaperones or degradation of the misfolded proteins by the ubiquitin proteasome system. B: Upon chronic stress the capacity of the proteostasis network is exceeded and toxic aggregate species develop. These species interfere with stress response and proteostasis collapses (adapted from Hipp *et al*, 2014).

Another loss of function phenotype present in muscular myopathies involves the recycling of filamin at the muscular attachment sites by chaperones. Here the small heat-shock protein HSPB8, Hsc70 and its cofactors Bag3 and CHIP identify misfolded filamin proteins, which are subsequently degraded via autophagy. This chaperone controlled process is termed chaperone-assisted selective autophagy (CASA) and is essential for the correct assembly of muscular structures such as the Z-disc, involved in anchoring actin to the muscular striature. The 400 kDa filamin cannot be processed normally by the proteasome, thus the cellular quality control system has to take alternative routes to remove the protein and replace it by a new functional version. Chaperones recognize the damaged protein and target it to the autophagosomes (Arndt *et al*, 2005; Ulbricht *et al*, 2013). Certainly more examples exist, in which chaperones and the cellular quality system are connected to the severity of diseases making the cellular proteostasis system a promising target for drug development (Papsdorf & Richter, 2014).

The gain of function mechanism can be envisioned for mutated superoxide dismutase in amyotrophic lateral sclerosis, α-synuclein in PD, the Aß peptide in Alzheimer's disease or

mutated huntingtin in HD (Rosen *et al*, 1993; Kang *et al*, 1987; Rubinsztein *et al*, 1993). Age is a major risk factor for several of these proteostasis diseases. Studies in *C. elegans* showed that with a decline in activity of the proteostasis network the adequate response to protein aggregates is hindered and cellular homeostasis is not maintained (Ben-Zvi *et al*, 2009). It has been discussed that an evolutionary advantage exists by focusing cellular resources to reproduction rather than to maintenance of the somatic proteasome integrity (Kirkwood, 1977). And indeed a decrease in proteostasis is observed shortly after progeny production in *C. elegans* (Ben-Zvi *et al*, 2009). Although a decline in the proteostasis network is a short process in the nematode system similar scenarios can be envisioned for mammals (Hipp *et al*, 2014). Neurons and muscle cells are mostly affected by proteostasis impairment, as these postmitotic cells lack the ability to retain aggregates in their mother cell during cell division (M. A. Rujano et al., 2006). The occurrence of the named diseases can be either sporadic as seen in many cases of Alzheimer's or hereditary as observed for HD (Chiti & Dobson, 2006). Investigating the molecular mechanism of a hereditary disease thereby provides the chance to dissect the mechanisms leading to cellular toxicity in the end.

2.6.1 Polyglutamine Diseases

Several related neurodegenerative diseases with extended polyglutamine stretches exist: Spinocerebellar ataxia 1-4 with mutated ataxin, spinal and bulbar muscular atrophy with a mutated androgen receptor, dentatorubral-pallidoluysian atrophy with mutated atrophin and Huntington's disease with mutated huntingtin (La Spada *et al*, 1991; Orr *et al*, 1993). These genetically similar, progressive neurodegenerative diseases share common features such as an extended polyglutamine stretch within the mutated protein and the presence of insoluble protein aggregates.

In Huntington's disease the protein huntingtin with yet unattributed function is mutated and exposes large extended polyglutamine stretches (Rubinsztein *et al*, 1993). The length of the stretch correlates with the age of onset of the disease and the aggregation propensity (Rubinsztein *et al*, 1993). The role of the large aggregates is controversially discussed. Originally a correlation between severity of the disease and aggregation occurrence was suggested (Todd & Lim, 2013). Later on large aggregates have been proven cytoprotective and smaller oligomeric huntingtin species have been assigned as the toxic species (Figure 4, Takahashi *et al*, 2008; Arrasate *et al*, 2004; Todd & Lim, 2013). This is explained by the

reduction of interactive, solvent exposed surfaces whereas toxic species are thought to expose hydrophobic amino acid residues on unpaired β-strands which can act as sticky ends for other cellular proteins (Chiti & Dobson, 2006; Miller *et al*, 2012a).

The origin of toxicity of Huntington´s diseases is under debate and several hypotheses have been discussed. One is that the aggregating species may tie all available chaperone activity to it, thereby interfering with the proteostatis network (Gidalevitz *et al*, 2006; Balch *et al*, 2008; Park *et al*, 2013). Supporting this hypothesis more than 200 proteins have been found to colocalize to aggregates (Olzscha *et al*, 2011). In accordance with that idea is the fact that overexpression of Hsc70 chaperone members leads to a suppression in polyQ toxicity (Hageman *et al*, 2010). Additionally factors involved in Hsc70 expression including the transcription factor NF-Y are sequestered into polyQ aggregates (Yamanaka *et al*, 2008). Moreover polyglutamines are thought to interfere with the proteostasis system regarding ubiquitination and degradation. Ubiquitinated aggregates are found in inclusions in accordance with the idea that these proteins fail to be degraded when their levels exceed proteasome capacity (Waelter *et al*, 2001). On the other hand the aggregation of polyglutamine seems to cause the malfunction of the UPS (Hipp *et al*, 2012; Verhoef *et al*, 2002). Besides this, the impairment of membrane integrity and a purely mechanical model of huntingtin aggregates blocking neuronal axons was postulated (Lashuel & Lansbury, 2006; Parker *et al*, 2001). Although extensively studying the mechanism of toxicity no disease-modifying treatments exist so far (Labbadia & Morimoto, 2013).

2.6.2 Polyglutamine Toxicity in Yeast

The simplest and genetically most accessible eukaryotic model organism is *Saccharomyces cerevisiae*, in which several systems to study polyQ aggregation have been established (Kaiser *et al*, 2013; Muchowski *et al*, 2000; Krobitsch & Lindquist, 2000). Despite the evolutionary distance between mammals and yeast a number of mechanism such as cell death are highly conserved (Braun *et al*, 2010). In yeast diverse morphological events have been described as a reaction to polyglutamine-expression, including DNA-fragmentation, damage to mitochondrial respiratory chain complexes, apoptosis-like effects, spindle formation defects, mislocalization of septin proteins and altered regulation of the prion state [PSI^{+}] (Kaiser *et al*, 2013; Treusch & Lindquist, 2012; Manogaran *et al*, 2011; Solans *et al*, 2006; Sokolov *et al*, 2006).

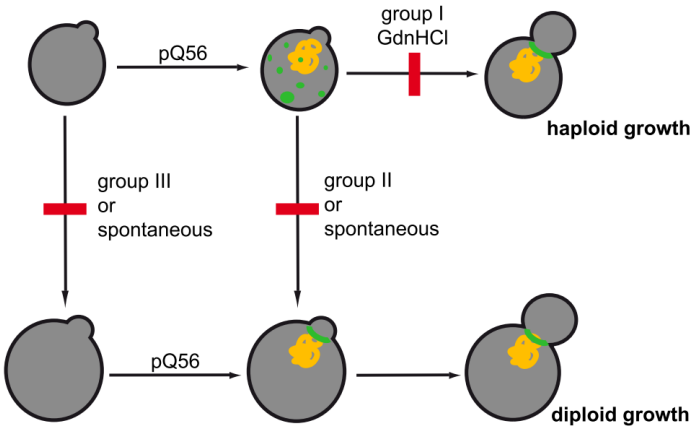

Figure 5 A model for the development and the escape from pica. The pica phenotype is generated by the expression and presumable aggregation of Q_{56}-YFP (yellow) and the subsequent inability of cells to follow the normal haploid growth cycle, potentially caused by compromised septin deposition (green). Deletion of Group I genes results in growth as haploid yeast cells and correct septin ring assembly. An alternative route is switching to diploid growth, which under normal conditions is blocked by Group II and Group III genes. Deletion of these genes lead to a transformation to a higher ploidy status and resistance to pica, as well as a restored capability to assemble septin rings (taken from (Kaiser *et al*, 2013)*).*

As the critical threshold for toxicity lies around 40 glutamine residues three different constructs with either 0, 30 or 56 polyglutamine residues fused to a fluorophore were designed (Krobitsch & Lindquist, 2000; Kaiser *et al*, 2013). In the model system designed by Dr. Kaiser, the polyQ-induced cellular arrest phenotype (*pica*) is evident from small colony growth, augmented cell size and fragmentary septin assemblies during budding (Kaiser et al., 2013, Figure 5). In contrast to other systems it is independent of the prion state of Rnq1 but dependent on the ploidy status of the yeast cell (Kaiser *et al*, 2013). Here this model system is used to dissect the molecular mechanism leading to toxicity. Polyglutamine induced toxicity can be suppressed by a set of mitochondrial genes (Kaiser, 2012, Table 1). Most of the reported toxicity-suppressors participate in metabolic processes or directly localize to mitochondria. Fourteen genomic deletion strains were uncovered that act synergistically with the polyQ induced phenotype, which were mostly associated with mitochondrial functions, including the mitochondrial fusion mediator Ugo1, the subunit of the F1F0-ATPase Atp15 and the protein Nfu1, which is involved in Fe-S cluster synthesis. Thus these mitochondrial proteins optimize systems, which are functional under normal growth conditions but become dysfunctional at conditions of polyQ intoxication.

Table 1 Genes, whose knock-out leads to an enhanced phenotype. The intensity of the phenotype is indicated on a semi-quantitative scale. --- very strong toxicity, no residual growth, --: residual growth detectable, but stronger toxicity than in the WT background (Kaiser, 2012).

Gene Knockout	Strain Number	Gene function	Growth of Q_{56}-YFP
arg82Δ	3531	Inositol polyphosphate multikinase (IPMK)	--
atp15Δ	1021	Epsilon subunit of mitochondrial ATP synthase	--
cem1Δ	198	Mitochondrial beta-keto-acyl synthase	--
his7Δ	3388	Imidazole glycerol phosphate synthase	---
hom6Δ	6933	Homoserine dehydrogenase	--
ies2Δ	1997	Essential for growth under anaerobic conditions	--
kre28Δ	4366	Subunit of a kinetochore-microtubule binding complex	--
map1Δ	5153	Methionine aminopeptidase	--
ncl1Δ	3050	S-adenosyl-L-methionine-dependent tRNA	---
nfu1Δ	4889	Protein involved in iron metabolism in mitochondria	--
rpb9Δ	4437	RNA polymerase II subunit	--
rrn10Δ	3051	Subunit of UAF (upstream activation factor) for RNA polymerase I	---
ugo1Δ	4304	Outer membrane component of the mitochondrial fusion machinery	--
ybr196c-aΔ	7457	Putative protein of unknown function	--

2.6.3 The Poliovirus Precursor VP0

The poliovirus belongs to the group of picornaviruses with a single-stranded RNA surrounded by an icosahedral capsid. The virus can paralyze its host *homo sapiens* by manifesting in poliomyelitis (De Jesus, 2007). The viral RNA can be divided into 3 subunits: The structural region P1 and the non-structural regions P2 and P3. The latter thereby contain information for proteases and RNA dependent RNA polymerases whereas P1 encodes the capsid polypeptide with the subunits VP0, VP2 and VP1 (Kitamura *et al*, 1981). Besides the known metastable disease related proteins, the viral protein VP0 was investigated as a model protein in yeast. Dr. Rehn detected in 2014 that yeasts expressing the poliovirus precursor VP0 resemble the *pica* phenotype (Rehn, 2014). Mutation of the

myristoylation domain glycine to alanine at position 2 results in a loss of toxicity in yeast (Rehn, 2014). Interestingly aggregation in this case does not correlate with toxicity as VP0 and VP0 G2A both aggregate when expressed in yeast (Rehn, 2014). In this thesis it is addressed how the toxicity is mediated and which cellular pathways are affected as toxicity culminates in the same growth phenotype as observed for polyglutamine.

3. Aim of the Work

Studying the proteostatis network in *C. elegans* and *S. cerevisiae* and its relevance in disease models was the mayor task of this PhD thesis. Cellular proteostasis encompasses a complex network of regulators ensuring the correct folding state of the proteome, hindering aggregation of proteins, refolding aggregates or triggering client degradation. These factors are connected in a system which, if misbalanced, results in deleterious effects for cellular survival. Here the Hsc70 system and its cofactors in context of muscular homeostasis in *C. elegans* were studied. Additionally a challenged proteostasis network was created by the production of toxic polyglutamine stretches in *S. cerevisiae* to dissect the response of a unicellular organism to toxic protein aggregates.

3.1 Studying the Hsc70 System in Relation to Muscular Deficiencies in Nematodes

Hsc70 activity is regulated by NEFs and J-proteins (Mayer & Bukau, 2005). The knockout of *unc-23*, a BAG-domain containing protein, reveals a strong muscular phenotype in *Caenorhabditis elegans*. How this phenotype is connected to the Hsc70 system was not understood to date. The impact of Hsc70 misregulation on the muscular homeostasis and how the muscular structures were connected to the Hsc70 system were addressed in this thesis. Here the focus was set on the functional regulation of Hsc70 and UNC-23 together with cytosolic Hsp40 proteins in isolated protein assays and with respect to muscular attachment *in vivo*.

3.2 Analyzing the Underling Mechanism of Polyglutamine Induced Toxicity

Polyglutamine stretches within certain proteins trigger the onset of several neurodegenerative diseases. Multiple effects of toxic aggregates in *S. cerevisiae* have been described. Here isolated polyglutamine stretches fused to YFP were used in the model organism *Saccharomyces cerevisiae*. Toxicity was shown to be ameliorated by altering the yeasts ploidy status and septin ring formation fails in intoxicated cells. Nevertheless the mechanisms of polyglutamine induced toxicity remained enigmatic. The transcriptional response of yeasts upon polyglutamine intoxication was addressed. These results were

further inspected by metabolic analyses to dissect which metabolic processes are affected. Detailed microscopic investigations were carried out to visualize the affected processes.

4. Material and Methods

4.1 Material

4.1.1 Reagents

Table 2 Reagents. If not stated otherwise the reagents were of the highest purity. All chemicals not listed were obtained from Roth (Karlsruhe, Germany. Chemicals were diluted in $_{dd}H_2O$.

Name	Source
Acrylamide (38%, 2% Bisacrylamide)	Roth (Karlsruhe, Germany)
Agarose, ultra pure	Roth (Karlsruhe, Germany)
Agar	Serva (Heidelberg, Germany)
Ammoniumperoxodisulfate (APS)	Roche (Mannheim, Germany)
Ammoniumsulfate	Merck (Darmstadt, Germany)
Ampicillin	Roth (Karlsruhe, Germany)
Antifoam	Sigma Aldrich (St. Louis, USA)
ATP	Roche (Basel, Switzerland)
Bacto Agar	Difco (Detroit, USA)
Bacto Tryptone	Difco (Detroit, USA)
Bacto Yeast Extract	Difco (Detroit, USA)
Bromphenolblue S	Serva (Heidelberg, Germany)
Cholesterol	Sigma (St. Louis, USA)
Coomassie Brilliant-Blue R-250	Serva (Heidelberg, Germany)
Coomassie Protein Assay Reagent	Pierce (Rockford, USA)
Desferrioxamine (DFO)	Sigma Aldrich (St. Louis, USA)
Dithiothreitol (DTT)	Roth (Karlsruhe, Germany)
Diethylenetriamine pentaacetic acid (DETAPAC)	Sigma Aldrich (St. Louis, USA)
ECL-Westernblot Detection System	GE Healthcare (Munich, Germany)
Ethanol	Merck (Darmstadt, Germany)
Ethidiumbromide	Sigma (St. Louis, USA)
Ethylendiamintetraacidic acid (EDTA)	Merck (Darmstadt, Germany)
Formaldehyde, 37% p.A.	Roth (Karlsruhe, Germany)

Galactose	Sigma (St. Louis, USA)
Glass beads 4±0.3 mm	Carl Roth (Karlsruhe, Germany)
Glass beads 0.25±0.05 mm	Carl Roth (Karlsruhe, Germany)
Glucose	Sigma (St. Louis, USA)
Glutaraldehyd, 25% in water	Serva (Heidelberg, Germany)
Glycerol, 99 %	ICN, Costa Mesa, USA
Glycine	Roth (Karlsruhe, Germany)
Imidazole	Sigma (St. Louis, USA)
Ipegal CA630	Biochemika GmbH (Düsseldorf, Germany)
Isopropanole	Roth (Karlsruhe, Germany)
Isopropyl-β-D-thiogalaktopyranosid (IPTG)	Roth (Karlsruhe, Germany)
Kanamycin	Roth (Karlsruhe, Germany)
LB_0 Media	Sigma-Aldrich (Hamburg, Germany)
LiO_2Ac	Roth (Karlsruhe, Germany)
Milk powder	Roth (Karlsruhe, Germany)
N-(2-Hydroxyethyl)-piperazin-N´2-Ethansulfonic acid (HEPES)	ICN (Costa Mesa, USA)
N,N,N´,N´-Tetramethylethylendiamine (TEMED)	Roth (Karlsruhe, Germany)
NADH	Roche (Basel, Switzerland)
peqGOLD 1 kb DNA ladder	Peqlab (Erlangen, Germany)
Phosphoenolpyruvate (PEP)	Sigma (St. Louis, USA)
Polyoxyethylen-Sorbitan-monolaurat (Tween 20)	Merck (Darmstadt, Germany)
Ponceau S	Sigma-Aldrich (Hamburg, Germany)
Propidium iodide	Sigma-Aldrich (Hamburg, Germany)
Protease Inhibitor Mix HP	Serva (Heidelberg, Germany)
Roti Mark pre-stained	Roth (Karlsruhe, Germany)
SDS-PAGE Standard Low Weight	BioRad (Hercules, USA)
Sodiumdodecylsulfate (SDS)	Roth (Karlsruhe, Germany)
StainG	Serva (Heidelberg, Germany)
StainG	Serva (Heidelberg, Germany)
Tetracycline	Roche (Basel, Switzerland)
Tris-(Hydroxymethyl)-aminomethane (Tris)	ICN, Costa Mesa, USA

Yeast Nitrogen Base w/o phosphate w/o amino acids	MP Biomedicals (Santa Ana, USA)
β-Mercaptoethanol, pure	Merck (Darmstadt, Germany)
1,4-Dithiothreitol (DTT)	Roth (Karlsruhe, Germany)
5-(and-6)-Carboxyfluorescein succinimidyl ester (FAM)	Invitrogen (La Jolla USA)
5,5' Dithio-bis-Nitrobenzoic acid (DTNB)	Sigma (St. Louis, USA)

4.1.2 Buffers

Table 3 Buffer

Name	Substance	Concentration
ATP buffer	HEPES/KOH, pH 7.8	50 mM
	$MgSO_4$	4mM
ATP pre-mix buffer	Potassium phosphate buffer, pH 7.8	100 mM
	Glycylglycine	25 mM
	EDTA	20 µM
	BSA	0.05 mg ml^{-1}
	Luciferin	70 µM
	Luciferase	100 nM
ATPase pre-mix buffer	Phosphoenolpyruvate	2.6 mM
	NADH	260 nM
	Lactate dehydrogenase	0.5 U ml^{-1}
	Pyruvate kinase	0.024 U ml^{-1}
	$MgCl_2$	5 mM
	in standard assay buffer	
Bleach	NaOH	330 mM
	Bleach	400 ml
	H_2O	Ad 1 l
CD buffer	Potassium phosphate, pH 7.5	40 mM
DNA sample buffer (10x)	Glycerol	50 (v/v)
	EDTA/NaOH, pH 8.0	10 mM

	Bromphenol blue	0.2% (w/v)
	Xylene cyanol	0.2% (w/v)
Dialysis buffer	HEPES/KOH, pH 7.5	40 mM
	KCl	20 mM
	EDTA	1 mM
	DTT	1 mM
EPR buffer	HEPES/KOH, pH 7.0	40 mM
	KCl	150 mM
	DETAPAC pH 7.0	10 mM
	DFO	20 mM
Extracellular phosphatase assay	Sodium acetate, pH 4.2	0.1 M
	p-nitrophenylphosphate	5.62 mg ml $^{-1}$
FACS assay buffer	Trisodium citrate, pH 7.0	50 mM
Fairbanks A	Coomassie Brilliant Blue R	2.5 g
	Ethanol	250 ml
	Acetic acid	80 ml
	$_{dd}H_2O$	ad 1 l
Fairbanks D	Ethanol	250 ml
	Acetic acid	80 ml
	$_{dd}H_2O$	ad 1 l
HisTrap loading buffer	HEPES/KOH pH 7.5	40 mM
	KCl	20 mM
	DTT	1 mM
	DNase I	1 µg ml^{-1}
HisTrap elution buffer	HEPES/KOH, pH 7.5	40 mM
	KCl	20 mM
	Imidazole	400 mM
	DTT	1 mM
HsHsc70 purification buffer	Tris/HCl, pH 7.6	50 mM
	Phenylmethylsulfonyl fluoride	1 mM
	Lysozyme	0.4 mg ml^{-1}

	DNAse I	1 µg ml^{-1}
Ion exchange loading buffer	HEPES/KOH pH variable	40 mM
	KCl	20 mM
	EDTA	1 mM
	DTT	1 mM
Ion exchange elution buffer	HEPES/KOH, pH adapted according to pI	40 mM
	KCl	1 M
	EDTA	1 mM
	DTT	1 mM
Laemmli loading buffer (5x)	Tris/HCl, pH 6.8	312.5 mM
	SDS	10 % (w/v)
	β-mercaptoethanol	25 % (v/v)
	Glycerol	50 % (v/v)
	Bromphenolblue	0.05 % (w/v)
M9	KH_2PO_4	3 g
	Na_2HPO_4	6 g
	NaCl	5 g
	1 M $MgSO_4$	1 ml
	$_{dd}H_2O$	ad 1 l, autoclave
PBS	KH_2PO_4	5.44 g
	Na_2HPO_4	7.11 g
	NaCl	2.34 g
	$_{dd}H_2O$	Ad 1 l
PBST	PBS	See above
	Tween 20	0.05 % (v/v)
PLATE- mix	PEG4000	40 % (w/v)
	LiOAc	100 mM
	Tris/HCl (pH 7.5)	10 mM
	EDTA	1 mM
S buffer	K_2HPO_4 0.05 M	129 ml

	KH_2PO_4 0.05 M	871 ml
	NaCl	5.85 g
SDS running buffer	Tris/HCl, pH 6.8	25 mM
	Glycine	200 mM
	SDS	0.1 (w/v)
SDS-PAGE stacking gel	Tris/HCl, pH 6.8	125 mM
	SDS	0.2 (w/v)
	Acrylamide	5 % (w/v)
	Polymerization is started by the addition of	
	TEMED	2.5 µl/gel
	APS	25 µl/gel
SDS-PAGE separation gel	Tris/HCl, pH 8.8	62.5
	SDS	0.2 % (w/v)
	Acrylamide	12.5% (w/v)
	Polymerization is started by the addition of	
	TEMED	5 µl/gel
	APS	50 µl/gel
	DTT	1 mM
Soft agar freezing solution	NaCl	0.58 g
	KH_2PO_4	0.68 g
	Glycerol	30 g
	NaOH, 1 M	0.56 ml
	Agar	0.4 g
	$_{dd}H_2O$	ad 100 ml, autoclave
Standard assay buffer	HEPES/KOH, pH 7.5	40 mM
	KCl	150 mM
TAE buffer (50x)	Tris/acetat, pH8.0	2 M
	EDTA/NaOH, pH 8.0	50 mM
Western blot buffer	PBS	1 %

	Milk powder	1 %
	Tween 20	0.05 % (v/v)
Western blot blocking buffer	PBS	1 %
	Milk powder	5 %
	Tween 20	0.05 % (v/v)
Yeast preparation buffer	Tris/HCl pH 7.5	100 mM
	NaCl	50 mM

4.1.3 Media

Table 4 Media. All media were autoclaved if not indicated otherwise.

Name	Substance	Concentration
LB	LB medium	20 g l^{-1}
	For plates: agarose	20 g l^{-1}
Fermenter feeding solution	Yeast extract	500 g
	Glucose	250 g
	$_{dd}H_2O$	ad 1 l, autoclave
Fermenter media	Yeast extract	300 g
	NH_4Cl	3 g
	Antifoam A	1 ml
	$_{dd}H_2O$	Ad 5 l, autoclave
	After autoclaving add	
	KH_2PO_4 (13.2 w/v)	500 ml
	$MgSO_4$ (1.6 w/v)	250 ml
	Glucose (6% w/v)	250 ml
NGM	NaCl	3 g
	Peptone	2.5 g
	Agar	17 g
	$_{dd}H_20$	ad 1 l
	After autoclaving add	1 M $CaCl_2$, autoclaved, 1 ml
		5 mg/ml cholesterol, 1 ml

		1 M $MgSO_4$, autoclaved, 1 ml
		1 M KPO_4, pH 6.0, autoclaved, 25 ml
No-phosphate medium	Amino acid drop-out mix	0.7 g
	Glucose/galactose	20 g
	Agar	20 g
	YNB w/o phosphate, w/o ammonium sulfate	5.6 g
	NaCl	0.1 g
	$_{dd}H_20$	ad 1 l
RNAi plates	Following chemicals were added to NGM plates	
	IPTG	1 mM
	Tetracycline	6 µg ml^{-1}
	Ampicillin	50 µg ml^{-1}
TB-medium	NaAc, pH 5.5	69 mM
	$CaCl_2$	100 mM
	$MnCl_2$	70 mM
	$_{dd}H_20$	ad 1 l
	sterile filtered	
SMM	Amino acid drop-out mix (Table 5)	0.7 g
	Glucose/galactose	20 g
	Agar	20 g
	YNB	6.7 g
	$_{dd}H_20$	ad 1 l
SOB	Yeast extract	0.5 % (w/v)
	Tryptone	20% (w/v)
	NaCl	10 mM
	KCl	2.5 mM
	$MgCl_2$	10 mM
	$MgSO_4$	10 mM

	$_{dd}H_2O$	Ad 1 l
YPD	YPD media	50 g l^{-1}
	For plates: Agarose	20 g l^{-1}

4.1.4 Amino Acid dropout-mix

Table 5 Amino acid dropout-mixt. All amino acids were purchased from Sigma (St.Louis, USA).

Name	Amount
Adenine	0.5 g
Arginine	2 g
Histidine	2 g
Leucine	10g
Lysine	2 g
Methionine	2 g
Phenylalanine	2 g
Threonine	2 g
Tryptophan	2 g
Tyrosine	2 g
Uracil	2 g

4.1.5 Enzymes and Kits

Table 6 Enzymes and Kits

Enzymes	Source
Antarctic phosphatase	New England Biolabs (Ipswich, USA)
DNAse	Sigma Aldrich (St. Louis, USA)
GoTaq polymerase	New England Biolabs (Ipswich, USA)
Lactat dehydrogenase	Roche (Basel, Switzerland)
Pfu polymerase	New England Biolabs (Ipswich, USA)
Proteinase K	Sigma Aldrich (St. Louis, USA)
Pyruvate kinase	Roche (Basel, Switzerland)
Restriction enzymes	New England Biolabs (Ipswich, USA)

RNAse A	Sigma Aldrich (St. Louis, USA)
T4 ligase	New England Biolabs (Ipswich, USA)

Kits	Source
Aconitase Activity Assay Kit	Sigma (St. Louis, USA)
NAD/NADH Quantification Kit	Sigma (St. Louis, USA)
Wester Blot detection system, Western-Bright™	Advansta (Menlo Park, USA)
Wizard® *Plus* SV Minipreps DNA Purification	Promega (Fitchburg, USA)
Wizard® SV Gel and PCR Clean-Up System	Promega (Fitchburg, USA)

4.1.6 Fluorophores

Table 7 Fluorophores

Fluorophore	Excitation wavelength	Laser	Emission wavelength	Source
Alexa Fluor 488 C_5-maleimid	496 nm		519 nm	Invitrogen (Carlsbad, USA)
CFP	476 nm	Argon	478-501 nm	Clontech (Mountainview, USA)
eYFP	514 nm	Argon	520-540 nm	Clontech (Mountainview, USA)
GFP	458 nm	Argon	505-530 nm	EUROSCARF (Frankfurt, Germany)
mCherry	543 nm	Helium-Neon	577-634 nm	Clontech (Mountainview, USA)
MitoTracker fused to rhodamine	507 nm		529 nm	Life Technologies (Darmstadt, Germany)
SYPRO Orange	470 nm		570 nm	Life Technologies (Carlsbad, USA)
5- (and 6-) carboxyfluorescein succinimidylester	494 nm		518 nm	Invitrogen (Carlsbad, USA)

4.1.7 Antibodies

Table 8 Antibodies

Name	Organism	Origin	Target
UNC-23	rabbit	Pineda (Berlin, Germany)	UNC-23
α-rabbit IgG (whole molecule) peroxidase	goat	Sigma (St. Louis, USA)	rabbit

4.1.8 Strains and Organisms

Table 9 Strains and Organisms

Name	Genotype	Source
	E.coli	
BL21-CodonPlus-RIL (DE3)	F– *ompT hsdS*(rB– mB–) *dcm*+ Tetr *gal* λ	Merck (Darmstadt,Germany)
DH10B	F– *mcr*A Δ(*mrr-hsd*RMS-*mcr*BC) Φ80*lac*ZΔM15 Δ*lac*X74 *rec*A1 *end*A1 *ara*D139 Δ(*ara leu*) 7697 *gal*U *gal*K *rps*L *nup*G λ–	Life Technologies (Carlsbad, USA)
OP50	Unknown	CGC (Minneapolis, USA)
HT115(DE3)	F-, mcrA, mcrB, IN(rrnD-rrnE)1, rnc14::Tn10	CGC (Minneapolis, USA)
	S. cerevisiae	
BY4741	MAT a; *his3Δ1; leu2Δ0; met15Δ0; ura3Δ0*	(Brachmann *et al*, 1998)
PY4995	MAT **a**/**a**; *his3Δ1/1; leu2Δ0/0; met15Δ0/MET15;LYS2/lys2Δ0; ura3Δ0/0,* PY5006	(Storchová *et al*, 2006)
Single ORF deletion strains	MAT**a**; *his3Δ1; leu2Δ0; met15Δ0; ura3Δ0; ORF::kanMX4*	(Winzeler *et al*, 1999)
GFP-fusion strains	EY0986 (MAT**a**; his3*Δ*1; leu2*Δ*0; met15*Δ*0; ura3*Δ0*; ORF::GFP-*HIS3MX6* (S288C)	(Huh *et al*, 2003)

C. elegans		
CB25	*unc-23* (e25)	CGC (Minneapolis, USA)
CB611	*unc-23* (e611)	CGC (Minneapolis, USA)
RB1301	*unc-23* (ok1408)	CGC (Minneapolis, USA)
CB324	*unc-23* (e324)	CGC (Minneapolis, USA)
N2	*Wild-type*	CGC (Minneapolis, USA)

4.1.9 Plasmids

Table 10 Plasmids

Name	Selection Marker	Backbone	Source
L4440	Amp	L4440	Thermo Scientific (Darmstadt, Germany)
Unc-23/ H14N18.1	Amp	L4440	Thermo Scientific (Darmstadt, Germany)
ceHsc70/ F26D10.3	Amp	L4440	Thermo Scientific (Darmstadt, Germany)
Dnj-19/ T05C3.5	Amp	L4440	Thermo Scientific (Darmstadt, Germany)
Dnj-13/ F54D5.8	Amp	L4440	Thermo Scientific (Darmstadt, Germany)
Dnj-12/ F39B2.10	Amp	L4440	Thermo Scientific (Darmstadt, Germany)
Bag-1/ F57B10.11	Amp	L4440	Thermo Scientific (Darmstadt, Germany)
Q_0-eYFP	Amp	p425-GPD	Christoph Kaiser
Q_{30}-eYFP	Amp	p425-GPD	Christoph Kaiser
Q_{56}-eYFP	Amp	p425-GPD	Christoph Kaiser

Q_0-mCherry	Amp	p425-GPD	Christoph Kaiser/Julia Eckl
Q_{56}-mCherry	Amp	p425-GPD	Christoph Kaiser/Julia Eckl
VP0-CFP	Amp	p426-GPD	Alexandra Rehn
VP0 G2A-CFP	Amp	p426-GPD	Alexandra Rehn
C34B2.5-CFP	Amp	PD95.97	Veronika Haslbeck
CeHsc70 CFP	Amp	PD95.97	Klaus Richter
Dnj-12-YFP	Amp	PD95.97	Katharina Papsdorf, Franziska Edelmann
Dnj-13-YFP	Amp	PD95.97	Katharina Papsdorf, Franziska Edelmann
Dnj-19-YFP	Amp	PD95.97	Katharina Papsdorf, Franziska Edelmann
Δ129-unc-23-YFP	Amp	PD95.97	This work
Δ285-unc-23-YFP	Amp	PD95.97	This work
Δ371-unc-23-YFP	Amp	PD95.97	This work
HsHsc70	Amp	pMPM - A4	Harald Wegele
Bag-1	Kan	pET28	Li Sun
Dnj-12	Kan	pET28	Klaus Richter
Dnj-13	Kan	pET28	Li Sun

Dnj-19	Kan	pET28	Li Sun
Δ129-unc-23	Kan	pET28	This work
Δ285-unc-23	Kan	pET28	This work
Δ371-unc-23	Kan	pET28	This work

4.1.10 Oligonucleotides

Table 11 Oligonucleotides. All oligonucleotides were ordered from MWG Eurofins (Ebersberg, Germany).

Name	Sequence	Application
	Primer for *in vitro* application	
Δ129-unc-23 F	ATT GCA GCT AGC ATG CAA GGA TAC AGG AGA AGT C	Protein expression
Δ258-unc-23 F	ATT GCA GCT AGC ATG CCA CTA ACC TCC CCA ATC ACC G	Protein expression
Δ371-unc-23 F	ATT GCA GCT AGC GAT GCA ACT TTG ATG ATC GAT G	Protein expression
Unc-23 F	ATT GCA GCT AGC ATG TTT CAG AAC ATA CCA ATC AAA ATA C	Protein expression
Unc-23 R	TGC AAT GGA TCC CTA TTC GCT TTG ATC ATC CAT C	Protein expression
GATC-GPD-FW-228935	AAA GAC GGT AGG TAT TG	Sequencing
	Primer for *in vivo* application	
Dnj-12 YFP R	GGT TTT TCT AGA AGA CTG TTG GCA TTG AAC GCC TTG TGG C	Protein localization in *C. elegans*
Dnj-12-YFP F	GGT TTT GCG GCC GCC CGA AGT CTG ACG GCC AAA TGT	Protein localization in *C. elegans*

	GTA ATT CC	
Dnj-13 YFP F	GGT TTT GCG GCC GCG TCT CCG TGG CAG GAC CAT ACT GTG CGC CG	Protein localization in *C. elegans*
Dnj-13 YFP R	GGT TTT GCT AGC GAA GTT CCT CAG AAT CAC TTC CCG TTG AGT T	Protein localization in *C. elegans*
Dnj-19-YFP F	GGT TTT GCG GCC GCG GCA AGC GAA GTT GCG GCT GAC GCG TTA TTG G	Protein localization in *C. elegans*
Dnj-19-YFP R	GGT TTT GCT AGC TTG GTG TTG GCA TCT GAC GCC TTG TCC G	Protein localization in *C. elegans*
Hsc70 promoter F	GCA TGC GCG GCC GCT CGT CAC CAA CCA AAA GC	Promoter activity in *C. elegans*
Hsc70 promoter R	GGT TTT GCT AGC CTT ACT CAT TTT TAC TGT AAA AAA TAA TTT AAA AAT CAA G	Promoter activity in *C. elegans*
Unc-23 promoter F	AGT CCA GCG CGG CCG CCA CTT TGA AAA GTA G	Promoter activity in *C. elegans*
Unc-23 promoter R	CGG ACT GCT AGC GCT GAA TAT TAG GAT GG	Promoter activity in *C. elegans*
Unc-23-YFP F	ATT GCA GCT AGC ATG TTT CAG AAC ATA CCA ATC AAA ATA C	Protein localization in *C. elegans*
Unc-23-YFP R	CAG CCT GCT AGC TTC GCT TTG ATC ATC CAT C.	Protein localization in *C. elegans*
Δ129-*unc-23* F	ATT GCA GCT AGC ATG CAA GGA TAC AGG AGA AGT C	Protein localization in *C. elegans*
Δ258-*unc-23* F	ATT GCA GCT AGC ATG CCA CTA ACC TCC CCA ATC ACC G	Protein localization in *C. elegans*
Δ371-*unc-23* F	ATT GCA GCT AGC GAT GCA ACT TTG ATG ATC GAT G	Protein localization in *C. elegans*

4.1.11 Equipment

Table 12 Equipment

Name	Origin
Analytical Balances	
1409 MP	Satorius (Göttingen, Germany)
BL 310	Satorius (Göttingen, Germany)
BP 121 S	Satorius (Göttingen, Germany)
Blotting device	
FastBlot B44	Biometra (Göttingen, Germany)
CD spectrometer	
Jasco J-710	Jasco (Gross-Umstadt, Germany) equipped with a PFD-350S Peltier- type FDCD attachment unit Jasco (Gross- Umstadt, Germany
Centrifuges	
Avanti J25 (Rotors: JA-10 and JA-25.50)	Beckmann (Vienna, Austria)
Eppendorf-Centrifuge 5415 C	Eppendorf (Hamburg, Germany)
Gel electrophoretic device	
Hoefer Mighty Small II	Hoefer Inc (Holliston, USA)
Microscopes	
Axiovert 200 inverted microscope	Carl Zeiss (Oberkochen, Germany) equipped with Hamamatsu C4742-95 camera Hamamatsu (Herrsching, Germany equipped with injection device Eppendorf (Hamburg, Germany
Leica SP-5 laser scanning microscope	Leica (Wetzlar, Germany)
MZ16- FA stereo microscope	Leica (Wetzlar, Germany)
Stemi stereo microscope	Carl Zeiss (Oberkochen, Germany) Equipped with SCHOTT KL1500 LCD unit (Mainz, Germany)
Power amplifier	

LKB-GPS 200/400	Amersham Bioscience (Freiburg, Germany)
Pharmacia EPS 3500, 1001 and 601	GE Healthcare (Freiburg, Germany)
Purification	
Äkta FPLC	GE Healthcare (Little Chalfont, UK)
Cell disrupter	Basic Z Constant Systems (Warwick, UK)
Silent Crusher M	Heidolph (Schwabach,Germany)
Purification columns	
DEAE-Sepharose column	GE Healthcare (Chalfont St Giles, UK)
Fluoroapatite column	Bio-Rad (Hercules, USA)
HisTrap HP 5 ml	GE Healthcare (Little Chalfont, UK)
Resource Q/S 6 ml	GE Healthcare (Little Chalfont, UK)
Superdex 200 Prep grade (130 ml)	GE Healthcare (Little Chalfont, UK)
Superdex 200 Prep grade (240 ml)	GE Healthcare (Little Chalfont, UK)
Superdex 75 prep grade (130 ml)	GE Healthcare (Little Chalfont, UK)
Superdex 75 Prep grade (240 ml)	GE Healthcare (Little Chalfont, UK)
UV/VIS spectrometer	
Cary100 UV/Vis spectrometer	Varian (Palo Alto, USA)
EnVision Xcite Multilabel Plate Reader	PerkinElmer (Waltham, USA)
NanoDrop ND-2000	Peqlab (Erlangen, Germany)
Others	
AVANCE-III 500 NMR instrument	Bruker (Rheinstetten, Germany) equipped with a QNP cryo probe optimized for 31Pdetection.
BD FACS CANTO II	BD Bioscience (Heidelberg, Germany)
Biometra BioDOC II	Biometra (Göttingen, Germany) equipped with an Canon EOS600D (Tokyo, Japan)
Centricon (10,000 MWCO) microconcentrators	Millipore (Bedford, USA)
Dialysis tubes Spectra/Por (6-8 kDa)	Spectrum (Huston, USA)
Eppendorf-Thermomixer	Eppendorf (Hamburg, Germany)
EPR Spectrometer JEOL JES FA 200	JEOL (Tokyo, Japan)

EPR Tubes (Clear Fused-Quartz Non-Precision)	Wilmad (Vineland, USA)
ImageQuant LAS4000	GE Healthcare (Little Chalfont, UK)
Incubator	New Brunswick Scientific (Nürtingen,Germany)
Magnetic stirrer Heidolph MR2000	Heidolph (Kehlheim, Germany)
MM400 bead mill	Retsch (Haan, Germany)
Needle puller	Narishige PB-7 (Tokyo, Japan)
pH-Meter – WTW	WTW (Weilheim, Germany)
Sonoplus 2200 series	Bandelin (Berlin, Germany)
Tecan GenIOS microplate reader	Tecan (Männerdorf, Switzerland)
Water bath Haake F6-K	Haake (Karlsruhe, Germany)

Computer Programs and Databases

Table 13 Computer programs and databases

Name	Company
Computer programs	
Adobe Illustrator CS3	Adobe Systems (San José, USA)
BD FACSDIVA	BD Biosystems (Heidelberg, Germany)
Fiji	Open source (Schindelin *et al*, 2012)
HMMER	(Eddy, 2009)
Leica Application Suite	Leica Microsystems (Wetzlar, Germany)
MestReNova 8.1.	MestreLab Research (Santiago de Compostela, Spain)
Microsoft Office 2010	Microsoft (Redmond, USA)
OriginPro 8.6 G	OriginLab Corperation (Northampton, USA)
SerialCloner 2.6.1	Franck Perez (Serial Basic)
UltraScan	(Demeler *et al*, 2010)
Databases	
BLAST	http://blast.ncbi.nlm.nih.gov/Blast.cgi
Euroscarf	http://web.uni-frankfurt.de/fb15/mikro/euroscarf/yeast.html
ExPAsy	http://expasy.org/
IUPred	http://iupred.enzim.hu/
Saccharomyces gene database	http://www.yeastgenome.org
Saccharomyces regulator database	www.yeastmine/yeastgenome.org
Wormbase	http://www.wormbase.org

4.2 Methods

4.2.1 E. coli

Cultivation and Storage

E. coli cells were cultivated in LB media. Selection was achieved by adding either 35 µg ml^{-1} kanamycin or 100 µg ml^{-1} ampicillin, depending on the plasmids resistance cassette.

Cells were incubated in liquid media or on plates at 37 °C. The cultures were inoculated with single colonies derived from LB plates and the growth is monitored at OD_{600}.

For storage 500 µl of an overnight culture is mixed with 500 µl 60% autoclaved glycerol, transferred to cryo-vials, frozen in liquid nitrogen and stored at – 80 °C.

Transformation

Chemical competent *E. coli* cells were prepared according to the following protocol (Inoue *et al*, 1990). 5 ml SOB were inoculated with *E. coli* cells and incubated over night at 37 °C. Subsequently the cells were transferred into 250 ml SOB and incubated to an OD_{600} of 0.5. After a 15 minutes cold shock the cells were harvested at 4 °C with 4000 rpm for 10 minutes. Subsequently the cells were resuspended in 80 ml ice cold TB medium and kept on ice for the following 10 minutes. The competent cells were spun down, resuspended in 20 ml TB-medium containing 14 % DMSO, aliquoted, frozen in liquid nitrogen and stored at -80°C.

100 ng DNA were added to 100 µl of the prepared competent cells and incubated for 15 minutes on ice. A subsequent heat-shock at 42 °C was performed and the cells were incubated for additional 15 minutes on ice. Subsequently the cells recovered in LB_0 at 37 °C for 45 minutes and spun down at 5000 rpm for 5 minutes. The pellet was resuspended in 100 µl LB_0 plated on $LB_{Antibiotic}$ plates. The plates were incubated over night at 37 °C.

4.2.2 S. cerevisiae

Cultivation and Storage

S. cerevisiae was cultivated in liquid cultures or on plates at 30 °C. WT and knockout library strains were cultivated in YPD. Selection of transformed yeasts was achieved using standard minimal media (SMM). The amino acid encoded on the plasmid was omitted in the amino acid mix used for the SMM media. Generally, cultures were inoculated using single colonies and cell densities were monitored at OD_{600}. 2 % (w/v) glucose was used as a carbon source if not indicated otherwise.

For storage 500 µl of a stationary culture was mixed with 500 µl 60% autoclaved glycerol, transferred in cryo-vials, frozen in liquid nitrogen and stored at -80°C.

Transformation

Transformation was performed with slight modifications according to the following protocol (Elble, 1992). For transformation 300 µl of a stationary yeast culture was spun down for 1 minute at 13 000 rpm. The supernatant was discarded and the pellet was resuspended in 150 µl PLATE mix. 40 mM DTT, 5 µg ml^{-1} salmon sperm DNA as well as 100 ng plasmid DNA were added to the transformation mixture. The cells were incubated at room temperature for 16 h and subsequently heat shocked for 1 h at 42 °C. Cells were pelleted to 1 minute at 13 000 rpm, resuspended in 50 µl autoclaved $_{dd}H_2O$ and plated on SMM plates with glass beads (4± 0.05 mm). Plates were shaken horizontally to distribute the cells evenly. If not stated otherwise cell growth was monitored after 3 days.

Cell Disruption

Mechanical disruption of 950 µl of cell suspension was achieved by adding 900 mg of 0.25–0.50 mm glass beads and subsequent shaking at 4 °C in 4 pulses of 2 min at 30 Hz in a bead mill. Cell disruption was checked microscopically.

Bradford Assay

To determine the protein concentration of cell lysates, concentrations were determined by Bradford assays. Coomassie Protein Assay Reagent was diluted according to the manufacturer's protocol and the absorption determined at 595 nm.

Fluorescence Activated Cell Sorting (FACS)

In order to dissect the yeasts ploidy status FACS analysis was executed. Therefore the cells were transformed and washed off plates with yeast preparation buffer. Cells were fixed in 70 % (v/v) ethanol overnight. Yeasts were washed with FACS assay buffer and sonicated for 30 s. Cell densities were normalized to OD_{600} 2 in 1 ml in FACS assay buffer and treated overnight with 0.25 mg ml^{-1} RNAse A at 37 °C. 1 mg ml^{-1} Proteinase K were added and incubated at 50 °C for 2 h. Cells were stained with propidium iodide at 20 µg ml^{-1} for 90 minutes and investigated in a BD FACS CANTO II. Cells were gated as shown in Figure 29 to avoid scoring cell debris. The number of events of each plot was normalized and histograms plotted logarithmically (Kaiser *et al*, 2013). No cross-talk of the aggregates YFP or CFP fluorescence is observable in the propidium iodide channel (data not shown).

In vivo NMR

To investigate phosphate levels in vivo ^{31}P NMR was performed. As ^{31}P is the most abundant stable isotope of phosphate cells no additional labelling procedure is necessary. Yeasts cells were washed off transformation plates with standard assay buffer. Several plates of Q_{56}-YFP expressing yeasts had to be harvested due to the toxicity of the construct (Kaiser *et al*, 2013). Large colonies were removed to analyze the dominant colony pattern. Cells were washed three times to remove extracellular phosphate and normalized to an OD_{600} to 300. 450 µl were transferred to 5 mm NMR tubes, 10 % D_2O was added. Cells were directly measured to avoid artefacts due to starving of the cells. The spectra were recorded using an AVANCE III 500 NMR instrument. 256 scans were assembled with 5 seconds repetition time. Spectra processing and analysis was performed using the MestReNova software. Prior to Furiertransformation the FID was multiplied with an exponential function (lb=5). The spectra were referenced to 0 ppm for external phosphoric acid (Papsdorf *et al*, 2015).

Glucose metabolism of transformed yeasts was analyzed by addition of ^{13}C labeled glucose to live yeast cells. Therefore transformed yeasts were washed off plates with standard assay buffer and washed three times to avoid external glucose. 20 mg ml^{-1} [U^{13}-C_6] glucose was added to yeast cells with an OD_{600} 150 in 500 µl. Subsequently 50 µl D_2O were added and the sample measured immediately. The metabolism of the yeasts was recorded at the same instrument as described above. ^{1}H decoupled ^{13}C spectra were recorded at intervals with 256 scans and a 5 second repetition time. Spectra were processed and analysis performed with the MestReNova software, using an exponential window function (Papsdorf et al., 2015a). Peak intensities of the different metabolites were plotted. As slight variations in glucose levels already are visible in the metabolic kinetics, one experimente is shown (Papsdorf *et al*, 2015).

Analysis of Intracellular Iron Levels via EPR

Noninvasive electro paramagnetic resonance (EPR) spectroscopy can be used to analyze the intracellular iron levels. Fe^{3+} in contrast to its reduced form Fe^{2+} can be visualized by EPR. Therefore yeast cells were washed off plates with standard assay buffer. To enable analysis of the dominant colony population, large colonies were removed from pQ56 transformed plates. Cells were resuspended in EPR buffer and incubated at 30 °C for 15 minutes. DETAPAC thereby blocks iron import, while DFO binds free iron in an EPR

detectable form (Woodmansee & Imlay, 2002). Cells were centrifuged at 4 °C, washed with standard assay buffer, centrifuged again and resuspended in 300 µl standard assay buffer supplied with 10 % glycerol. Yeast densities were normalized to an OD_{600} 300 in 200 µl, which were transferred to 4 mm quartz EPR tubes. Samples were slowly frozen on dry ice and stored at -80°C until assayed. EPR signals were scored in a JEOL JES FA 200 instrument. The spectrometer settings were adjusted as follows: temperature, -125 °C; microwave power, 10 mW; field center, 152 mT; field sweep, 100 mT; modulation amplitude, 0.25 mT; receiver gain, 1200; time constant, 0.3 s. Prior to measurement samples were stored in a dewar containing liquid nitrogen to ensure a constant temperature from sample to sample. Ferric chloride standards were prepared with DFO and EPR measurements were conducted as described above. The detected EPR signals were normalized according to the determined cell density. Based on three independent experiments the relative concentration of free iron in the yeast cells was calculated (Papsdorf *et al*, 2015).

Aconitase Activity

One of the most prominent Fe-S cluster containing enzymes of the yeast is aconitase. Aconitase catalyzes the isomerization from citrate to isocitrate in the tricarboxylic acid cycle (TCA cycle) (Beinert *et al*, 1996). In order to analyze aconitase activity in yeast lysate an aconitase acitivty assay kit was used. To enable analysis of the dominant colony population, large colonies were removed from pQ56 transformed plates. Cells were washed off plates, resuspended in aconitase assay buffer and disrupted using glass beads and a bead mill. The manufactures protocol was followed. In short cell debris were removed via centrifugation with 13300 rpm at 4 °C for 10 minutes. Isocitrate was processed to get a colorimetically detectable product at 450 nm. A standard curve was prepared using isocitrate and the activity determined according to the following equation:

$$Aconitase\ activity\ \left[\frac{mU}{mL}\right] = \frac{B * SDF}{T * V}$$

B [nmol], amount of isocitrate generated; SDF, sample dilution factor; T [min], time reaction incubated in minutes; V [ml], sample volume.

The calculated aconitase activities were normalized to the protein concentration detected by a Bradford assay (Papsdorf *et al*, 2015).

Determination of ATP-level

ATP levels of yeast cells were analyzed as described before (Yang *et al*, 2002; Gray *et al*, 2014). Slight modifications of the protocol were used, as harsher disruption methods had to be applied. Yeasts were washed off transformation plates with ATP level buffer. Several plates of Q_{56}-YFP expressing yeasts had to be harvested due to the toxicity of the construct (Kaiser *et al*, 2013). Large colonies were removed to analyze the dominant colony pattern. Cell densities were normalized to an OD_{600} of 5 and heated for 4 minutes at 95°C. Subsequently the cells were disrupted using glass beads and a bead mill as described above. After disruption cells were kept on ice and the ATP-level of the cell was analyzed using a luciferase coupled system. 60 µl of ATP pre-mix buffer was added to 60 µl of cell lysate and bioluminescence detected in a Tecan GENios microplate reader. The assay was performed at 20 °C for 60 minutes. Additionally an ATP standard curve was measured. The plateau value of the relative light units was plotted scored and the data of 5 different experiments was normalized to enable comparison between different samples.

Determination of the NADH level

NADH levels were quantified using the NAD/NADH Quantification Kit. Yeasts cells were washed off transformation plates with PBS. Several plates of Q_{56}-YFP expressing yeasts had to be harvested due to the toxicity of the construct (Kaiser *et al*, 2013). Large colonies were removed to analyze the dominant colony pattern. The assay was performed according to the manufactures protocol. In short, yeasts were resuspended in NAD/NADH extraction buffer and OD_{600} was determined. Cells were disrupted in a bead mill as described above and lysate treated according to the protocol. The total NAD/NADH levels were quantified colorimetrically at 450 nm. An NADH standard curve was prepared and the total NAD/NADH level calculated.

Extracellular Phosphatase Activity

The extracellular phosphatase activity of yeasts phosphatases can be investigated by shifting yeast cells to phosphate free media and analyze the phosphatase activity in the supernatant (Huang & O'Shea, 2005). Therefore yeasts cells were washed off transformation plates with no-phosphate media. Several plates of Q_{56}-YFP expressing yeasts had to be harvested due to the toxicity of the construct (Kaiser *et al*, 2013). Large colonies were removed to analyze the dominant colony pattern. Cells were washed twice

with no-phosphate medium and normalized to an OD_{600} of 5 in 1 ml. Yeasts were incubated at 30 °C and phosphatase activity was determined at different time points. Therefore 50 µl of the culture were added to 100 µl extracellular phosphatase assay buffer at 20 °C for 15 minutes. Afterwards 200 µl of a saturated carbonate solution was added, mixed and spun at 3000 rpm for 10 minutes. The OD_{420} of the supernatant was recorded in quarz cuvettes in a Cary 100 UV/Vis spectrometer. The extracellular phosphatase ratio is calculated according as follows: $OD_{420}/OD_{600}*1000$. Triplicates were measured and one representative experiment shown.

Mitochondrial Staining

Yeast mitochondria were stained with MitoTracker fused to rhodamine, which accumulates in mitochondria dependent on their membrane potential. Cells were washed of plates with PBS as described before and stained according to the manufactures protocol. In short 250 nM MitoTracker was added for 15 minutes to the cells. Subsequently fluorescence was examined without further fixation steps the cells using the Axiovert 200.

Microarray

Microarrays were performed by Mr. Grötzinger and Dr. Kaiser as described previously (Kaiser, 2012; Papsdorf *et al*, 2015). Analysis was performed by Dr. Richter. In short, the microarray data originated from different experimental sets. Q_0 at day 3, and Q_{56} at day 3 were processed together, likewise Q_0 at 2 and Q_{56} at day4. The data provided by the Kompetenzzentrum für Fluoreszente Bioanalytik had already been normalized within one assay set, using the multi-chip analysis (RMA) algorithm (Speed *et al*, 2003; Irizarry, 2003) and MAS5 (Pepper *et al*, 2007). To obtain relative expression differences between two samples, the MAS5 value for each gene was used, the ratio (e.g. Q_0 at day 3/Q_{56} at day 3) was calculated and the full dataset of 5900 probes sorted regarding this value. The least-affected gene should then be at position 2950 with a quotient of 1. Thus the ratio column was divided by the median value obtained from position 2950. This approach was also used in the other data sets for normalization. All ratios were then converted to logarithmic values. For the comparison of Q_0-YFP and Q_{56}-YFP samples, all possible combinations of the datasets were calculated and included. From the relative logarithmic expression differences the average expression change and the standard deviation was determined. The full set was then sorted according to this average relative expression change. Genes were

included in the final hit list, if they showed expression differences of at least threefold. Expression changes below these values were not included in the hit list (Papsdorf *et al*, 2015).

Cluster analysis

The cluster analysis was performed by Dr. Richter. All hits above noise level for either up- or down-regulation were included in the cluster analysis. To this end, the 20 highest ranking co-regulated genes for each of hit was obtained from the SPELL database, which provides this information based on the analysis of more than 10,000 microarray data sets (Hibbs *et al*, 2007). Being listed together was considered an incidence of co-regulation. A pairwise co-regulation matrix was built including the information of all the hits. This matrix was used to draw a map with the open-source software CytoScape (Saito *et al*, 2012). The layout function "Edge-weighted Spring Embedded" was used for initial visualization of the clusters and the final maps were obtained by moving the nodes to prevent graphical overlap for better visualization (Papsdorf *et al*, 2015).

Common Regulator Analysis

Numerous genes are found up and down-regulated in the microarray datasets obtained by Dr. Christoph Kaiser and analyzed by Dr. Klaus Richter (Kaiser, 2012; Papsdorf *et al*, 2015). In order to investigate if these genes share common regulators a more detailed examination was executed. Therefore the common regulators of the 72 genes up-regulated and the 76 genes down-regulated were compared to a random dataset. The 30 most prominent regulators were retrieved via yeastmine (www.yeastmine/yeastgenome.org). If a regulator was enriched to more than 33% and appeared in the up- and down-regulated section it was marked grey. These hits were named "common regulators". To analyze the specific regulation of a cluster all genes within a cluster were analyzed via yeastmine and the transcription factors which appeared more than 3 times were listed. Three random gene list of 8 genes were analyzed and standard deviations calculated.

4.2.3 C. elegans

Cultivation and Storage

C. elegans was cultured according to general handling protocols described by Sydney Brenner (Brenner, 1974). For maintenance, *C. ele*gans was cultured on NGM plates seeded

with OP50 bacteria at 20 °C. Pieces of these plates were transferred onto new NGM plates by chunking whenever necessary.

For storage freshly starved *C. elegans* were washed off plates with S buffer, transferred into a cryo-vial and incubated on ice for 15 minutes. An equal volume of soft agar freezing solution was added to the worms and subsequently the frozen to -80°C at a constant freezing rate of -1°C min^{-1}.

Backcrossing

The backcrossing of the knockout RB1301 nematodes was performed three times as described by Ahringer et al. (Ahringer, 2006).

Synchronizing

In order to investigate the development of the worm it is necessary to synchronize the developmental stages of *C. elegans*. Adult nematodes were washed off plates with M9, pelleted at 1000 rpm for 1 minute and the supernatant is discarded. Next, the pellet is resuspended in 15 ml bleaching solution and shaked for 5 minutes. The mixture was again pelleted at 1000 rpm for 1 minute and washed at least 5 times with M9 buffer. The adult worms are killed during the procedure whereas the eggs will hatch in the solution overnight and develop to L1 larvae. At this larval stage the worms development arrests until fed.

RNA Interference

RNA interference (RNAi) experiments were performed by feeding nematodes with dsRNA expressing *E. coli* HT115 strains as described before (Timmons & Fire, 1998; Kamath *et al*, 2003). The RNAi constructs directed against *dnj-12, dnj-13, dnj-19, unc-23, hsp-1* and the empty control vector L4440 were sequenced prior to transformation. Transformed bacteria are incubated in LB_{Amp} overnight at 37 °C. DsRNA expression is induced by the addition of 1 mM IPTG. After 4 h 300 µl bacteria are transferred to RNAi plates. Synchronized L1 larvae are added to the plates and investigated after 1-3 days. RNAi phenotypes were scored using a Stemi stereo microscope equipped with a SCHOTT KL1500 LCD unit.

Thrashing and Life Span Assay

Lateral swimming movements of three days old young nematodes were scored in a droplet of M9 buffer for 1 minute. To determine the average lifespan of N2 and *unc-23* mutated nematodes (ok1408) synchronized L1 larvae were cultivated on NGM/RNAi plates at 20 °C. The nematodes are transferred to new plates every second day. Absent pharyngeal pumping and no movement after touching with an eyelash were criteria for scoring dead nematodes.

Microinjection

Microinjection was performed as described by Mello and colleges (Mello *et al*, 1991). Glass needles were pulled with a Narishge needle puller and subsequently loaded with 2 µl of a 10 ng μl^{-1} concentrated DNA solution. Young adult worms were immobilized on a dry 2 % agarose injection pad in a halocarbon oil droplet. Using an Axiovert 200 inverted microscope equipped with an injection device the DNA was injected into the nematodes distal gonads. Worms were transferred to a new NGM plate and observed after 2 days for fluorescent offspring at the Leica MZ16-FA stereomicroscope.

4.2.4 Imaging

Agarose Plate Imaging

Agarose plates imaging of petri dishes to monitor the yeasts colony pattern was performed with a Canon EOS 60D digital camera on a Repro camera stand.

Low Magnification Imaging

Nematodes were observed directly in the petri dishes using a Zeiss stemi stereo microscope equipped with a Schott KL1500 LCD unit.

High Magnification Imaging

A Leica MZ16-FA stereo microscope was used for imaging and observing non fixed worms. Therefore no special mounting technique was applied. Fluorescent and bright field images of yeasts and immobilized nematodes were taken using a Zeiss Axiovert 200 inverted microscope equipped with a Hamamatsu camera C4742-95. Yeast were mounted

on a 2 % agarose SMM media pad, covered with a coverslide an observed with 63x and 100 x magnification. Worms were immobilized in a droplet of 2 mM tetramisol for at least 15 minutes and further mounted on a 2 % agarose M9 pad. Worms were covered with a cover slide and observed in a range from 20x to 100x magnification.

Confocal Microscopy

For a more detailed view on localization of fluorescent proteins, high resolution microscopy was performed using a Leica SP5 laser scanning microscope. Samples were prepared as described for the Zeiss Axiovert 200 inverted microscope. Scanning speed and laser intensity were adapted to avoid photobleaching. Gain and offset were adjusted to utilize the dynamic range of the photomultipliers. The fluorophores were exited and emission observed as described in the Table 7.

4.2.5 Molecular Biology

Polymerase Chain Reaction (PCR)

The polymerase chain reaction (PCR) was performed in order to amplify genomic DNA of *C. elegans, S. cerevisiae* or generate constructs for protein expression. GoTaq or Pfu Polymerase (Table 6) were utilized according to the manufacture's protocol in the corresponding buffers. A total concentration of 1 ng μl^{-1} template, 1 pmol μl^{-1} forward and reverse primer and 2 mM dNTPs was used. The annealing temperatures were set according to primer characteristics ranging between 50 °C and 65 °C. The amplification time was adapted according to the length of the corresponding product and the speed of the polymerase. The product was analyzed via agarose gel electrophoresis and purified with the Wizard® SV Gel and PCR Clean-Up System.

Agarose Gel Electrophoresis

1 % agarose was dissolved in TAE buffer and 0.1 ‰ Stain G was added to the solution. DNA sample buffer (10x) was added to the DNA and loaded onto the polymerized agarose gel. 1 µl mm^{-1} peqGOLD 1 kb DNA ladder was used as a standard to determine the size of the DNA sample. Electrophoretic separation was performed at 120 V for 25 minutes. Visualization of the sample was recorded in a Biometra BioDOC II.

DNA Purification and Storage

PCR products or DNA subjected to enzymatic digestion was purified using Wizard® SV Gel and PCR Clean-Up System. Separation of bacterial DNA was performed with the Wizard® *Plus* SV Miniprep DNA Purification System. After isolation the DNA diluted in nuclease free water and stored at -20°C.

Enzymatic Digestion and Ligation of DNA

Enzymes used for digestion, dephosphorylation and ligation were supplied by New England Biolabs. Vectors were digested enzymatically over night at the enzyme´s optimal temperature. Smaller DNA fragments as PCR products were digested for 3 hours. The digestion was performed in the buffer provided by the manufacturer. Vectors were dephosphorylated for 1 h at 37°C with antarctic phosphatase to avoid self-ligation. Heat inactivation was performed if possible. Alternatively the DNA was isolated via gel electrophoresis. Ligation was performed in 10 µl at 4°C overnight using T4 ligase and the corresponding buffer. A molar ration of 1:9 vector to insert were used. The reaction was transformed in *E. coli* the next day.

Determination of the DNA Concentration

The DNA concentration was measured using the NanoDrop ND-1000 spectrometer. By UV/Vis spectrometry the DNA concentration was determined at A_{260}.

DNA Sequencing

30 µl of plasmid DNA or PCR products with a concentration range between 10 and 100 ng were send to GATC (Konstanz, Germany).

4.2.6 Protein Purification and Analysis

Protein Expression in Flasks

Protein expression was carried out in the BL21-CodonPlus (DE3) strain. The plasmids listed in Table 10 were used for protein expression. 6 l LB_{Kan} where inoculated with 100 ml of an *E. coli* overnight culture. Cells were cultivated at 37 °C to an OD_{600} of 0.6-0.8. At this OD the culture is incubated for 15 minutes on ice and subsequently 1 mM IPTG was

added to start the protein expression. The culture was incubated overnight at 20 °C. Cells were harvested at RT at 5000 rpm in a Beckmann centrifuge and the pellet was resuspended in 100 ml HisTrap loading buffer. Either the resuspended pellet was directly processed or frozen in liquid nitrogen and stored at -80°C.

Protein Expression in the Fermenter

Protein expression for nematode Hsc70 was performed in the BioStat C fermenter culture of 7 liters. The fermenter media containing the 30 µg ml^{-1} Kanamycin was inoculated with 300 ml of the transformed BL21-CodonPlus (DE3). The fermenter constantly controlled O_2 content and pH. glucose levels were monitored. Feeding solution was added stepwise after the reduction of the glucose levels. At an OD_{600} of 25 the fermenter was cooled to 18°C before adding 1 mM IPTG. After 12 h expression cells were harvested at RT with 5000 rpm in a Beckman centrifuge and the pellet was stored at -80 °C. For purification 30 g pellet was thawed in HisTrap loading buffer.

Protein Purification

All nematode proteins were purified according to the following protocol. The bacterial pellet, resuspended in HisTrap loading buffer is homogenized with a Silent Crusher M and the solution processed with the cell disrupter at 1.8 bar. Two cell disruption steps were applied, separated by a sonification step. Sonification was performed on ice 5 times for 30 seconds with 30 seconds pause after each sonification step. The disrupted pellet was centrifuged at 20 000 rpm for 30 minutes at 4 °C. The supernatant was loaded in a superloop and transferred on the HisTrap column using the Äkta FPLC. The protein tagged with five histidines reversibly binds to the HisTrap column. The column with the protein bound was washed with 10 column volumes of loading buffer and 5 column volumes of 4 % elution buffer. To elute the protein an imidazole containing buffer competes with the binding of the proteins histidines to the nickel matrix. An elution step of 10 column volumes with 100 % elution buffer is applied. The relevant fractions were analyzed via SDS-Page, pooled and dialyzed in dialysis buffer overnight. In the following purification step the protein is separated according to its ionic charge. To ensure that the protein is charged before being loaded to the Resource Q/S column the pH of the puffer is adapted two units above or below the proteins pI. For proteins with a pH lower than 6 the Resource Q with a negatively charged column matrix was applied. The Resource S column was used

for proteins with a proteins pI above 6. The protein is loaded to the column and washed for 5 column volumes with ion exchange wash buffer. A gradual increase the salt concentration competes with the proteins-matrix interaction. During a 100 ml gradual elution profile from 0 to 100 % ion exchange elution buffer the protein is eluted. The relevant fraction were analyzed via SDS-PAGE and pooled. The volume was reduced to 10 ml and loaded on a Superdex column. During size exclusion chromatography proteins can be separated by size due to their retention time in the matrix. The relevant samples are analyzed via SDS-PAGE and dialyzed in dialysis buffer overnight. The clean proteins volume is reduced, aliquoted, frozen in liquid nitrogen and stored at -80°C. All columns are cleaned and stored according to the manufactures protocol.

Non tagged *homo sapiens* Hsc70 (HsHsc70) was purified as described before (Bendz *et al*, 2007). In short HsHsc70 (GeneBank accession number P08107) was produced in *E. coli*. General treatment was performed as described above and only variations named. For cell disruption the pellet was diluted in HsHsc70 purification buffer. After pellet centrifugation at 20 000 the supernatant was purified via anion exchange chromatography on a DEAE-Sepharose followed by a Resource Q and a Fluorapatite column. As a last purification step the protein was loaded on a Superdex200 and dialyzed against dialysis buffer and stored as described above

Denaturing Gel Electrophoresis (SDS-PAGE)

Proteins can be investigated regarding their purity using denaturing gel electrophoresis. Therefore 5x Laemmli was added in the appropriate amount to protein samples with a concentration of 0.5 µg μl^{-1}. The samples were boiled for 5 minutes at 95 °C and loaded onto 12.5 % SDS-Pages consisting of a stacking and a separation gel as described before (Laemmli, 1970). To monitor the size of the analyzed proteins 8 µl of the SDS-PAGE standard low weight were loaded. For gels which are further processed via western blotting Roti marker pre-stained was used. Electrophoretic separation was performed at 45 mA for 1 h in SDS running buffer. Gels were either stained with Coomassie blue or used for western blot analysis. For staining according to Fairbanks, the gel was boiled in Fairbanks A and incubated for 15 minutes. Destaining was performed using Fairbanks D until the protein fractions were visible (Fairbanks *et al*, 1968) .

Western Blot

Semi-dry western blots were performed to analyze specific proteins in yeast and worm lysate. Worms subjected to analysis were harvested from 3 NGM plates and lysed in Laemmli by a 5 minute heating step. The worm lysate was applied to SDS-PAGE and blotted subsequently. Thereby proteins separated by gel electrophoresis were blotted onto a PVDF membrane. The PVDF membrane was activated by rinsing with methanol. Further gel and filter paper were incubated in western blot transfer buffer. The components were arranged in the following order from anode to cathode: three filter paper, gel, PVDF membrane, three filter paper. Blotting was performed with 1.5 mA cm^{-2} for 1 h in a Blot device. The blot was blocked for one hour in western blot blocking buffer followed by adding a 1:100 000 dilution of the first antibody overnight. After three washing steps with PBS-T for 15 minutes the second antibody is added in a 1:50 000 dilution. It binds the Fc-part of the first antibody and is incubated with the blot for 1 h followed by three additional washing steps with PBS-T. The second antibodies Fc part is coupled to horse radish peroxidase, which is detected by the Western-Bright^{TM} system in an ImageQuant LAS4000. Detection times were adapted according to the signals intensity. All antibodies used in this work are diluted in western blot buffer (Table 8).

Mass Spectrometric Analysis

To guarantee the identity of the purified proteins mass spectrometry was applied. Therefore protein bands were isolated from SDS-PAGEs. Tryptic digestion was performed and the samples analyzed via MALDI-TOF.

Absorption Spectroscopy

Proteins absorb UV light with absorption maxima at 200 and 280 nm. The peptide backbone and aromatic amino acids are the mayor cause for these maxima. Protein concentration was determined using a NanoDrop ND1000 with 2 µl sample volume. The dialysis buffer is used as a blank. The protein concentration is calculated using lambert-beers law:

$$A = \varepsilon * c * d$$

With A is the absorption, ε the absorption coefficient in M^{-1} cm^{-1}, c the concentration in M and d the path length in cm.

Based on the amino acid composition ε is calculated with ProtParam using www.expasy.org (Gasteiger *et al*, 2005).

Circular Dichroism Spectroscopy (CD-spectroscopy)

Secondary structure elements can be characterized by using CD-spectroscopy. Thereby left and right handed circulized light is interacting differently with chiralically active chromophores of a protein. CD instruments report the difference in absorption between left and right polarized light in molar ellipticity in degreed. Far UV CD spectra thereby provides information about the proteins secondary structure (Kelly *et al*, 2005). Protein samples are dialyzed in CD buffer with a concentration of 0.2 mg ml^{-1}. Measurements were performed in a 0.1 cm quartz cuvette in a thermostated holder on a Jasco J-710. Spectra were measured with 10 accumulations and the molar ellipticity θMRW was determined using the following equation:

$$\theta_{MRW} \frac{\theta * 100}{c * d * N_{Amino\ acid}}$$

θ is the observed ellipticity in degrees, d is the path length in cm, c is the protein concentration in mM and $N_{Amino\ acid}$ the number of amino acids in the respective protein. Temperature transitions were normalized for a better comparability.

Thermal Stability Assay (TSA)

Besides CD-spectroscopy the TSA assay is another method to determine protein stability. In contrast to CD-spectroscopy not the change in secondary but the change tertiary structure is observed. By monitoring the fluorescence of SYPRO Orange (1:5000 v/v dilution, Table) the melting curve of the protein is analyzed. SYPRO Orange binds to hydrophobic patches and fluorescence is increased upon unfolding of the protein. The assay is performed in 96 well format with a sample volume of 20 µl. 0.2 mg ml^{-1} proteins are applied and measured in triplicates (Sun *et al*, 2012; Papsdorf *et al*, 2014). The samples are heated from 20 to 95 °C with a heating rate of 0.5 °C min^{-1}.

Steady state ATPase activity

Several chaperones are known to use the hydrolysis of ATP to trigger conformational changes and client folding. Here the ATPase activity is observed with an enzyme-coupled

system as described before (Ali, Jackson, Howells, & Maxwell, 1993; Sun et al., 2012). In short, the ATPase hydrolyzes one molecule of ATP to ADP. ADP is used by the pyruvate kinase to catalyze the reaction from phosphoenolpyruvate to pyruvate. Next, lactatdehydrogenase catalyzes the reaction from pyruvate to lactate whereby NADH is transformed to NAD^+. The last step can be visualized by measuring the absorption at 340 nm. The assay was measured in standard assay buffer and the different components listed in the ATPase pre-mix buffer (Table 3). The reaction was started by adding 2 µM ATP. Measurements were performed at 340 nm, at 25 °C, in quartz cuvettes in a Cary100 UV/Vis spectrometer. The ATPase activity was calculated as follows:

$$Activity = \frac{\frac{\Delta A_{340}}{\Delta t} - \frac{\Delta A_{340}}{\Delta t} background}{\varepsilon_{NADH} * c_{ATPase}}$$

A is the ATPase activity per minute $\frac{\Delta A_{340}}{\Delta t}$ *is the slope after addition of ATP,* $\frac{\Delta A_{340}}{\Delta t} background$ *is the slope before addition of ATP,* ε_{NADH}*the extinction coefficient of NADH and* c_{ATPase}*the concentration of the ATPase.*

If not indicated otherwise the following protein concentration were used. For the activity determination without J-domain containing proteins 3 µM Hsc70 and 5 µM NEF (BAG-1 or UNC-23 and the corresponding fragments) were used. The titration assays were performed with 3.2 µM Hsc70 and 0.8 µM of DNJ-12 or DNJ-13. If the cofactors were titrated the activities were used to calculate the K_D according to the following equation:

$$v = v_0 + (v_{max} - v_0) * \frac{L_{tot}}{L_{tot} + K_D}$$

Simple substoichiometric binding model. v = turnover rate, v0 = initial turnover rate, vMax =maximum turnover rate, Ltot = absolute concentration of the binding partner, KD = apparent dissociation constant according (Li *et al*, 2013).

High Throughput Steady state ATPase Measurement

In order to modify Hsc70s activity a 10 000 substance library was screened for Hsc70 ATPase activity modulators in cooperation with Max Planck Institute Research Unit for Enzymology and Protein Folding (Halle/Saale, Germany). The described ATPase assay was used with slight modifications. The assay setup was measured in a 96 well format and modulators were added to a concentration of 500 µg ml^{-1}. The reaction was performed in standard assay buffer and the reaction was started by the addition of 500 nM ATP.

Measurements were performed at 25 °C at 340 nm in an *EnVision Xcite* Multilabel Plate Reader.

Luciferase Refolding

In presence of certain cofactors Hsc70 is capable of refolding chemically denatured luciferase (Sun *et al*, 2012; Papsdorf *et al*, 2014). 10 µM of recombinant luciferase was denatured at RT for 45 minutes. The denatured luciferase was diluted 1:125 in luminescence buffer. Luminescence was scored at RT for 60 minutes in white 96 well LIA plates in a Tecan GENios microplate reader. 3.2 µM CeHsc70 and 0.8 µM DNJ-13 were used and different NEF added. Plateau values of luciferase activities were scored to obtain refolding yields and plotted against the NEF concentrations.

Cross-link Experiments

To analyze the interaction of proteins crosslink experiments were performed. Therefore the compound D6/H6-Disulfo-succinimidylglutarat (D6/H6-DSSG) is used. It carries two functional amine-reactive groups and either 6 protons or 6 deuterium atoms, which enables mass spectrometric identification. A 50 fold molar excess of the cross-linker was used according to the manufactures protocol (Seebacher *et al*, 2006; Green *et al*, 2001; Schilling *et al*, 2003). To a 10 µM protein solution 50 µM cross-linker was added and incubated for either 1 or 5 minutes. The reaction was performed in the standard assay buffer and stopped with 1 M TRIS/HCl pH 8.0. Subsequently the samples were analyzed on a SDS-PAGE.

Analytical Ultracentrifugation

If the protein binding was observed by cross-link experiments, a more detailed analysis was performed using analytical ultracentrifugation coupled with fluorescence detection. The Δ258-UNC-23 was labeled randomly at its lysine residues with 5- (and 6-) carboxyfluorescein succinimidylester (Papsdorf *et al*, 2014). BAG-1 was labeled at its introduced cysteine at position 7 with Alexa Fluor 488 C_5-maleimid. Proteins were added to the labeled cofactors as described in the figure legends. Labeled proteins are marked by a star.

Sedimentation properties of *BAG-1 and *Δ258-UNC-23 were analyzed in the presence of different Hsc70 concentrations to analyze binding affinity. Therefore the weight average

sedimentation coefficient was used, which is calculated from sedimentation coefficients and the concentration of each species in the solution. The coefficient was received from analysis of the sedimentation velocity using the C(s) module of UltraScanII (Demeler *et al*, 2010). For comparability reasons the coefficient is normalized. These weight average sedimentation coefficients can be used for K_D calculations (Dam & Schuck, 2005). Oligomerization of unlabeled UNC-23 fragments was analyzed in a XL-A analytical ultracentrifuge and listed in Table 14. The UV detection system was used at 280 nm to inspect the sedimentation of the fragments. Data analysis of sedimentation velocity experiments was performed using the C(s)-analysis tool of the UltraScanII software. Sedimentation coefficients (s20,w), diffusion coefficients (D20,w) and molar masses were obtained from this analysis (Dam & Schuck, 2005; Stafford, 1994).

4.2.7 Statistical Analysis

Statistical analysis was performed by either using a double paired t-test or a Mann-Whitney test with the OriginPro 8.6 software.

4.2.8 Data Acquisition

All activity measurements were performed at least in duplicates if not stated otherwise. *In vivo* measurements were recorded in triplicates.

5. Results

5.1 The Balanced Regulation of Hsc70 by UNC-23 and DNJ-13 is Required for Muscle Functionality[1]

Hsc70 activity is regulated by two classes of proteins: the NEFs and the J-domain/Hsp40 proteins (Mayer & Bukau, 2005). The knockout of *unc-23*, encoding a BAG-domain containing protein, reveals a strong muscular phenotype in *C. elegans* (Waterston *et al*, 1980). In this thesis the structure of UNC-23 together with its domain composition and its role in Hsc70 binding and regulation was analyzed. The Hsc70 system was further studied with respect to muscular functionality in connection with other cofactors such as Hsp40.

5.1.1 UNC-23 Contains a Disordered N-terminal Domain with PXXP Motifs

In *C. elegans* two cytosolic BAG proteins, BAG-1 and UNC-23, were found using the HMMER3-based algorithm with known human and nematode BAG proteins as a starting set (Eddy, 2009; Papsdorf *et al*, 2014). BAG-1 consists of an N-terminal BAG-domain with an amino acid identity of 30 % compared to the human homolog. Additionally it possesses a C-terminal ubiquitin domain. The nematode protein was shown to interact with components of the ubiquitin pathway (Li *et al*, 2004). The second BAG protein detected, UNC-23, contains an N-terminal BAG-domain and a long C-terminal tail (Figure 6A and B). The BAG-domain of UNC-23 shares a 40 % amino acid identity with its human homolog Bag2 (Figure 6A). Surprisingly, the long C-terminal tail is absent in its assigned human homolog. This tail consists of 9 PXXP motifs, two polyglutamine rich regions and various phenylalanine/proline (F/P) repeats (Figure 6A and B). PXXP motifs can be found in other human BAG proteins such as Bag3 and Bag4, but with lower homology within the BAG domain. PXXP sequences are known to interact with SH3 motifs (Lee *et al*, 1996; Feller *et al*, 1994). Thus UNC-23 possibly represents a protein which combines features of the different human BAG proteins Bag2, Bag3 and Bag4.

[1] This chapter is published in the *Journal of Biological Chemistry* (Papsdorf *et al*, 2014)

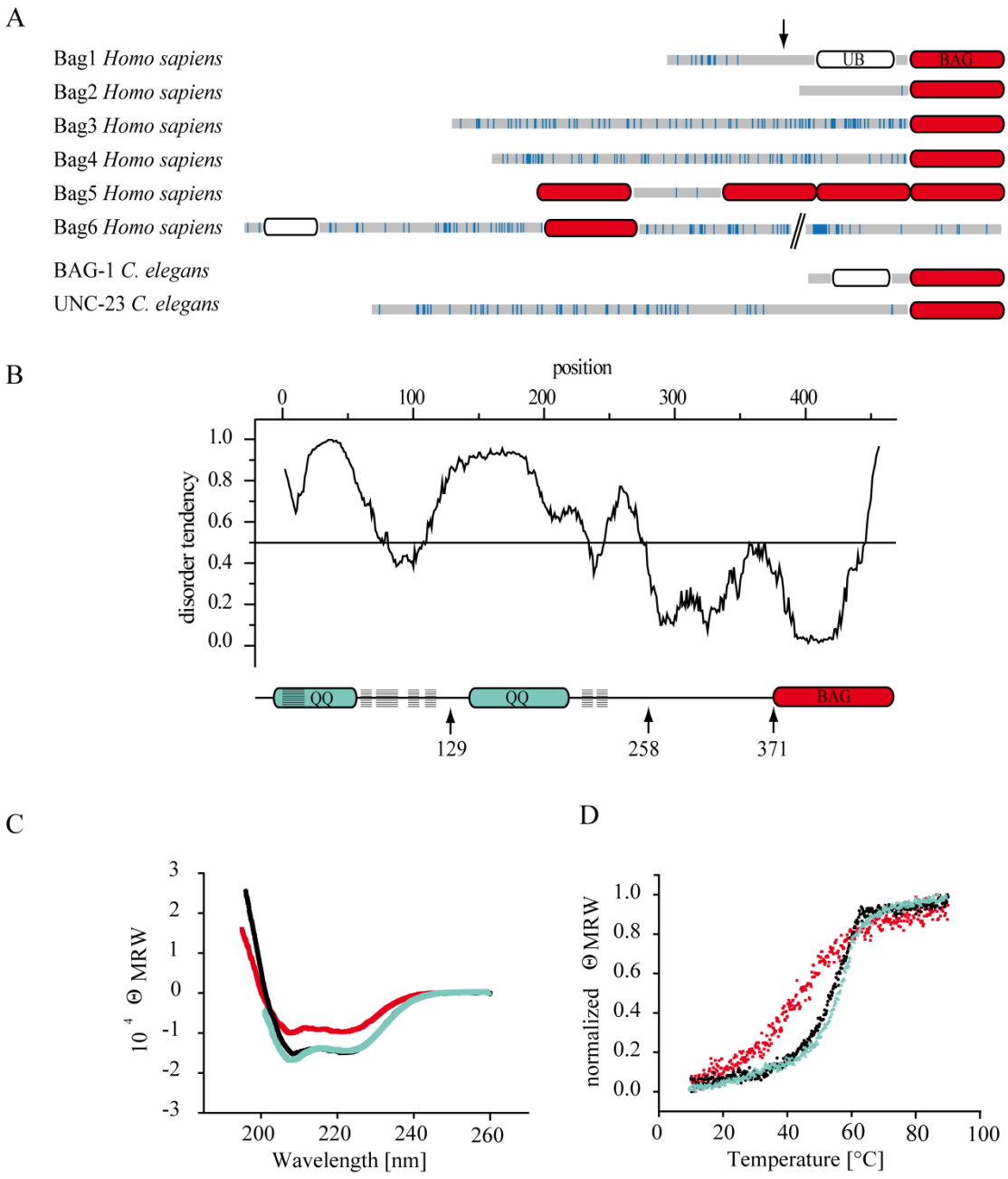

Figure 6 Characterization of BAG-proteins. A: Domain composition of C. elegans and Homo sapiens BAG-domain containing proteins. The BAG-domain (BAG) is depicted in red, the ubiquitin domain (UB) in white. Proline residues are highlighted by blue bars. The arrow indicates the length of the human Bag1S splicing isoform. B: IUPred intrinsically unstructured domain search and correspondingly designed UNC-23 protein fragments. Numbers mark the truncation points starting from the N-terminus. Polyglutamine regions are depicted in green, PXXP motives represented by stripes and the BAG-domain is highlighted in red. C: Circular dichroism spectra of the three truncation fragments Δ371-UNC-23 (red), Δ258-UNC-23 (black) and Δ129-UNC-23 (blue). D: Thermal transitions of Δ371-UNC-23 (red square), Δ258-UNC-23 (black circle) and Δ129-UNC-23 (blue triangle) as measured by circular dichroism at 222 nm. Starting values were normalized for better comparability.

Table 14 Characteristics of different UNC-23 truncation fragments. Values were obtained by protein expression, CD thermal transitions to determine the melting temperature T_m, analytical ultracentrifugation to analyze the sedimentation coefficient $s_{20,w}$, the molecular mass MW_{UC} and the K_D. Mass spectrometry was used to analyze the molecular mass MW_{MS}. Evaluation of ATPase assays of the Hsc70/DNJ-12 and Hsc70/DNJ-13 system were used to determine the $K_{D,app}$. Data was analyzed as described in the materials and methods section. The standard error is given (s.e.m.). Values for BAG-1 are obtained from Sun et al. (Sun *et al*, 2012). *ND: not determined.*

	Expression	T_m [°C]	$s_{20,w}$ [S]	$D_{20,w}$ [m^2s^{-1}]	MW_{UC} [kDa]	MW_{MS} [kDa]	$K_{D,app}$ 12 [µM]	$K_{D,app}$ 13 [µM]	$K_{D,UC}$ [µM]
UNC-23	---								
Δ129-UNC-	+	56	3.17 ± 0.19	$4.04 * 10^{-7}$ ± $0.5 * 10^{-7}$	68.8 ± 9.9	39.438	6.84 ± 3.9	ND	ND
Δ258-UNC-	+++	55	3.01 ± 0.12	$4.5 * 10^{-7}$ ± $0.6 * 10^{-7}$	57.9 ± 7.3	24.921	15.06 ± 6.0	ND	0.5 ± 0.4
Δ371-UNC-	+	46	2.92 ± 0.1	$11.0 * 10^{-7}$ ± $0.6 * 10^{-7}$	23.2 ± 1.45	11.964	138 ± 23.4	ND	ND
BAG-1	+++	ND	2.1 ± 0.4	$7.36*10^{-7}$ ±$1.5*10^{-7}$	23.5	24.0102	0.39 ± 0.12	1.35 ± 0.48	0.02 ± 0.02

The unusual N-terminal tail of UNC-23 is thought to be regulated via three different splicing isoforms H14N18.1a-c with a protein length of 458, 399 and 457 amino acids. The cDNA obtained by OpenBiosystems encodes the splicing variant H14N18.1 c suggesting that this is the relevant isoform *in vivo*. To analyze the structural organization of the N-terminal tail in UNC-23 an unstructured domain search with the IUPred algorithm was performed (Dosztányi *et al*, 2005). This algorithm is based on the possibility of neighboring amino acids to form stable interactions with their partner (Dosztányi *et al*, 2005). It revealed a high tendency of the N-terminus to be unstructured while the C-terminus with the BAG-domain was predicted to be folded (Figure 6).

To investigate the domains and their functions experimentally, three truncation constructs at position 129, 258 and 371 were designed. The fragment corresponding to the human homolog Bag2 expressed stably. Thus the presence of polyglutamine rich regions and PXXP motifs reduces the expression of the protein. The full length protein could not be expressed in a sufficient amount. Nevertheless the fragment containing half of the N-terminal tail Δ129-UNC-23 was isolated and purified to an adequate yield. The structure and stability of all three truncations was compared by CD spectroscopy. The secondary structure content was inspected with far UV light CD spectroscopy. A similar α-helical

content was detectable in Δ129- and Δ258-UNC-23 (Figure 6C). This implies secondary structural elements within amino acids 129-258. Thermal transitions showed a similar melting temperature for Δ129- and Δ258-UNC-23. Unfolding midpoints were detected at 55 °C for Δ258-UNC-23 and 56 °C for Δ129-UNC-23 (Figure 6D, Table 14). This indicates that the presence of the extended N-terminal domain does not influence the overall stability of the protein. Analyzing the isolated BAG-domain Δ371-UNC-23 a reduced α-helical content and decreased thermal stability was found (Figure 6). Hence the amino acids 258 until 371 contribute structure and stability to the BAG-domain and may form an interdependent structure. Nevertheless all fragments are stable at the experimental conditions from 20 to 25 °C.

5.1.2 UNC-23 Mutated Nematodes Show Severe Muscular Deficiencies

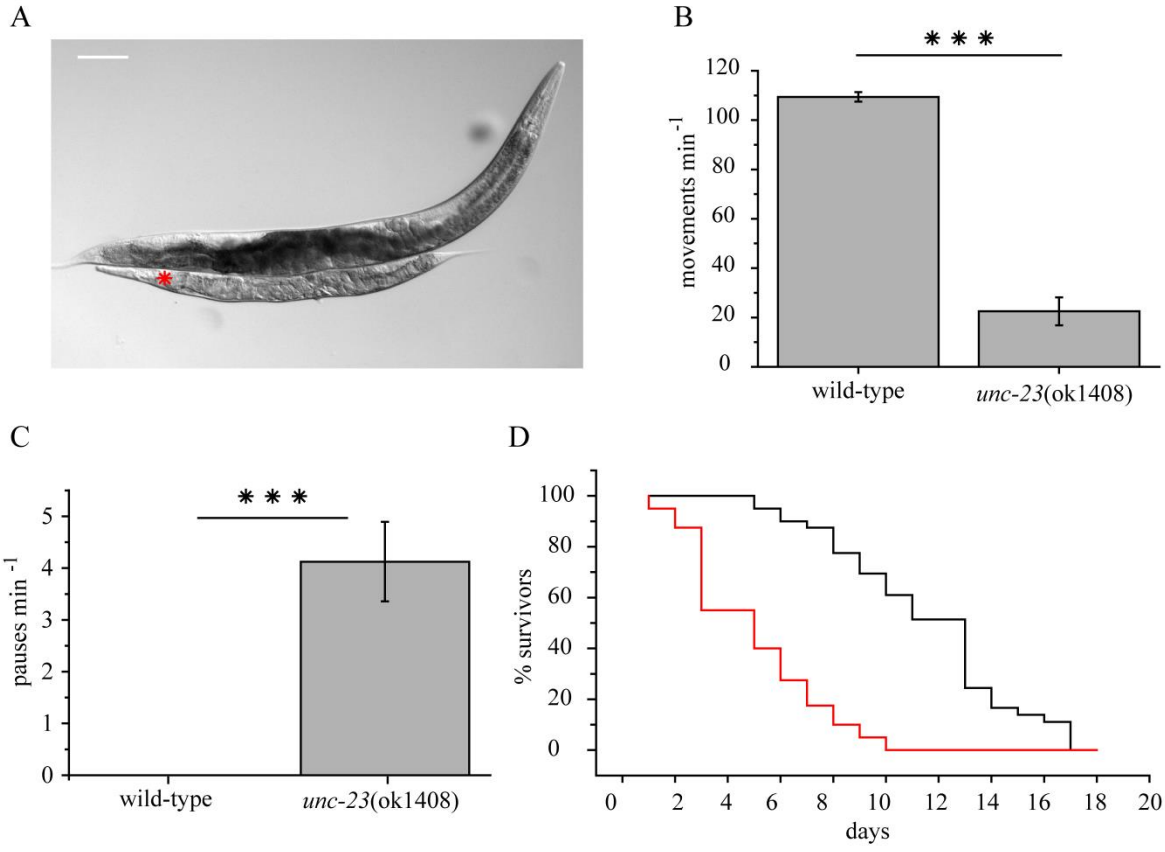

Figure 7 Unc-23 mutated nematodes exhibit a strong muscular phenotype. A: N2 nematode compared to an unc-23 (ok1408) mutated worm (red star). Scale Bar: 100 µm. B: Thrashing assay of three days old young wild-type and unc-23 mutated nematodes. Means with standard errors (s.e.m.) are plotted. Statistical analysis was performed with the Mann-Whitney Test. Significance is indicated by three stars $p=2.38*10^{-6} < \alpha=0.001$. C: Irregularities in pharyngeal pumping monitored in three days old young adult wild-type and unc-23 mutated nematodes. Means with standard errors (s.e.m.) are plotted. Statistical analysis was performed with the Mann-Whitney Test. Significance is indicated by three stars $p=3.22*10^{-6} < \alpha=0.001$. Kaplan Meyer plot of life span assay of wild-type (black) and unc-23 mutated (red) nematodes. All assays were performed with at least 10 animals.

Different mutations in *unc-23* were found in the late 80ies and a detailed characterization of those strains exists (Waterston *et al*, 1980). If *unc-23* is mutated in *C. elegans* the nematodes are reduced in size and exhibit a strong muscular phenotype coinciding with a head-bent phenotype (Plenefisch *et al*, 2000; Waterston *et al*, 1980). The OMRF Knockout Group provides a strain with a large deletion within the *unc-23* gene named RB1301 (ok1408). All studies in this thesis were performed on a backcrossed RB1301 strain. These nematodes are smaller, thinner and more translucent compared to wild-type animals as shown in Figure 7A (Waterston *et al*, 1980; Plenefisch *et al*, 2000). *Unc-23* mutated worms show an impaired muscular function, which worsens during development including the head-bent phenotype present in other *unc-23* mutations (Waterston *et al*, 1980; Rahmani, 2002; Rahmani *et al*, 2015) (Figure 7A). This strong phenotype can be scored by lateral swimming movements. Three days old young adult wild-type nematodes swam with about 100 strokes min^{-1} whereas *unc-23* mutated worms only stroked 20 times min^{-1} (Figure 7B). Additional irregularities in pharyngeal pumping with up to 4 pauses min^{-1} during normally regular swallowing movements were observed (Figure 7C). Ultimately these significant impairments in muscular functions culminate in a decreased life span from an average of 12 days in N2 nematodes to 5 days in *unc-23* mutated nematodes (Figure 7D).

5.1.3 Muscular Expression Pattern of UNC-23 and CeHsc70

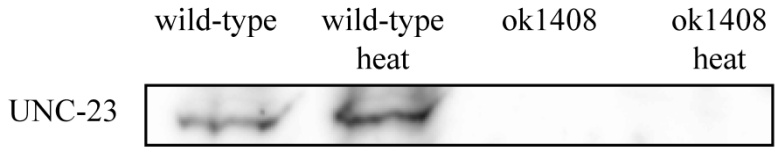

Figure 8 Western blotting of UNC-23 with the polyclonal antibody against UNC-23 derived in rabbit. Nematodes were harvested from plates after normal growth conditions and 1 hour heat-shock at 30 °C. Wild-type (N2) and unc-23 mutated nematodes (ok1408) were subjected to analysis.

The UNC-23 protein can be visualized in wild-type nematodes by western blotting (Figure 8). UNC-23 is up-regulated during 1 hour of heat-shock at 30 °C. This is in agreement with data published with a 5 fold up-regulation of UNC-23 during heat-shock (Guhathakurta *et al*, 2002). As a control *unc-23* mutated nematodes were analyzed. No signal is observed at

the corresponding UNC-23 band (Figure 8). Hence UNC-23 is absent in the *unc-23* mutated strain.

To address the role of UNC-23 in the living nematode further, its tissue specific expression was investigated. Therefore transgenic wild-type nematodes expressing YFP controlled by the *unc-23* promoter (*unc-23*::YFP) were generated.

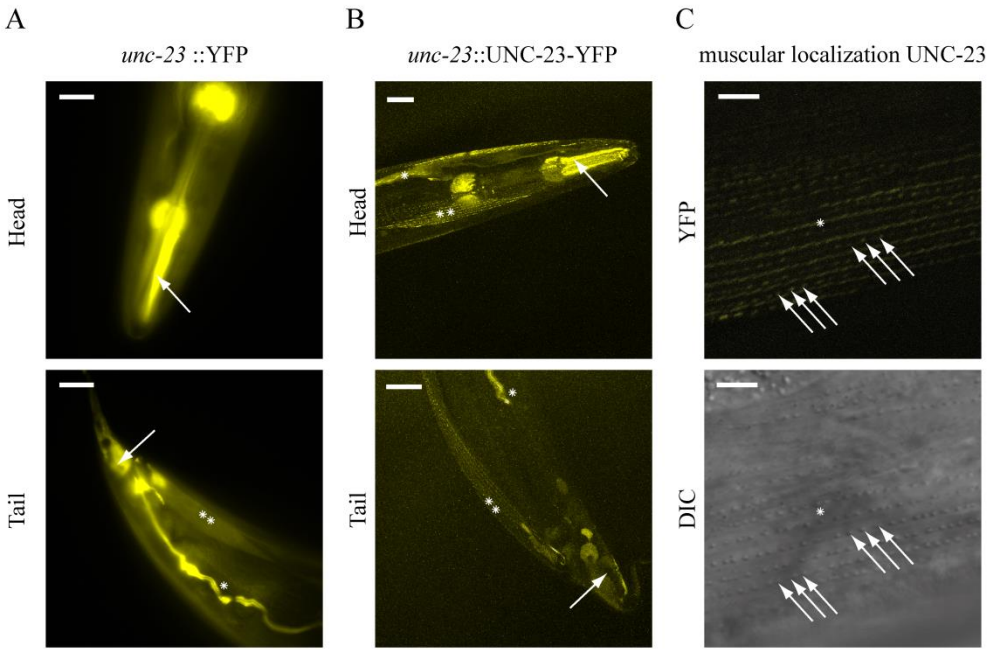

Figure 9 UNC-23 is ubiquitously expressed in C. elegans. Transgenic modified wild-type nematodes expressing different constructs. A: Expression pattern of YFP under the control of the unc-23 promoter (unc-23::YFP). Head of the nematode with a strong fluorescence in the pharyngeal muscle cell (arrow) and the bulb. Nematode tail with a strong fluorescence in the anal depressor cell (arrow), the excretory channel (star), and the body wall muscles (two stars). B: Expression pattern of UNC-23 fused to YFP under the control of the unc-23 promoter (unc-23::UNC-23-YFP). Nematode head with a strong fluorescence in the pharyngeal muscle cell (arrow), the excretory channel (star) and the body wall muscles (two stars). Nematode tail with a strong fluorescence in the anal depressor cell (arrow), the excretory channel (star), and the body wall muscles (two stars).C: A more detailed look on the basallamina side of the muscle cell. The dense bodies are visible in the DIC image highlighted by arrows. The star indicates the M-line. Scale bar represents 5 µm. n= 14.

Under normal growth conditions the *unc-23* promoter was active in the pharyngeal non-striated muscle cells and in the somatic striated body wall muscles (Figure 9A). A strong expression was observed additionally in the anal depressor cell and in the excretory channel. Further, UNC-23 was fused to YFP controlled by the endogenous *unc-23* promoter (*unc-23*::UNC-23-YFP) to investigate the exact localization of UNC-23-YFP. Upon injection the progeny showed fluorescence in the same tissues as the isolated promoter (Figure 9B). A more detailed look on the muscular localization of UNC-23 was achieved with confocal microscopy. Dense bodies are muscular attachment structures, which are clearly visible in the DIC image and were used as a marker in the muscle cell

(Waterston *et al*, 1980). UNC-23 localized with the dense bodies and was additionally observed in the M-lines of muscular ultrastructure shown in Figure 9C (Gaiser *et al*, 2011; Waterston *et al*, 1980; Papsdorf *et al*, 2014). No stable line could be obtained for this construct, however this pattern was constantly observed in all fluorescent progeny.

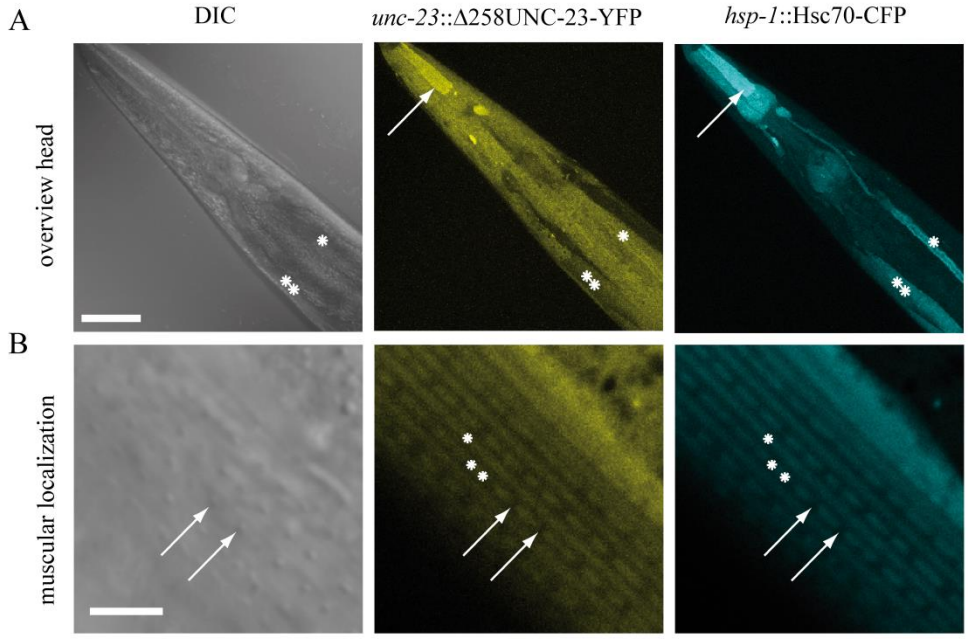

Figure 10 Transgenic wild-type nematodes expressing Δ258-UNC-23-YFP controlled by the unc-23 promoter (unc-23::Δ258-UNC-23-YFP) and Hsc70-CFP under the hsp-1 promoter (hsp1::Hsc70-CFP). A: Tissues expressing the corresponding fusion proteins. Fluorescence of both proteins can be observed in the pharynx (arrow), the excretory channel (star) and the body wall muscles (two stars). Δ258 UNC-23-YFP can be additionally observed in the intestine. Scale bar: 40 µM. B: Detailed look on basallamina side of body wall muscles. No localization to the dense bodies of Δ258-UNC-23-YFP or Hsc70-CFP is detectable (arrow). Δ258-UNC-23-YFP and Hsc70-CFP show a diffuse localization to the M- (star) and the I-band (two stars). Scale bar: 5µM.

Next, the fragment Δ258-UNC-23 corresponding to the human Bag2 was analyzed regarding its localization. Fused to YFP with the *unc-23* promoter (*unc-23*::Δ258-UNC-23-YFP), the fragment showed expression in the same tissues as the full-length fragment such as in the pharyngeal muscles, the excretory channel and the body wall muscles (Figure 10A). Having a closer look on the muscular ultrastructure a large difference in localization became evident. Strikingly, the fragment was completely absent from the dense body ultrastructure but enriched in the space in between the dense bodies (Figure 10B). Hence the correct localization of UNC-23 to the dense body ultrastructure requires the full length N-terminus.

With respect to UNC-23´s potential interaction with Hsc70, Hsc70-CFP was coinjected in nematodes. During these injections it became evident that transgenic nematodes with

Hsc70-CFP exhibit a similar head-bent phenotype as the *unc-23* mutated nematodes (Figure 11A). In 40 % of the F1 progeny expressing solely Hsc70-CFP the phenotype was elicited (Figure 11B). This strongly suggests that de-regulation of Hsc70 can develop a harmful gain of function phenotype, indicating that changes within the Hsc70 system lead to weakened attachment structures in the sensitive muscular homeostasis.

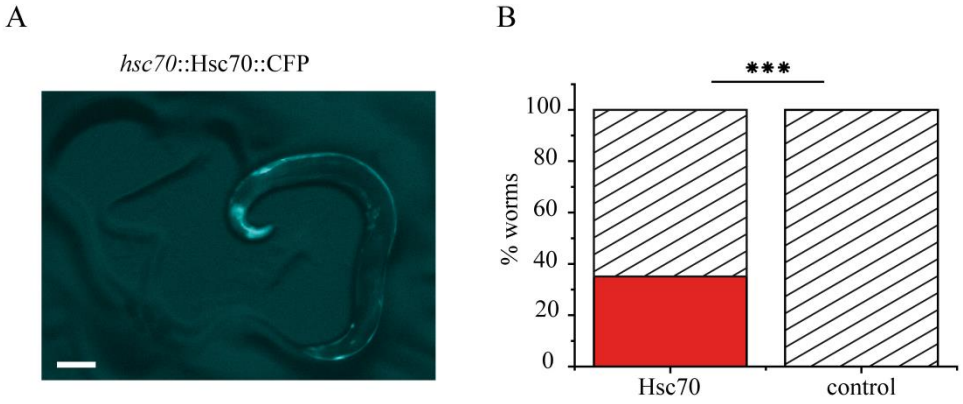

Figure 11 Nematodes expressing solely Hsc70-CFP under the control of the endogenous hsp-1 promoter (hsp1::Hsc70-CFP). A: The head-bent phenotype in the F1 progeny. Scale bar 100 µM. B: Quantification of the F1 progeny possessing the phenotype (red) compared to the control (C34B2.5::CFP). Statistical analysis was performed with the Mann-Whitney-Test: $p=1.5*10^{-9}<\alpha=0.001$. Statistical significance is indicated by three stars.

5.1.4 UNC-23 Binds to Hsc70 with its BAG-domain

Having seen changes in localization of the UNC-23 constructs *in vivo* the binding to Hsc70 was characterized next. As UNC-23 possesses a BAG-domain the binding to Hsc70 was analyzed by investigating the purified proteins. As a first approach a cross-link experiment was carried out and binding of Δ258-UNC-23 to Hsc70 was analyzed by SDS-PAGE (Figure 12A). Δ258-UNC-23 was able to form dimers upon cross-linker addition. Addition of Hsc70 to Δ258-UNC-23 resulted in oligomer formation in presence of the cross-linker. This data is in agreement with earlier yeast two-hybrid studies (Rahmani, 2002). The interaction was further characterized by investigating the sedimentation properties of fluorescently labeled *Δ258-UNC-23 in the presence of Hsc70 (Figure 12B). The labeled *Δ258-UNC-23 sedimented with the same sedimentation properties of 3.3 S as the unlabeled protein Δ258-UNC-23 (Table 14). Thus, dimer formation of *Δ258-UNC-23 is still possible after the labeling reaction. Adding Hsc70 to *Δ258-UNC-23 resulted in complex formation with a sedimentation coefficient of 6.1 S. As a control nematode Hsp110 (C30C11.4), a distant homolog of Hsc70, was added to *Δ258-UNC-23. Hsp110 itself is a cochaperone for Hsc70 which facilitates nucleotide exchange. Here no complex

formation was observable and no increased S values were detectable suggesting that UNC-23 does not bind to Hsp110.

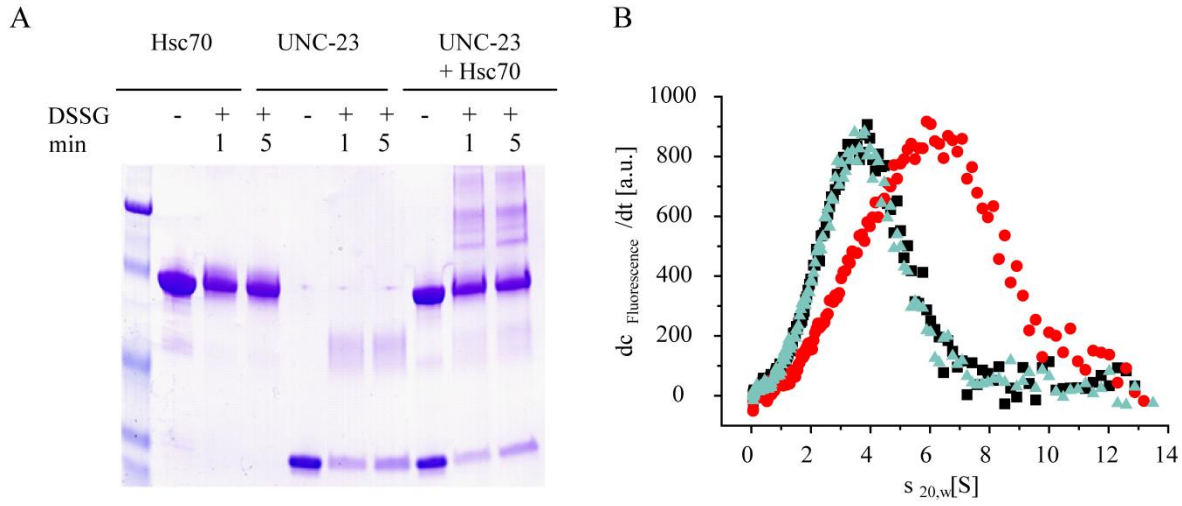

*Figure 12 UNC-23 binds Hsc70 in vitro. A: Cross-linking experiments performed with DSSG. Samples were taken after 1 and 5 minutes. Experiments were performed with either Δ258-UNC-23 or Hsc70 alone or both proteins in combination. B: dc/dt profiles of velocity sedimentation of 3 µM labelled *Δ258-UNC-23 alone (black square), in presence of 5 µM Hsc70 (red circle) or 5 µM Hsp110 (cyan triangle).The assay was carried out in standard assay buffer.*

BAG proteins are NEFs for Hsc70. To investigate the effect of nucleotides on the Hsc70/*Δ258-UNC-23 complex, different nucleotides were added to the sedimentation experiment (Figure 13A). ATP as well as ADP competed with *Δ258-UNC-23 for binding to Hsc70 (Figure 13A). This replacement was confirmed in the absence of $MgCl_2$ highlighting the possibility of Hsc70 to bind nucleotides independently of $MgCl_2$. Thus the complex of *Δ258-UNC-23 and Hsc70 dissociates in the presence of nucleotides. Next, the competition between *Δ258-UNC-23 and the Hsp40 proteins DNJ-12 and DNJ-13 for Hsc70 binding was tested. Here neither of the two Hsp40 proteins was able to replace *Δ258-UNC-23 from the Hsc70 chaperone (Figure 13B). This is in agreement with the finding that Hsp40 proteins require ATP for Hsc70 binding (Laufen *et al*, 1999). Lastly, different NEFs were tested with respect to their ability to replace *Δ258-UNC-23 from Hsc70. Unlabeled UNC-23 fragments were not able to disturb the complex (Figure 13C). The ability to disrupt the complex could not be realized by the smallest fragment Δ371-UNC-23. Only partial displacement of *Δ258-UNC-23 from the Hsc70 complex was achieved by the other UNC-23 fragments Δ258-UNC-23 and Δ128-UNC-23. BAG-1 was the only NEF which efficiently interfered with *Δ258-UNC-23´s binding to Hsc70 (Figure 13C). To prove the weaker affinity of *Δ258-UNC-23 to Hsc70 compared to BAG-1

average sedimentation velocity experiments were implemented, titrating Hsc70 to the respective cofactor. Here it became evident that BAG-1 binds Hsc70 with a much higher affinity than UNC-23 (Figure 13D, Table 14).

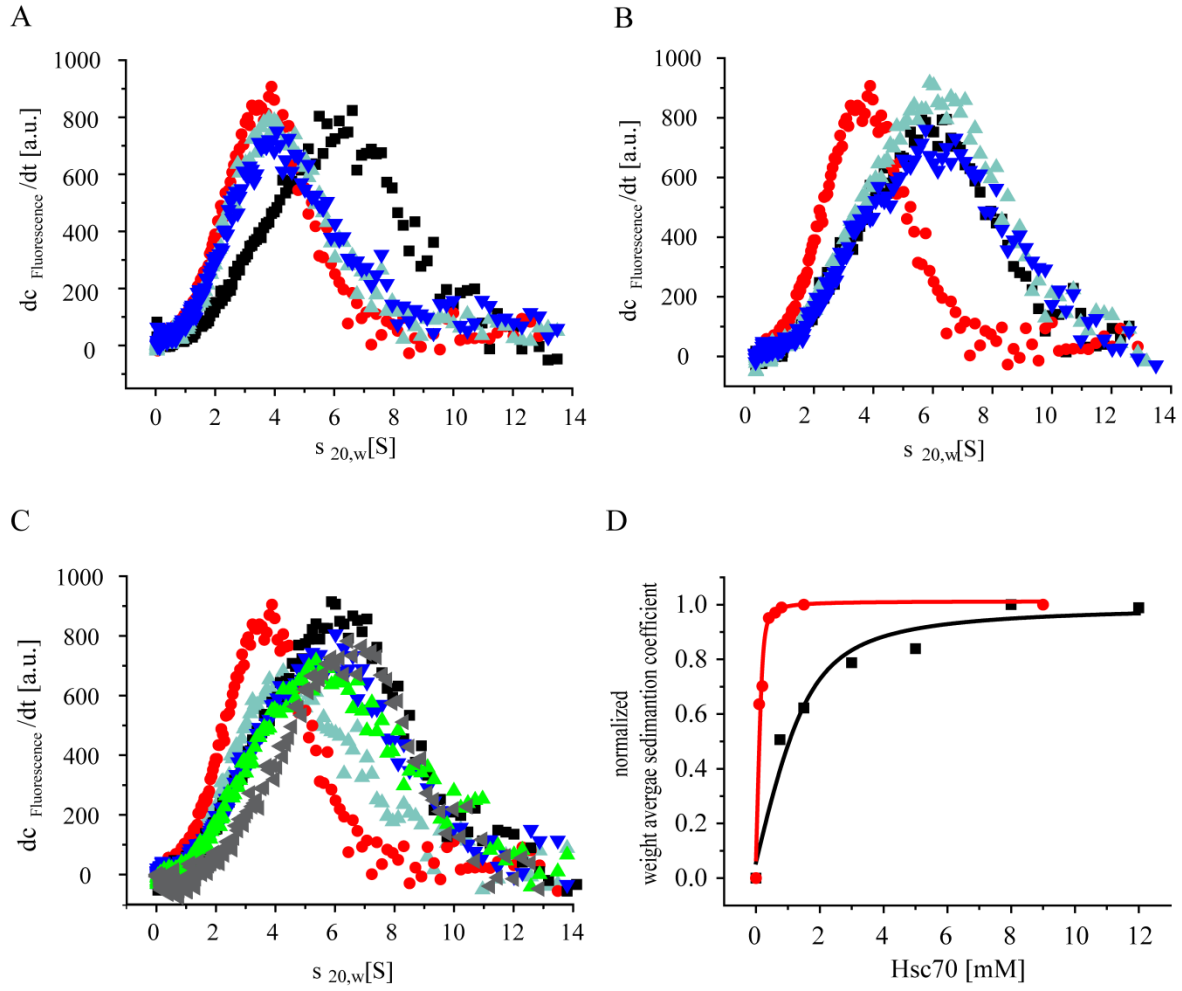

*Figure 13 Characterization of Δ258-UNC-23 Hsc70 interaction. A: dc/dt profiles of velocity sedimentation of labelled *Δ258-UNC-23 alone (red circle), in presence of Hsc70 (black square). Sedimentation profile of the *Δ258-UNC-23/Hsc70 complex upon addition of ATP (cyan triangle) or ADP (blue triangle). B: dc/dt velocity sedimentation profiles of *Δ258-UNC-23 alone (red circle) or in presence of Hsc70 (black square). Sedimentation profile of the *Δ258-UNC-23/Hsc70 complex in presence of DNJ-12 (cyan triangle) or DNJ-13 (blue triangle). C: Competitional binding of NEFs to the *Δ258-UNC-23/Hsc70 complex. *Δ258-UNC-23 alone (red circle) and in presence of Hsc70 (black square). Complex of Hsc70 and *Δ258-UNC-23 upon addition of BAG-1 (cyan triangle); Δ129-UNC-23 (blue triangle), Δ258-UNC-23 (green triangle) or Δ371-UNC-23 (grey triangle). D: Affinity of the two NEFs BAG-1 (red circle) and Δ258-UNC-23 (black square) to Hsc70. Weight averaged sedimentation coefficients were normalized and plotted against Hsc70 concentrations.*

5.1.5 Hsp40s Cooperate with UNC-23

Having characterized the binding of UNC-23 to Hsc70, the focus was set on the effect of UNC-23 on Hsc70s ATPase activity. The addition of the NEF BAG-1 resulted in the highest stimulation of Hsc70 steady state ATPase activity (Figure 14A). The stimulation of

the three UNC-23 fragments was very weak (Figure 14A). Previously it was shown that BAG proteins can stimulate Hsc70´s ATPase activity several fold in cooperation with Hsp40 proteins (Höhfeld & Jentsch, 1997). For the nematode BAG-1 this cooperativity became visible in the Hsc70/Hsp40 system (Sun *et al*, 2012). Thus, it was tested whether the stimulation is also a feature of UNC-23 (Figure 14B and C).

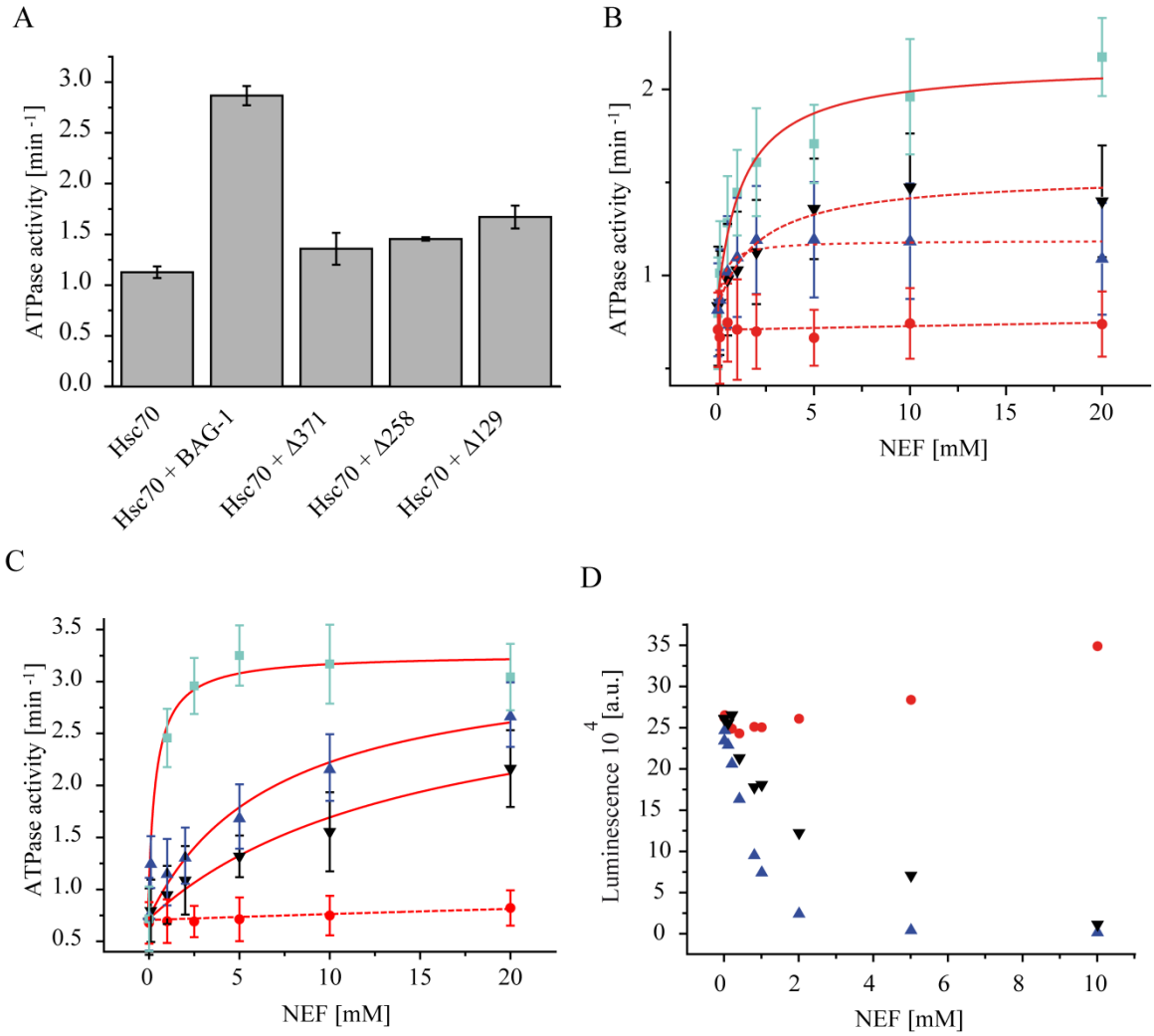

Figure 14 Hsc70s activity stimulation by UNC-23. Means with standard error were plotted. A: Steady state ATPase measurements of 3 µM Hsc70 with 5 µM of different NEFs. B: NEFs were titrated to 3.2 µM Hsc70 and 0.8 µM DNJ-12. ATPase activity of the system upon addition of increasing amounts of BAG-1 (cyan square), Δ129-UNC-23 (blue triangle), Δ258-UNC-23 (black triangle) and Δ371-UNC-23 (red circle) was monitored. Activities were plotted against the protein concentration and fitted as described in the material and method section (red line). Dotted lines were not evaluated any further due to small activity changes with respect to the error bars. C: Different NEFs were titrated to 3.2 µM Hsc70 and 0.8 µM DNJ-13. ATPase activity of the system upon addition of increasing amounts of BAG-1 (cyan square), Δ129-UNC-23 (blue triangle), Δ258-UNC-23 (black triangle) and Δ371-UNC-23 (red circle) was monitored. D: Refolding of firefly luciferase by the Hsc70/DNJ-13 system is analyzed in presence of Δ129-UNC-23 (blue triangle), Δ258-UNC-23 (black triangle) and Δ371-UNC-23 (red circle).

Indeed stimulation of Hsc70 ATPase activity was monitored in the presence of the Hsp40 protein DNJ-12. The two longer UNC-23 fragments Δ129-UNC-23 and Δ258-UNC-23

stimulated the chaperone whereas the isolated BAG-domain did not lead to a likewise effect (Figure 14B). In case of a sufficiently high stimulation in comparison to the error bars the curves were fitted and listed in Table 14. The stimulation of Hsc70 was also analyzed in the presence of DNJ-13. Here stimulations were observed for the longer UNC-23 fragments Δ129-UNC-23 and Δ258-UNC-23 (Figure 14C). This indicates that the N-terminal domain is not involved in Hsc70 stimulation. Again the isolated BAG domain was not sufficient to fulfil the stimulating activities in combination with the Hsc70 system (Figure 14C). It could be shown, that the affinity of the NEF UNC-23 for Hsc70 is in the low micromolar range and thus much lower compared to BAG-1.

To analyze whether UNC-23 has an influence on the refolding of urea denatured luciferase the folding was investigated in the presence of Hsc70. Refolding was analyzed for the Hsc70/DNJ-13 system together with the different UNC-23 fragments (Figure 14D). Therefore chemically denatured luciferase was given to the chaperone system mixture and the luciferase activity was recorded over time. Again, the two longer UNC-23 fragments influenced the refolding of luciferase in a comparable manner. The shortest fragment Δ378-UNC-23 did not alter the chaperone system´s activity (Figure 14D). Conclusively the isolated BAG-domain is not able to exert Hsc70s related effects of UNC-23. These data demonstrate that UNC-23 is able to alter Hsc70 activity and its refolding reaction in combination with DNJ-13 *in vitro*.

5.1.6 Knock-down of DNJ-13 Rescues UNC-23 Induced Motility Phenotype

The Hsp40 proteins DNJ-12 and DNJ-13 and UNC-23 cooperatively alter Hsc70 function *in vitro*. Is this effect also evident *in vivo*? To address this question living *unc-23* mutated nematodes were cultivated on Hsp40 knock-down conditions. For wild-type nematodes obvious changes in *dnj-12*, *dnj-13* or *dnj-19* knock-downs were not observed (data not shown). While RNAi against *dnj-12* or *dnj-19* did not lead to changes in life span of *unc-23* mutated nematodes, severe improvements were observable upon *dnj-13* RNAi (Figure 15A). Strikingly, if *dnj-13* was depleted the *unc-23* mutated worm lived nearly as long as wild-type nematodes (Figure 15A). *Unc-23* mutated nematodes had a half life time of 5 days which is increased up to 12 days upon *dnj-13* reduction. The debilitating growth phenotype was almost absent and worms were thicker and bigger, with only a slight head-bent phenotype remaining (Figure 15B). A significant improvement in the thrashing assay was monitored, compared to non-treated *unc-23* mutated worms (Figure 15C).

Furthermore, the head muscle cells and the dense body superstructure became visible in *dnj-13* RNAi treated nematodes, while they were absent in *unc-23* mutated worms (Figure 15D, Waterston *et al*, 1980). Hence large parts of the phenotype in *unc-23* mutated worms only arise in the presence of DNJ-13. The reduction of specifically DNJ-13 reduces the *unc-23* phenotype and restores growth and life span. The knock-down of other Hsp40 proteins such as *dnj-12* and *dnj-19* did not lead to likewise effects. As DNJ-13 and UNC-23 act antagonistically on the Hsc70 chaperone the Hsc70 cycle apparently is shifted out of balance. It is tempting to speculate that the loss of one cofactor traps Hsc70 in a conformation where no client binding and folding can occur. Another scenario can be envisioned by specifically directing Hsc70 to subcellular locations by either DNJ-13 or UNC-23. Upon disturbance of this system Hsc70 is not recruited to the place of need.

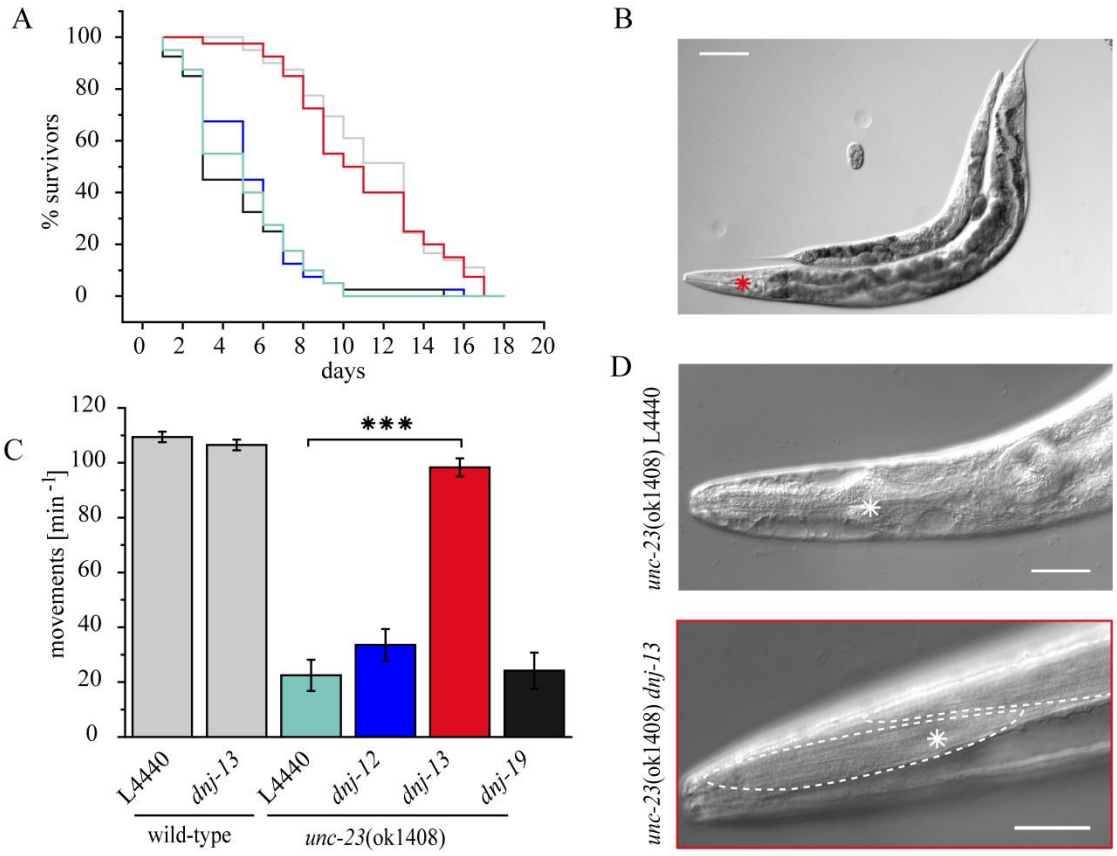

Figure 15 Dnj-13 knock-down recues the unc-23 mutated phenotype. A: Life span assay of wild-type (grey) and unc-23 mutated nematodes (ok1408) on dnj-12 RNAi (blue), dnj-13 RNAi (red), dnj-19 RNAi (black) and empty control vector L4440 (cyan). 20 animals were subjected to analysis. B: Unc-23 mutated nematodes fed on L4440 and dnj-13 RNAi (red star). C: Thrashing assay of wild-type nematodes (grey) fed on the empty control vector L4440 and dnj-13 RNAi. Unc-23 mutated nematodes fed on dnj-12 RNAi (blue), dnj-13 RNAi (red), dnj-19 RNAi (black) and empty control vector L4440 (cyan). Assay was performed with three days old young adult nematodes. Means with standard error (SEM) are plotted. Statistical analysis was performed with the Mann-Whitney-Test. $p=2.83*10^{-6}<\alpha=0.001$. *Significance is indicated by three stars. 10 animals were subjected to analysis. D: Head region of a young adult unc-23 mutated nematode fed on L4440 RNAi (upper panel) and on dnj-13 RNAi (lower panel). Metacorpus of the pharynx is indicated by a star. Muscular tissue with the characteristic dense body structure is highlighted by dotted lines. Dense body superstructure is not observable in unc-23 mutated worms* (Waterston *et al*, 1980).

To test whether selectivity for DNJ-13 is a result of lacking expression of DNJ-12 and DNJ-19 in muscular tissue, it was examined if all Hsp40 proteins are expressed in the body wall muscles (Figure 16). Therefore reporter constructs of full length fusions of Hsp40 to YFP controlled by the respective endogenous *hsp40* promoter (*hsp40*::Hsp40-YFP) were designed and injected into wild-type nematodes. Indeed expression for DNJ-12, DNJ-13 and DNJ-13 could be shown in the body wall muscles and other cell types of adult wild-type worms (Figure 16). This implies that the participation of DNJ-13 in muscle-related processes may occur as a selective Hsp40 cofactor, while DNJ-12 and DNJ-19 are thought to be related to other processes in nematodes.

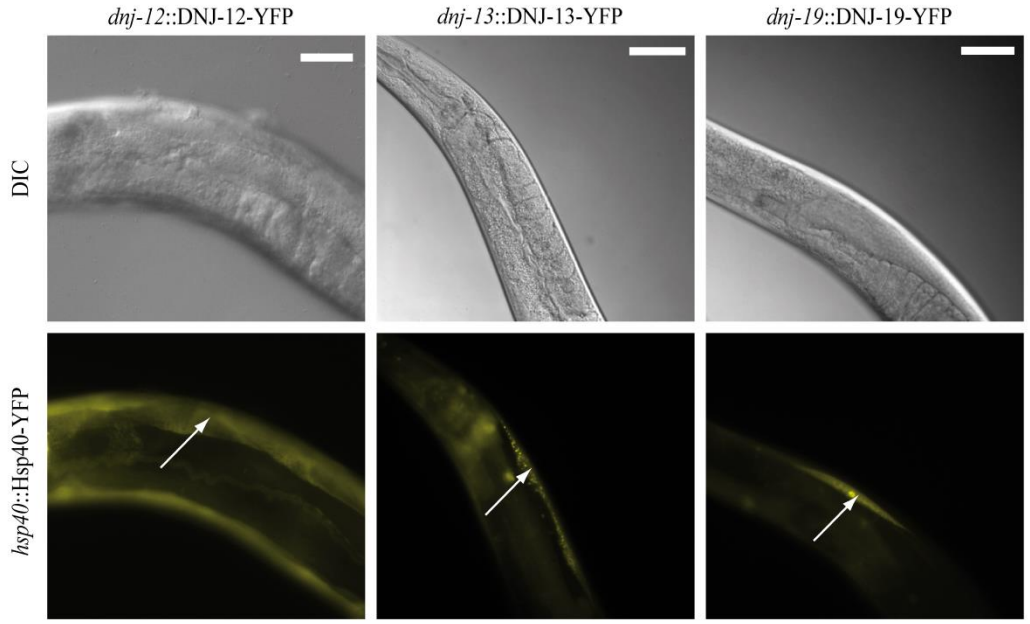

Figure 16 Expression of Hsp40 proteins in muscular tissue of C. elegans. Transgenic wild-type nematodes containing the endogenous promoter of the corresponding Hsp40 protein and YFP-fused either DNJ-12, DNJ-13 or DNJ-19 are seen. Upper panel: DIC images of the nematodes. Lower panel: YFP fluorescent images. Arrows indicate body wall muscle. All proteins are expressed in this muscular tissue. Scale bar: 50 µm.

5.2 Modulating the Nematode Hsc70 System

The molecular chaperone Hsc70 is one of the most conserved proteins among all kingdoms of life. The bacterial DnaK/DnaJ system was extensively studied to reveal molecular interactions and several activity modulators were detected. Studies on the human system were performed mostly with isolated proteins or in cell culture models. The nematode Hsc70 (CeHsc70) system was first addressed in 2012 by Richter and colleagues (Sun *et al*, 2012). It is a molecular chaperone whose ATPase cycle is tightly regulated by Hsp40 and BAG proteins. The chaperone is able to refold model substrates such as luciferase in combination with the Hsp40 protein DNJ-13 (Sun *et al*, 2012). As Hsc70 is known to be involved in diverse cellular processes interfering with its activity is of great interest. It provides a powerful platform to investigate protein interactions *in vitro* combined with the possibility to address functionality of the chaperone system in the whole organism. Investigating modulators in this context offers the chance to uncover the effect of regulatory changes.

To address this question, the optimal system for a screening approach was determined. Recombinant human and nematode proteins of the Hsc70 system were purified and analyzed in respect to their ATPase activity (Figure 17). First, steady state ATPase activity of human and nematode proteins in presence of human and nematode Hsp40 proteins was analyzed (Figure 17A). Nematode Hsc70 in the presence of DNJ-12 thereby exhibited the highest ATPase activity. Together with Dr. Kaiser the temperature regulation of human and nematode Hsc70 was analyzed. Nematode Hsc70 hydrolyzed ATP faster with a k_{cat} of 0.186 min^{-1} compared to the human homolog Hsc70 (HsHsc70) with a k_{cat} of 0.1 min^{-1} at 25 °C (Figure 17B). Interestingly both proteins exhibited a maximum in ATPase activity just below the organism´s lethal temperature (Sun *et al*, 2012, Figure 17B). A 10 000 substance library was screened in cooperation with the Max Planck Institute´s Research Unit for Enzymology and Protein Folding (Halle/Saale, Germany). The temperature of the assay was set at 25 °C and the nematode system was chosen for further analysis. Thus the system with the highest ATPase activity was selected in order to use lower protein amounts. The substances were added to 1.5 µM Hsc70 together with DNJ-12 and BAG-1 in a 96 well format. They were tested and rescreened directly. The first hits found during the screening are shown in Figure 17C. 8 compounds activating or inhibiting the assay system to more than 40 % were further characterized (Figure 17C, cyan). The inhibitory substances were strongly colored and increased the overall absorption at 340 nm. Thus an inhibitory an influence on Hsc70 ATPase activity was not observed (data not shown).

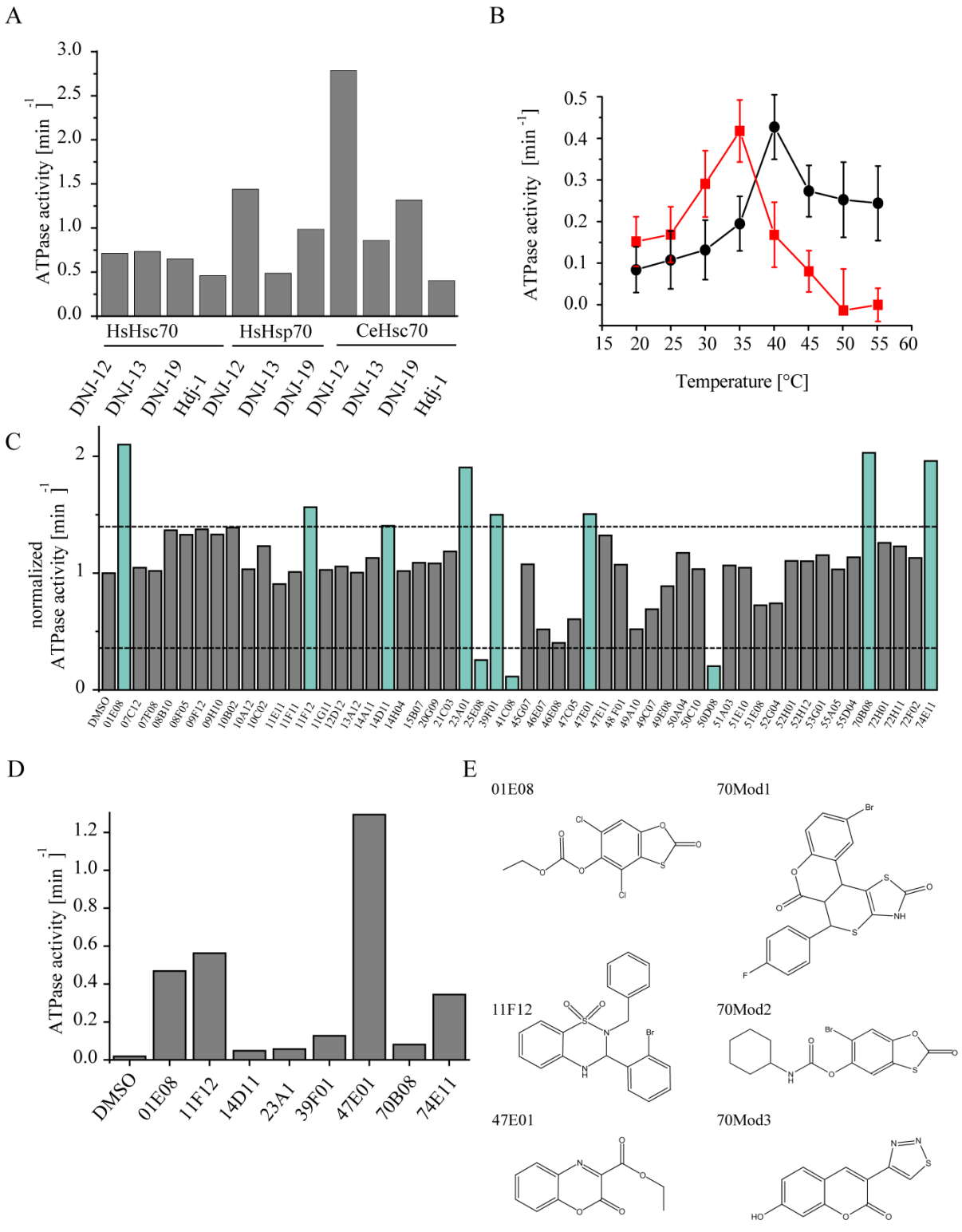

Figure 17: The Hsc70 steady state ATPase activity. A: The steady state ATPase activity of 3 µM human constitutive expressed Hsc70 (HsHsc70), human heat-shock induced Hsp70 (HsHsp70) and nematode Hsc70 (CeHsc70). The activity was measured in the presence 3 µM of different Hsp40 proteins: nematode DNJ-12, DNJ-13, DNJ-19 and the human Hdj-1. B: Temperature dependence of ATPase activity of CeHsc70 and HsHsc70. Black circles depict HsHsc70 activity, red squares depict CeHsc70 activity. The values represent the mean of three experiments with the corresponding standard deviation (Sun *et al*, 2012).*C: The ATPase activity of 1.5 µM Hsc70 together with DNJ-12 and BAG-1 was investigated in a 96 well format at 25 °C in presence of 500 µg/ml substance. The normalized ATPase activity of the rescreened substance library hits is listed. Substances with modifying activity above the threshold of 40 % (dotted lines) were chosen for further characterization (cyan). D: Modulating activity of substances on the ATP regenerating background system consisting of pyruvate kinase, lactate dehydrogenase and NADH.*

Next, the effect of the activating substances on the assay system was tested. Three substances, 01E08, 11D12 and 47E01 stimulated the assay system lactate dehydrogenase (LDH), pyruvate kinase (PK) and NADH in absence of Hsc70 (Figure 17D). These substances were excluded from further analyses regarding the Hsc70 system. Nevertheless investigating these compounds with respect to altering metabolic processes could be of future interest. The results obtained for 70B02 and 74E11 were not consistent and the substances were excluded from further analysis. The three substances 70Mod1 (14D11), 70Mod2 (23A01) and 70Mod3 (39F01) were the substances to stimulate the Hsc70 ATPase activity. Nevertheless long term storage likely leads to degradation of the compounds and effects were ambivalent. The chemical formulas are depicted in Figure 17E. It now remains to be addressed which components of the system is influenced directly, what is the binding affinity to the chaperones and which mechanism lies behind the regulating effect of the compound.

5.3 Polyglutamine Toxicity in Yeast Induces Metabolic Alterations and Mitochondrial Defects[2]

Polyglutamine toxicity is involved in a variety of human neurodegenerative diseases. Extended polyglutamine stretches within mutated proteins increase the aggregation propensity of the corresponding protein. Despite the variety of proteins which are affected all polyglutamine diseases share a common threshold of around 40 glutamine residues inducing neuronal toxicity. Longer polyglutamine stretches provoke an early onset of the disease and increase the aggregation propensity (Takahashi *et al*, 2010). The events generated by an aggregation prone protein resulting in neuronal death are still not fully understood. Different models have been established: The aggregating protein ties all chaperone capacity to it deranging cellular proteostasis (Gidalevitz *et al*, 2006). Additionally proteins with extended polyglutamine stretches are shown to interfere with the protein degradation machinery (Waelter *et al*, 2001). To dissect the mechanism related to toxicity independently of the respective protein function three different constructs of 0, 30 or 56 glutamines fused to either YFP or mCherry were used. The shorter two fragments were found not to be harmful whereas the 56 glutamine residues lead to the toxic *pica* phenotype (Kaiser *et al*, 2013). The system was investigated in the simplest and genetically most accessible eukaryote *S. cerevisiae*. Dr. Kaiser performed a knockout library screen to identify genes increasing or decreasing polyglutamine toxicity in yeast. Based on this screen and a transcriptomic analysis of the intoxicated yeast, light was shed on the events leading to polyglutamine induced toxicity.

5.3.1 Toxic and Non-Toxic PolyQ Stretches Alter the Phosphate Balance in Yeast

To obtain a more detailed comprehension of the events leading to the *pica* phenotype the transcriptomic status of the intoxicated yeasts was analyzed (Kaiser, 2012; Papsdorf *et al*, 2015). In short, expression levels of yeast cells expressing either Q_0- or Q_{56}-YFP were compared. Intoxicated and normally growing cells were analyzed after two and three days for Q_0-YFP and after three and four days for Q_{56}-YFP, to obtain the average relative transcription change for each gene. By this method 76 genes were identified as down-regulated to less than 33% comparing Q_{56}- to Q_0 –YFP expressing cells (Table 15). These genes were united into an interconnected network (Figure 18). To enlarge this network,

[2] This chapter is submitted to *BMC Genomics* (Papsdorf *et al*, 2015)

predicted co-regulated genes were integrated, which were not part of the initial hit list. These predicted co-regulators are highlighted with pink frames in Figure 18. A detailed description of the method performed by Dr. Richter can be found in Papsdorf et al., 2015.

Table 15 Genes down-regulated in Q_{56}- YFP compared to Q_0- YFP expressing yeast. The averaged expression difference obtained from four datasets is listed (Q_0-YFP day two, Q_0-YFP day three, Q_{56}-YFP day three and Q_{56}-YFP day four). Each combination is analyzed, the expression differences calculated and the standard deviations obtained by these calculations. The p-value was generated using the students t-test. Hits with a p-value > 0.05 were marked in grey.

ID	Gene Symbol	$\log_2 Q_0/Q_{56}$	Standard deviation	p-value
YPR192W	AQY1	3.61	0.93	0.00081737
YCR010C	ADY2	3.24	1.02	0.0290809
YLR377C	FBP1	3.17	2.18	0.08286075
YNR056C	BIO5	3.08	0.58	0.00470883
YNL117W	MLS1	2.99	1.60	0.0470131
YGL158W	RCK1	2.98	0.69	0.01950588
YHR139C	SPS100	2.97	1.91	0.04871947
YMR323W,	ERR1, ERR2,	2.95	2.01	0.05846673
YDR281C	PHM6	2.93	0.70	0.00069456
YOR032C	HMS1	2.87	1.00	0.02086733
YPL223C	GRE1	2.83	2.01	0.04599407
YJL045W	---	2.83	1.51	0.03996189
YGR236C	SPG1	2.81	1.69	0.04981097
YKR097W	PCK1	2.80	1.59	0.04787258
YOR388C,	FDH1, FDH2	2.79	0.86	0.00062556
YAL062W	GDH3	2.71	1.95	0.06091858
YMR175W	SIP18	2.68	1.83	0.04602545
YCR021C	HSP30	2.62	2.04	0.08092449
YIL057C	RGI2	2.61	1.04	0.04984244
YOR107W	RGS2	2.54	1.57	0.04738938
YBR296C	PHO89	2.45	0.81	0.0443598
YDR536W	STL1	2.39	2.07	0.15249177
YGR052W	FMP48	2.37	0.21	0.00832945
YBR066C	NRG2	2.33	0.32	0.00159371
YNR002C	ATO2	2.30	0.80	0.0017669
YBR157C	ICS2	2.24	0.51	0.01929475
YBR050C	REG2	2.19	1.25	0.09672312
YOL152W	FRE7	2.19	1.06	0.02945964
YML123C	PHO84	2.17	0.33	0.01136453
YOR178C	GAC1	2.13	1.44	0.0965377
YMR081C	ISF1	2.11	1.66	0.11743186
YBL075C	SSA3	2.04	0.54	0.02274132

YGR256W	GND2	1.99	1.42	0.03496092
YHR136C	SPL2	1.99	0.68	0.00472149
YPR065W	ROX1	1.98	0.92	0.00723834
YCL036W	GFD2	1.93	0.86	0.00410337
YHR160C	PEX18	1.91	1.01	0.05309219
YNL142W	MEP2	1.90	1.05	0.06594156
YLR142W	PUT1	1.89	1.52	0.13610642
YNR058W	BIO3	1.88	0.73	0.02455291
YNR057C	BIO4	1.85	1.05	0.02461184
YNL269W	BSC4	1.81	1.53	0.11786821
YBR093C	PHO5	1.79	0.33	0.02237015
YIL160C	POT1	1.78	0.78	0.02638647
YKL107W	---	1.77	1.14	0.06675667
YGL162W	SUT1	1.76	0.48	0.02785988
YJR115W	---	1.76	0.85	0.01625853
YBR072W	HSP26	1.74	1.66	0.08631927
YKR093W	PTR2	1.73	0.96	0.11303896
YKL043W	PHD1	1.73	0.34	0.00219033
YPL201C	YIG1	1.72	1.90	0.25307398
YNR014W	---	1.71	1.73	0.04996757
YLR053C	---	1.70	1.00	0.07572893
YOR376W-A	---	1.70	0.86	0.10732706
YPL054W	LEE1	1.69	1.42	0.10407407
YGR201C	---	1.68	1.29	0.04786668
YPL057C	SUR1	1.68	0.69	0.031226
YGR121C	MEP1	1.68	0.71	0.01771003
YDL218W	---	1.68	0.84	0.04976561
YHR022C	---	1.68	0.25	0.005146
YJR108W	ABM1	1.68	1.71	0.07610121
YJR095W	SFC1	1.67	1.93	0.23675555
YKL093W	MBR1	1.66	0.95	0.04478269
YMR303C	ADH2	1.65	0.49	0.0400323
YNL194C	---	1.65	0.87	0.10056003
YOR028C	CIN5	1.63	0.66	0.00347329
YMR175W-A	---	1.61	1.79	0.13563467
YOL084W	PHM7	1.59	0.29	0.01975799
YER150W	SPI1	1.59	0.68	0.02702445
YHR096C	HXT5	1.59	1.02	0.08141928
YPR013C	---	1.58	0.54	0.02577641
YGR249W	MGA1	1.58	0.36	0.02992433
YER065C	ICL1	1.58	1.62	0.2384934

YEL019C	MMS21	1.57	1.10	0.05747169
YHL024W	RIM4	1.57	0.52	0.07000804
YMR280C	CAT8	1.57	0.99	0.15233503

Having a closer look at the interconnected network two isolated clusters were detectable. A large cluster of genes involved in the diauxic shift was down-regulated in polyQ intoxicated yeast cells (Figure 18A). Presumably, Q_0 expressing cells undergo diauxic shift during the assay, due to faster colony growth compared to the *pica* yeast. This suggests that the *pica* phenotype and the smaller colony size does not origin from lack of glucose. Hence other metabolic irregularities possibly disturb colony growth.

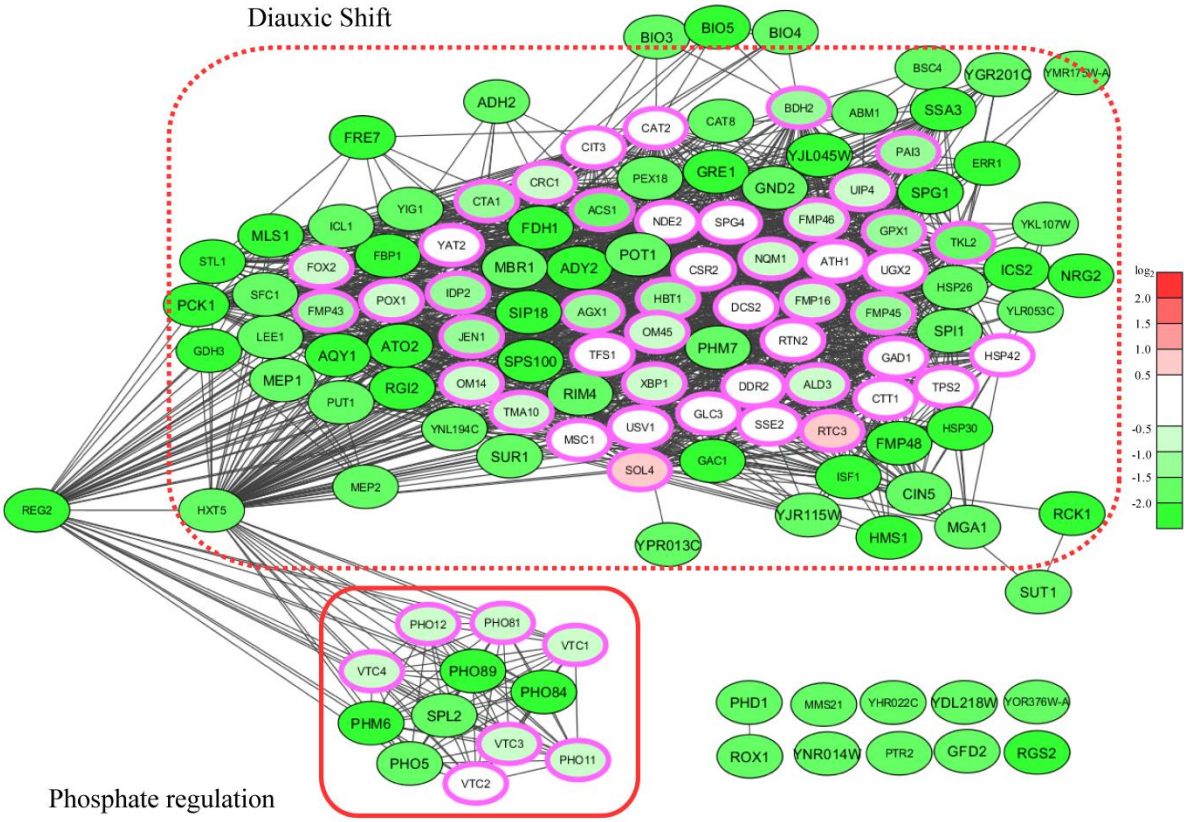

Figure 18 Network of genes down-regulated in Q_{56}-YFP compared to Q_0 expressing yeast. Genes are colored according to their log differences (100% green: 100% green: log2>2, 75% green: 2>log2>1.5, 50% green: 1.5>log2>1, 25% green: 1>log2>0.5, white: 0.5>log2>-0.5, 25% red: -0.5>log2>-1, 50% red: -1>log2>-1.5, 75% red: -1.5>log2>-2, 100% green: -2>log2. Pink frames highlight the co-regulated genes obtained from the additional analysis (Papsdorf *et al*, 2015)*. Large font size: p<0.05, small font size p>0.05. Red boxes highlight clusters according to their cellular pathways.*

Another cluster found differentially down-regulated in *pica* cells were genes of phosphate regulatory pathways (Figure 18A). The phosphate transporter PHO84 and PHO89, the extracellular phosphatase PHO5 and the proteins involved in phosphate metabolism SPL2

and PHM6 were part of this cluster. This is in agreement with previous studies using a non-toxic polyQ constructs in liquid cultures in which similarly phosphate related genes including PHO3, PHO5, PHO11, PHO12 and PHO84 were found down-regulated during the expression of mutated huntingtin fragments (Hughes *et al*, 2001). The robustness of the polyQ induced transcriptional response is remarkable as different constructs, diverse growth conditions and altered toxicity levels were investigated. The results imply that this reaction may be a very sensitive marker in the reaction chain leading to the formation of the *pica* phenotype, but it is barely dependent on the toxicity level.

5.3.2 Polyphosphate Levels are Elevated in Q_{56}-YFP Expressing Yeasts

Are the differences found in gene expression patterns also detectable on a metabolic level? To understand the impact of polyQ stretches on the phosphate metabolism different phosphate components of *pica* and normally growing cells were analyzed. Therefore suspensions of living Q_0-, Q_{30}- and Q_{56}-YFP expressing cells were prepared and ^{31}P spectra recorded by means of NMR (Figure 19A). Three distinguishable NMR signals were elicited resulting from intracellular inorganic phosphate and intracellular polyphosphate. Peak 1 at 2 ppm is assigned to inorganic phosphate, peak 2 at -5.5 ppm and 3 at -24 ppm were assigned to polyphosphate, which is a phosphate storage form located in the yeast vacuole and cytosol (Table 16).

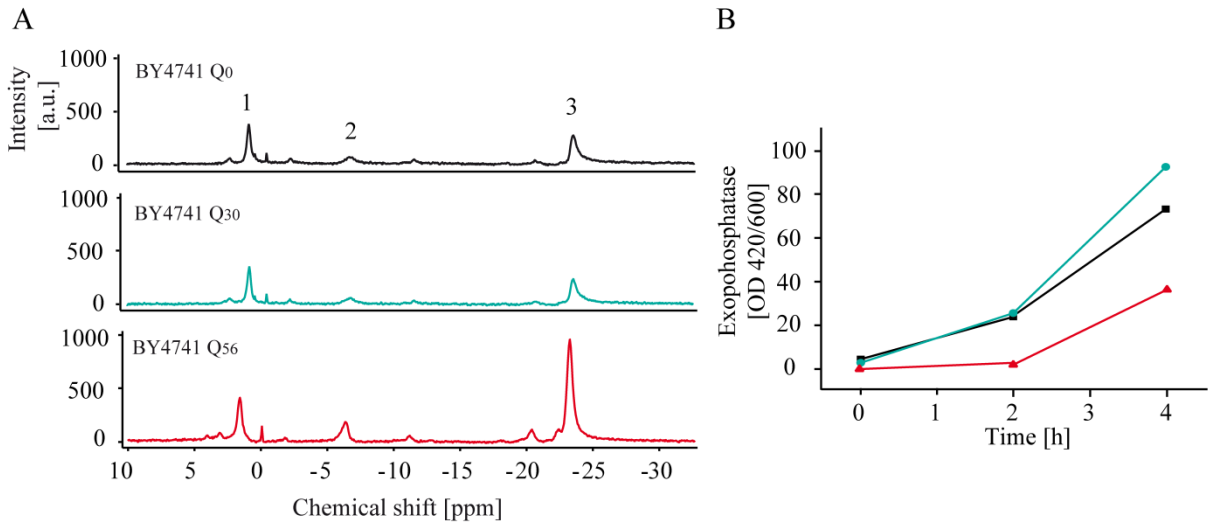

Figure 19 Phosphate metabolism in polyQ expressing yeast cells. A: ^{31}P spectra of yeast cells expressing either Q_0- (top), Q_{30}- (middle) or Q_{56}-YFP (bottom). Yeasts were resuspended in phosphate free buffer and spectra recorded immediately after. Peak assignments are listed in Table 16. 1: inorganic phosphate, 2: polyphosphate (end of chain), 3: polyphosphate (internal). B: Exopolyphosphatase activity was recorded by relocation of yeasts in phosphate free media. Extracellular phosphatase activity was recorded. Q_0-YFP (black), Q_{30}-YFP(cyan) or Q_{56}-YFP (red). Three independent experiments were performed.

No changes in the phosphate pattern were observable in yeast cells expressing Q_0-YFP compared to Q_{30}-YFP expressing yeasts (Figure 19A). Surprisingly, an almost two fold increase in the polyphosphate signal was recorded in *pica* cells (Figure 19A). Nevertheless inorganic phosphate levels were not altered (Figure 19A). This indicates that the phosphate balance in Q_{56}-YFP expressing yeasts indeed is disturbed. Having seen the down-regulation in the transcriptional response and changed polyphosphate levels it was analyzed next, whether the imbalances were also detectable on protein level. Therefore extracellular phosphatase activity of Pho5p was determined using an extracellular phosphatase activity assay. Q_0-, Q_{30}- and Q_{56}-YFP expressing cells were shifted to phosphate free media and the extracellular phosphatase activity measured by a dye coupled reaction (Figure 19B). A delay in Q_{56} expressing cells phosphatase activity became evident. Proteins responsible for phosphate uptake were less active suggesting that Q_{56}-YFP expressing cells contain reduced levels of the phosphatases.

Table 16 Assignment of ^{31}P NMR signals

Peak position [ppm]	Peak label	Assigned to
2	1	Inorganic phosphate
-5.5	2	Polyphosphate (end of chain)
-24	3	Polyphosphate (internal)

5.3.3 Expression Changes in Toxic Q_{56}-YFP Show a Specific Up-regulated Response

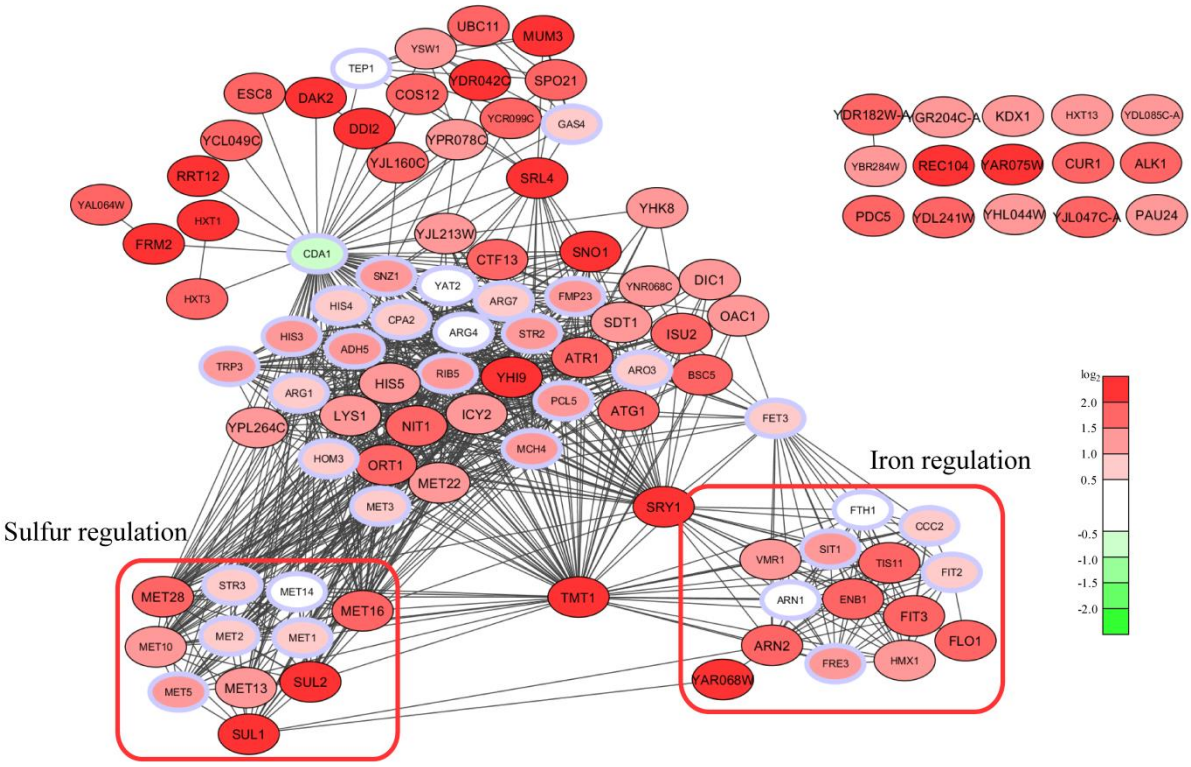

Figure 20 Network of genes up-regulated in Q_{56}-YFP compared to Q_0 expressing yeast. Genes are colored according to their log differences (100% green: 100% green: log2>2, 75% green: 2>log2>1.5, 50% green: 1.5>log2>1, 25% green: 1>log2>0.5, white: 0.5>log2>-0.5, 25% red: -0.5>log2>-1, 50% red: -1>log2>-1.5, 75% red: -1.5>log2>-2, 100% green: -2>log2. Blue frames highlight the co-regulated genes obtained from the additional analysis (Papsdorf *et al*, 2015)*. Red boxes highlight clusters according to their cellular pathways. Large font size: p<0.05, small font size p>0.05.*

Having investigated the down-regulation of *pica* cells the up-regulation was analyzed likewise. 72 genes were found up-regulated more than 2.5 fold on the $\log_2$ scale comparing Q_{56}-YFP to Q_0-YFP (Table 17). These up-regulated genes were similarly integrated into an interconnected network to visualize clusters of cellular processes (Figure 20). Again predicted co-regulated genes were obtained by Dr. Richter, integrated into the network and highlighted by a blue frame (Figure 20, Papsdorf *et al*, 2015). Thereby two defined clusters could be visualized. First, a cluster related to iron uptake with the iron transporters ENB1 and ARN2 was detected. Genes related to iron starvation such as FIT3, VMR1 and TIS11 were additionally part of this group. Secondly, a large cluster of the sulfur regulatory network was found. Genes participating in sulfur uptake and in early methionine synthesis such as SUL1, SUL2 and MET10 were contained in this cluster (Figure 20). These datasets strongly point to an iron depletion and methionine starvation in Q_{56} expressing yeasts.

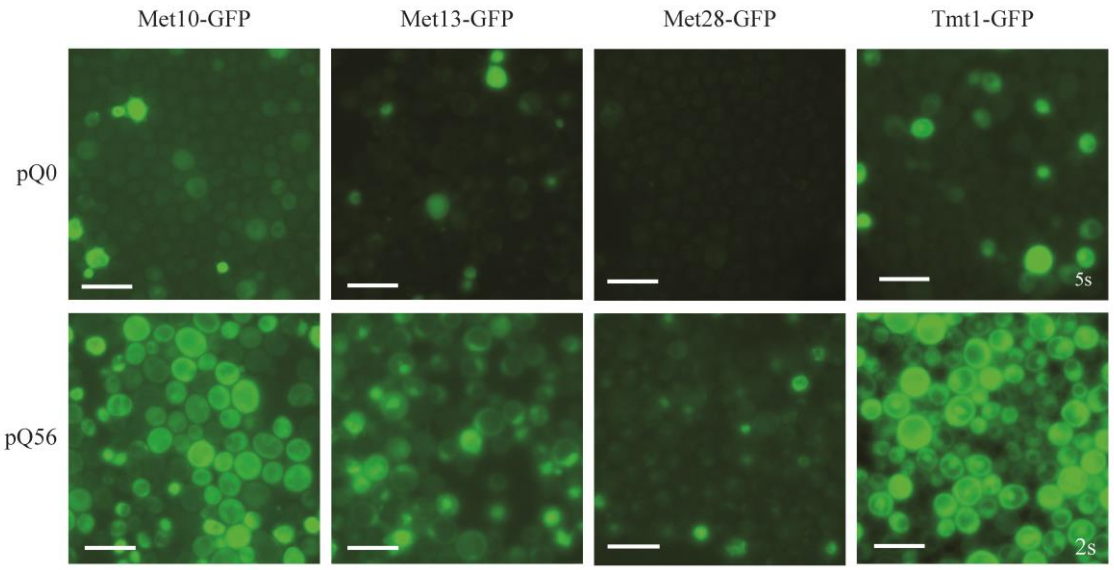

Figure 21 Up-regulation of Met10p, Met13p, Met28p and Tmt1p fused to GFP monitored on protein level. Cells express Q_0- and Q_{56}-mCherry. GFP fluorescence is monitored and exposure time not changed comparing Q_0- and Q_{56}-mCherry if not stated otherwise. Scale bar represents 10 µm.

Further it was tested if the up-regulation visible on transcriptomic level is present on protein level. Therefore the expression of genomic Met10p, Met13p, Met28p and Tmt1p fused to GFP was observed microscopically (Figure 21). Indeed for all proteins an increase in fluorescence was observed comparing pQ0 and pQ56-mCherry transformed yeasts. This implies that the up-regulation is also evident at the level of protein concentrations within the cell.

Table 17 Genes up-regulated in Q_{56}- YFP compared to Q_0- YFP expressing yeast. The averaged expression difference obtained from four datasets is listed (Q_0-YFP day two, Q_0-YFP day three, Q_{56}-YFP day three and Q_{56}-YFP day four). Each combination is analyzed, the expression differences calculated and the standard deviation obtained by these calculations. The p-value was generated using the students t-test. The hits with a p-value > 0.05 were marked in grey.

ID	Gene Symbol	$\log_2 Q_{56}/Q_0$	Standard deviation	p-value
YAR075W	---	5.94	2.65	0.0118319
YFL053W	DAK2	4.89	1.71	0.00278943
YDR042C	---	3.80	0.46	0.00311027
YPL033C	SRL4	3.51	0.77	0.00062449
YHR029C	YHI9	2.67	1.11	0.00511175
YAR068W, YHR214W-A	---	2.65	0.77	0.01328436
YKL183C-A	---	2.64	0.87	0.00025251
YHR094C	HXT1	2.57	3.19	0.14289571
YMR095C	SNO1	2.51	0.68	0.00057467
YER175C	TMT1	2.46	0.63	0.0013498

YCR045C	RRT12	2.36	1.04	0.02183959
YOR298W	MUM3	2.35	0.32	0.0158274
YLR092W	SUL2	2.35	0.90	0.0133767
YKL218C	SRY1	2.29	0.67	0.00024098
YBR294W	SUL1	2.25	1.04	0.04034834
YCL026C-A	FRM2	2.22	0.66	0.01227384
YHR157W	REC104	2.22	0.50	0.02986818
YFL061W, YNL335W	DDI2, DDI3	2.05	0.78	0.00025123
YOL158C	ENB1	1.99	0.88	0.06596865
YAR050W	FLO1	1.95	0.79	0.0109145
YIR017C	MET28	1.93	0.69	1.6798E-06
YJL160C	---	1.92	0.45	0.0101294
YOL017W	ESC8	1.91	0.02	0.01078285
YHL047C	ARN2	1.89	0.32	0.02217488
YGL263W	COS12	1.84	0.36	0.01414172
YML116W	ATR1	1.84	0.02	0.01141218
YOR226C	ISU2	1.84	1.56	0.02822063
YJL047C-A	---	1.83	0.60	9.4709E-06
YIL165C	NIT1	1.74	0.11	0.01479371
YOR339C	UBC11	1.71	1.09	0.00519265
YMR094W	CTF13	1.67	0.31	0.00633299
YDL241W	---	1.65	0.53	0.00370141
YGL021W	ALK1	1.65	0.15	0.01451989
YPR167C	MET16	1.65	0.99	0.00475723
YJL213W	---	1.64	0.40	0.01616031
YDR345C	HXT3	1.64	1.57	0.06695841
YOR130C	ORT1	1.61	0.26	0.0089673
YLR136C	TIS11	1.59	0.40	0.05823717
YCL049C	---	1.58	0.54	0.00032344
YNR069C	BSC5	1.58	1.32	0.20898065
YDR182W-A	---	1.56	0.61	0.04964433
YPR158W	CUR1	1.55	0.31	0.00351943
YOR383C	FIT3	1.54	0.21	0.00790573
YGL180W	ATG1	1.54	0.95	0.1502267
YLR134W	PDC5	1.52	0.47	0.0013838
YAL064W	---	1.52	0.66	0.10343767
YCR099C	---	1.52	1.05	0.1736527
YOL091W	SPO21	1.51	0.14	0.01044166
YDL085C-A	---	1.48	2.11	0.13607594
YNR068C	---	1.48	0.72	0.11929763
YLR348C	DIC1	1.48	1.19	0.02931345

YEL069C, YNR072W	HXT13, HXT17	1.46	2.34	0.36657784
YHL035C	VMR1	1.45	0.87	0.14859112
YKL161C	KDX1	1.42	0.39	0.04934333
YPR078C	---	1.42	0.36	0.00868702
YKL120W	OAC1	1.41	0.54	0.01183173
YGR204C-A	---	1.41	1.24	0.01785192
YGL224C	SDT1	1.41	0.84	0.00101731
YBR148W	YSW1	1.40	0.46	0.08312594
YLR205C	HMX1	1.40	0.58	0.07670162
YBR301W	PAU24	1.40	0.05	0.02729238
YGL125W	MET13	1.40	0.50	0.00150402
YIL116W	HIS5	1.38	0.18	0.01325996
YPL250C	ICY2	1.38	0.55	0.00059314
YHR048W	YHK8	1.38	0.11	0.03031932
YOL064C	MET22	1.36	0.36	0.01465976
YPL264C	---	1.36	0.50	0.00238525
YBL005W-A (+ Homologs)	---	1.35	0.25	0.04921427
YBR284W	---	1.35	0.69	0.13582784
YIR034C	LYS1	1.35	0.54	0.00506078
YHL044W	---	1.33	0.80	0.00121048
YFR030W	MET10	1.33	0.49	0.07926356

5.3.4 Iron-homeostasis is Affected in Q_{56}-YFP Expressing Yeasts

To investigate if the changes on transcriptional level were generated by a lack of iron, a closer investigation of the cellular iron levels was carried out. Cells were transformed with the three different polyglutamine constructs and the intracellular iron levels were measured. The total intracellular iron per OD was determined using EPR spectroscopy. Membrane permeable DFO was used to oxidize Fe^{2+} to detectable Fe^{3+} ions. Contrary to the expectations two fold increased iron levels were found in Q_{56}-YFP expressing cells (Figure 22). Iron levels were not altered comparing Q_0-YFP and Q_{30}-YFP expressing cells. At first this observation seems to contradict the microarray studies, as iron transporter expression usually is induced by iron starvation (Philpott *et al*, 2002). However, iron regulation and its metabolism are very complex and additionally related to iron sulfur (Fe-S) biosynthesis. Up-regulation of iron-related genes is generally controlled via the Aft1 transcription factor and induced if Fe-S clusters are not produced to sufficient amount in mitochondria (Rutherford *et al*, 2005; Lill *et al*, 2012). Fe-S cluster are multipurpose

protein cofactors and the proteins containing those take part in essential cellular functions such as protein synthesis, DNA replication and energy metabolism (Paul & Lill, 2015). One of the most abundant cellular Fe-S proteins is aconitase, catalyzing a step in the citric acid cycle. Great differences in the aconitase activity of cells expressing the different polyglutamine constructs were observed (Figure 22B). Only a slight variation was detectable in the aconitase activity in Q_0-YFP and Q_{30}- YFP expressing cells. Strikingly a strong reduction of aconitase activity was detectable in Q_{56}-YFP expressing cells (Figure 22B). Hence, the higher level of free iron in the cell is apparently not sufficient to ensure the production of the Fe-S cluster containing enzyme aconitase. The reduced production of Fe-S cluster proteins in the mitochondria of *pica* yeast might thus cause the up-regulation of the iron-regulatory expression cluster observed.

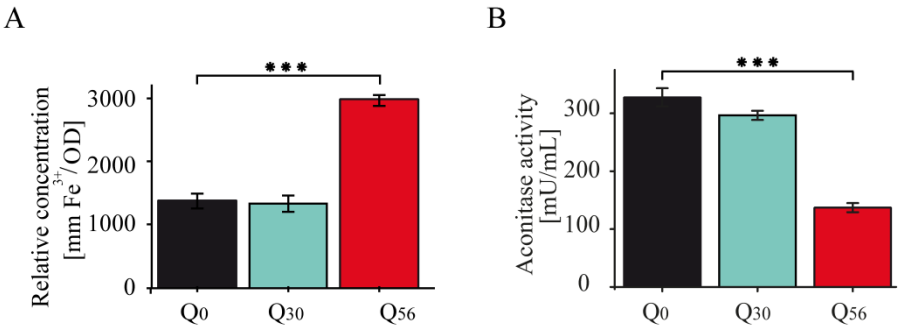

Figure 22 Iron homeostasis is disturbed in Q_{56} expressing cells. A: Relative Fe^{3+} concentration per OD determined by EPR spectroscopy. Q_0-YFP depicted in black, Q_{30}-YFP in cyan and Q_{56}-YFP in red. Standard deviation with means (s.e.m.) are depicted. Statistical analysis was performed using the students t-test $p < 0.05$. B: Aconitase activity of Q_0-YFP (black), Q_{30}-YFP (cyan) and Q_{56}-YFP (red). Means with standard errors are plotted. Statistical analysis was performed using the students t-test. $p < 0.05$.

5.3.5 Regulator Activity is Activated by Polyglutamine Constructs

Numerous genes are found up and down-regulated in the microarray datasets. In order to analyze if these genes share common regulators a thorough examination was performed. To this end the common regulators of the 72 genes up-regulated and the 76 genes down-regulated were compared to a random dataset. The 30 most prominent regulators were retrieved via yeastmine (www.yeastmine/yeastgenome.org). For a detailed description see the Material and Method section.

Table 18 Common regulators of genes detected up- or down-regulated in microarray datasets. Regulators were retrieved by analyzing the 30 most prominent regulators with yeastmine. For a detailed description see material and method section. Regulators found 33% decreased or increased compared to the random dataset were marked grey if they appear in both sections.

Name	Up-regulating	Random regulating	Fold change	Name	Down-regulating	Random regulating	Fold change
Gcn4	14	2	7	Msn2	5	1	5
Msn2	5	1	5	Cin5	5	2	2.5
Bas1	4	0	4	Gcn4	5	2	2.5
Met4	11	3	3.6	Spt20	5	2	2.5
Met32	12	4	3	Tup1	7	3	2.3
Tup1	9	3	3	Hsf1	8	4	2
Spt20	6	2	3	Cst6	6	3	2
Hfi1	8	3	2.6	Cyc8	6	3	2
Sin3	5	2	2.5	Met4	6	3	2
Spt7	5	2	2.5	Rpd3	6	3	2
Cst6	6	3	2	Skn7	6	3	2
Rpd3	6	3	2	Swi4	6	3	2
Spt10	14	9	1.5	Met32	7	4	1.7
Ixr1	15	11	1.3	Spt10	15	9	1.6
Rgr1	8	6	1.3	Bur6	6	4	1.5
Yap6	15	12	1.2	Hfi1	4	3	1.3
Rap1	7	6	1.2	Spt3	8	8	1
Tfc7	7	6	1.2	Rap1	6	6	1
Stp1	10	9	1.1	Fkh2	4	4	1
Xbp1	12	11	1.1	Ixr1	10	11	0.9
Gcn5	8	8	1	Xbp1	10	11	0.9
Spt3	8	8	1	Ume6	9	10	0.9
Yap1	7	7	1	Sfp1	22	26	0.8
Spt6	6	6	1	Tfc7	5	6	0.8
Med2	10	12	0.8	Yap5	5	6	0.8
Sua7	9	11	0.8	Sua7	9	11	0.8
Ume6	8	10	0.8	Fkh1	6	8	0.7
Rfx1	6	8	0.7	Gcn5	6	8	0.7
Sfp1	19	26	0.7	Yap6	8	12	0.7
Reb1	8	12	0.7	Stp1	6	9	0.7
Fkh1	5	8	0.6	Med2	6	12	0.5

Several regulators were found enriched compared to a random set of genes. Strikingly these regulators overlap in both sections. The 5 most prominent common enriched regulators are Gcn4, Msn2, Met32, Tup1 and Spt20. While Tup1 is a general repressor of transcription involved in a variety of cellular processes and Spt20 is part of a multi subunit histone modifying complex involved in general transcription, Msn2 is a stress response specific transcription factor activated in response to multiple stresses (Courey & Jia, 2001; Roberts & Winston, 1996; Martínez-Pastor *et al*, 1996). A more specific regulation is obtained by Gcn4 which is a regulator reacting to amino acid starvation and an activator of amino acid biosynthesis related genes. Thus although Q_{56}-YFP expressing yeast do not experience diauxic shift, amino acid shortage apparently occurs. Additionally Met32 is found which regulates sulfur metabolic genes (Natarajan *et al*, 2001; Blaiseau & Thomas, 1998; Blaiseau *et al*, 1997). This indicates that proteins exist which mutually up- and down-regulate the genes retrieved in the microarray studies. It is tempting to speculate that regulation in the clusters is connected via shared regulators. To address this assumption the analysis was performed for the isolated clusters.

Table 19 Common regulators of genes detected in the clusters retrieved from the microarray studies. The most prominent regulators were detected with yeastmine. For a detailed description see material and method section. The phosphate cluster contains 5 genes, the sulfur cluster 6 and the iron cluster 8 genes. #: times the transcription factor is found.

Name	#	Target	Name	#	Target	Name	#	Target
Phosphate cluster			Sulfur cluster			Iron cluster		
Spt10	5	PHM6, PHO5, PHO84, PHO89, SPL2	Ixr1	6	MET28, MET10, MET16, MET13, SUL1, SUL2	Spt10	5	ARN2, FIT2, FLO1, VMR1, YAR068W
Hsf1	5	PHM6, PHO5, PHO84, PHO89, SPL2	Met32	6	MET28, MET10, MET16, MET13, SUL1, SUL2	Stp1	5	ARN2, ENB1, FIT3, TIS11, VMR1
Pho2	5	PHM6, PHO5, PHO84, PHO89, SPL2	Met4	6	MET28, MET10, MET16, MET13, SUL1, SUL2	Aft1	3	ENB1, HMX1, VMR1
Rap1	5	PHM6, PHO5, PHO84, PHO89, SPL2	Cbf1	3	MET10, MET28, SUL2	Ixr1	3	ARN2, FIT3, YAR968W
Cbf1	4	PHM6, PHO5,	Sfp1	3	MET13, MET16,	Med4	3	HMX1, VMR1,

		PHO84, SPL2	SUL2		YAR968W
Hfi1	4	PHM6, PHO5, PHO84, PHO89	Rfx1	3	FIT3, FLO1, VMR1
Pho4	4	PHM6, PHO84, PHO89, SPL2	Rim101	3	ARN2, ENB1, FIT3
Spt20	4	PHM6, PHO5, PHO84, PHO89	Rtg3	3	ARN2, FIT3, YAR068W
Gcn4	3	PHM6, PHO5, PHO89	Stb1	3	ARN2, ENB1, FIT3
Gcr1	3	PHO5, PHO89, SPL2	Xbp1	3	ARN2, TIS11, YAR068W

The transcription factors regulating the phosphate, iron and sulfur cluster were retrieved via yeastmine. All factors which appear less than three times were not analyzed any further. 5 genes were regulated via SPT10 in the iron and the phosphate cluster. To test whether this enrichment is specific random genes were analyzed for their transcription factors. Here Spt10 also appeared but less frequent with 2 $\pm$ 2. Also the transcription factor IXR1 was found to regulate in the iron and sulfur cluster (Table 18). This transcription factor is involved in aerobic repression of gene (Brown *et al*, 1993). Here it was found to regulate 6 genes in the sulfate and 3 in the iron cluster compared to an incidence of only 0.67 $\pm$ 0.6 in the random gene set (Table 20). A similar enrichment was detectable for Cbf1 regarding its regulation of the phosphate and the sulfur cluster. Apart from these transcription factors regulating two clusters there are also cluster specific transcription factors. These are specifically detected in one cluster such as the Pho4 and Pho2 transcription factors for the phosphate cluster, the Met32 and Met4 transcription factors for the sulfur cluster and Aft1 for the iron cluster (Table 19). These factors either do not regulate the random gene list or just very few genes. These findings point to a specific involvement of transcription factors in the response to polyglutamine stress.

Table 20 Regulators of random regulated genes. Three studies with 8 random genes were performed to obtain the mean and standard deviation.

Name	Mean	standard deviation
Sfp1	3.00	1.73
Spt10	2.00	1.73
Hsf1	not retrieved	
Pho2	0.67	1.15
Rap1	1.67	1.15
Cbf1	0.33	0.58
Hfi1	0.33	0.58
Pho4	not retrieved	
Spt20	not retrieved	
Gcn4	0.67	0.58
Gcr1	0.33	0.58
Ixr1	0.67	0.58
Met32	0.33	0.58
Met4	0.33	0.58
Cbf1	0.33	0.58
Aft1	not retrieved	
Med4	0.67	1.15
Rfx1	not retrieved	
Rim101	0.33	0.58
Rtg3	not retrieved	
Stb1	not retrieved	
Xbp1	2.33	0.58
Stp1	0.66666667	0.57735027

5.3.6 Q_{56}-YFP Reduces Mitochondrial Carbon Source Utilization

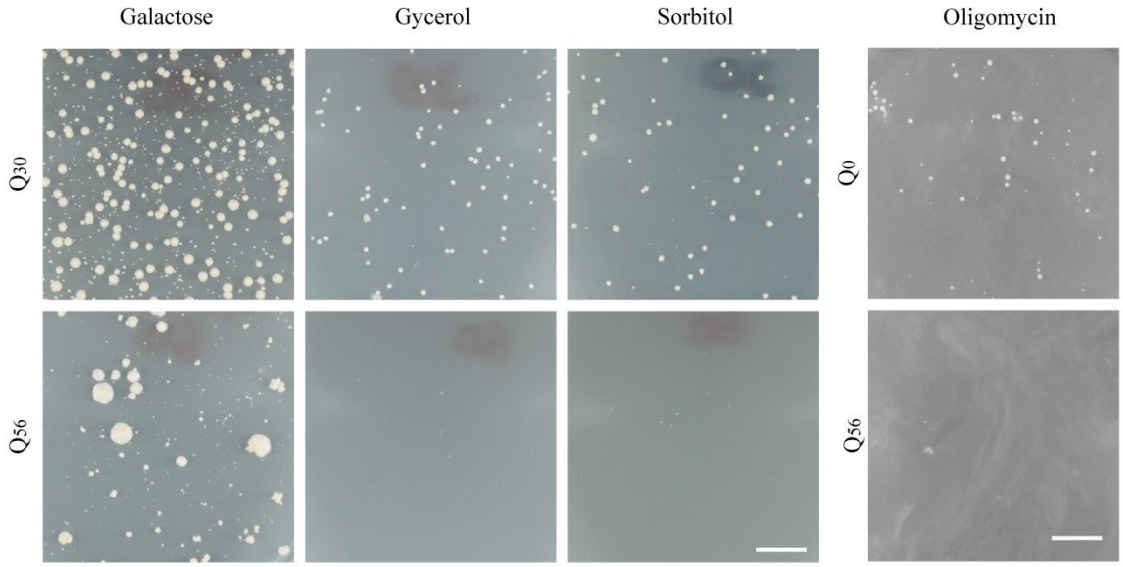

Figure 23. Carbon source utilization is impaired in Q_{56}-YFP expressing yeasts. Growth of transformed yeasts was monitored after 8 days of incubation. No growth of Q_{56}-YFP is observable if BY4741 cells are grown on media containing 2% sorbitol or 2% glycerol. The pica phenotype is unchanged if cells are grown on 2% galactose as a carbon source compared to glucose (Kaiser, 2012)*. Upon respiratory chain inhibition by adding oligomycin no growth is observable in Q_{56}-YFP expressing yeasts. The scale bar represents 10 mm.*

Several indications hint to an impaired mitochondrial system in *pica* cells including the increased amount of mitochondrial genes as suppressors of toxicity and the lack of Fe-S clusters in aconitase. Therefore Dr. Kaiser performed investigations on mitochondrial functions with respect to carbon source utilization. The *pica* phenotype was evident on either glucose or galactose (Figure 23, Kaiser, 2012). Galactose was used as a control because it can be metabolized by yeast in a similar manner as glucose. Yeasts grew generally slower on galactose as on glucose but the colony patterns resembled the patterns observed for glucose. Interestingly if glucose is supplemented by non-fermentable carbon sources, for example glycerol and sorbitol, *pica* yeasts do not grow any more (Figure 23). Here the yeasts are more dependent on respiration and functional mitochondria. This implies that the *pica* yeast is able to grow as long as the carbon source allows sufficient energy production via fermentation. To study the importance of the mitochondrial system additionally the respiratory chain inhibitor oligomycin was used. Challenging the mitochondrial system by oligomycin led to inhibited growth of Q_{56}-YFP expressing yeasts whereas the Q_0-YFP yeasts were still able to grow at the same oligomycin concentration.

Table 21 Assignment of ^{13}C signals detected via ^{13}C NMR.

Position	Signal type	Peak label	Attributed to
16.7	Doublet	Et	Ethanol
57.4	Doublet	Et	Ethanol
27.6	Doublet of doublet	Pyr	Pyruvate
169.9	Doublet of doublet	Pyr	Pyruvate
205.3	Doublet of doublet	Pyr	Pyruvate
60.5		G	Glucose
69.5	Triplett	G	Glucose
74.2		G	Glucose
75.8	Triplett	G	Glucose
92.1	Doublet	G	Glucose
95.9	Doublet	G	Glucose
62.5	Doublet	Glyc	Glycerol
72.0	Triplet	Glyc	Glycerol
160.3	Singlet	Carbonate	Carbonate
124			unassigned

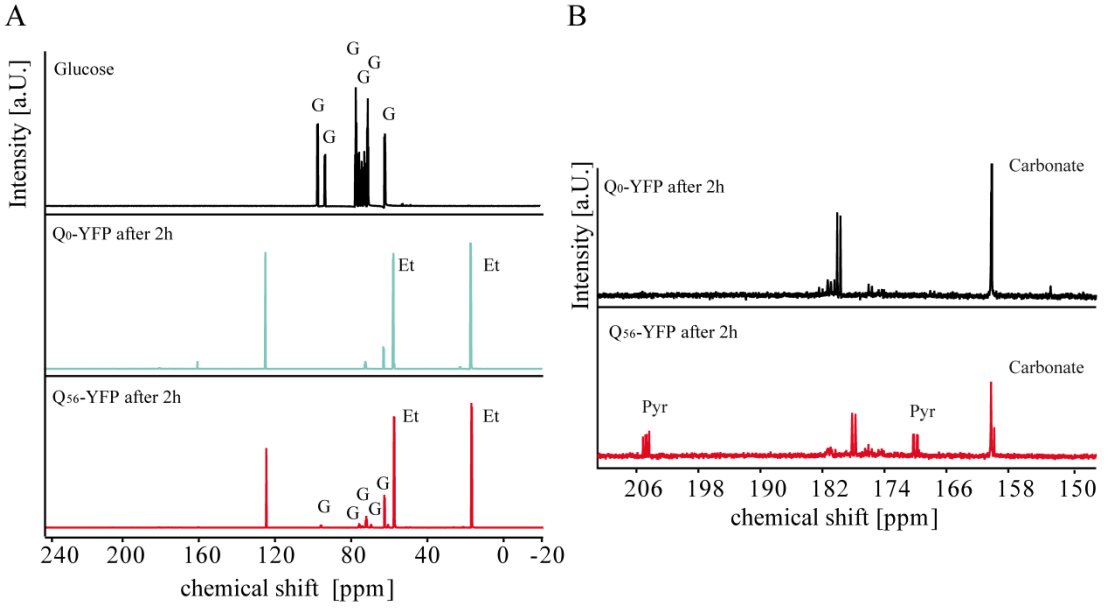

Figure 24 A: $U^{13}C_6$ glucose spectra and the assigned metabolic species monitored by NMR. Upper panel: $U^{13}C_6$ glucose, middle panel: $U^{13}C_6$ glucose consumption in the presence of BY4741 cells expressing Q_0-YFP, lower panel: $U^{13}C_6$ glucose consumption in the presence of BY4741 cells expressing Q_{56}-YFP. Peak assignment is listed in Table 21.Glucose is abbreviated with G, ethanol with Et, pyruvate with Pyr. B: Spectra range of 156 ppm to 210 ppm expose smaller peaks.

To unravel the metabolic processes which are affected, glucose utilization of living cells was monitored via NMR. Thereby [U$^{13}C_6$] glucose was added to cells harvested from SD media plates. Different peak sets are detectable via ^{13}C-NMR corresponding to the 6 C atoms of glucose (Figure 24A). The peak assignments are listed in Table 21. Within two hours yeast produced metabolites of different kinds including ethanol and the peak sets for glucose are diminished (Figure 24A). Having a closer look at the metabolites pyruvate peaks only appeared in Q_{56}-YFP transformed yeasts (Figure 24B). A kinetic investigation of yeast metabolism gave more detailed information on the impaired processes (Figure 25). Glucose consumption and ethanol production occurred with the same kinetic characteristics in Q_0-YFP and Q_{56}-YFP expressing yeasts. Hence fermentation of glucose is not hindered in *pica* yeasts. Interestingly peaks corresponding to pyruvate accumulated in Q_{56}-YFP yeasts and did not appear in Q_0-YFP expressing yeasts over the whole time course (Figure 25). Further a slight reduction in carbonate was detectable which is the last product of respiration. These two differences confirm an impaired respiratory activity of mitochondria as apparently the respiratory conversion of pyruvate to CO2 is reduced in the *pica* cells.

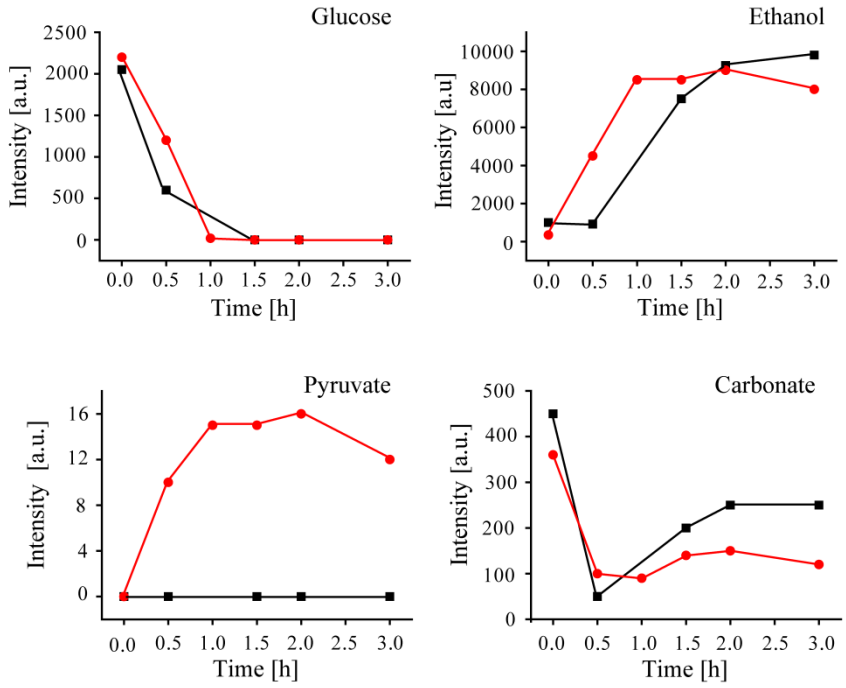

Figure 25. Kinetics of glucose metabolism by polyglutamine intoxicated yeast. Yeast were resuspended to an OD_{595}=150 and [U-$^{13}C_6$]-glucose was added at time point 0. Spectra were recorded for 3 hours by NMR. Kinetic of ^{13}C NMR signals of [U-$^{13}C_6$] glucose and metabolites produced by Q_0-YFP (black square) and Q_{56}-YFP (red circle) expressing yeasts. Glucose consumption is monitored by scoring the signal intensity at 75.8 ppm, ethanol production is observed at 16.7 ppm, pyruvate accumulation at 169.9 and carbonate production at 160.3 ppm. Chemical shift assignments are listed in Table 21. Replicates are performed and shown in (Papsdorf *et al*, 2015)

5.3.7 Q_{56}-YFP Intoxication Results in Decreased Cox4p Levels

Based on the data obtained two scenarios can be envisioned leading to the growth arrest in *pica* yeasts. Either energy shortage exists in the polyglutamine intoxicated yeasts or mitochondrial dysfunctions lead to impairment of Fe-S cluster synthesis and thereby are relevant for the yeasts. To this end cellular ATP levels were determined (Figure 26A). Although the metabolic activity is reduced the ATP level themselves were not affected in Q_{56}-YFP intoxicated yeasts. Additionally NADH-levels were determined, to check if they relate to the mitochondrial metabolic effects (Figure 26B). Only slight reductions were visible in the NADH levels of polyQ intoxicated yeasts compared to Q_0-YFP expressing yeasts, meaning these metabolic pathways are still functional in *pica* cells.

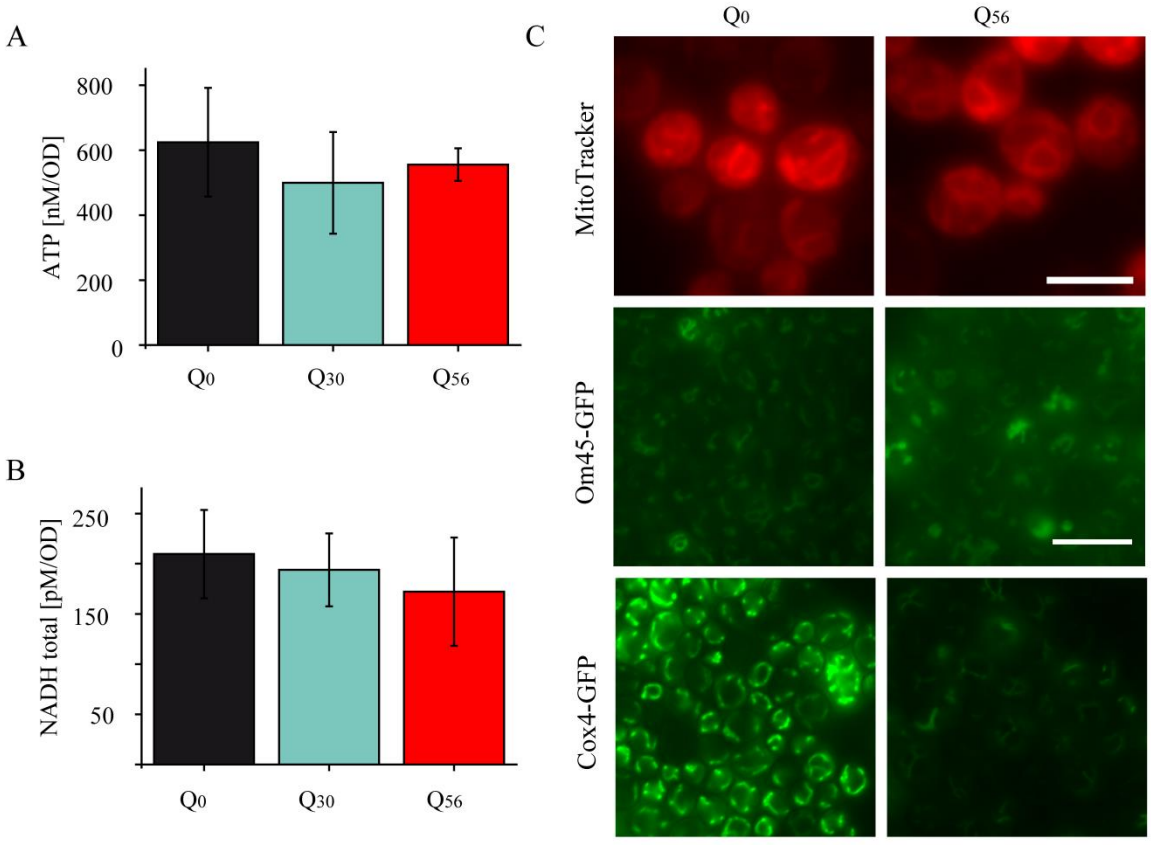

Figure 26ATP and NADH level in polyglutamine intoxicated cells and the effect on mitochondrial proteins. A: ATP level of Q_0-YFP, Q_{30}-YFP and Q_{56}-YFP expressing cells analyzed by a luciferase coupled assay. B: NADH level of Q_0-YFP, Q_{30}-YFP and Q_{56}-YFP expressing yeasts. C: Mitochondrial staining of Q_0-YFP and Q_{56}-YFP expressing cells with MitoTracker. Scale Bar: 5 µm. Expression pattern of Cox4p and OM45p fused to GFP in Q_0- and Q_{56}-mCherry expressing cells. Exposure time is not changed between Q_0- and Q_{56}- mCherry expressing yeasts. Scale bar represents 10 µm.

As differences in these markers are not detectable the general mitochondrial appearance was investigated via fluorescence microscopy (Figure 26C). In control and *pica* cells

mitochondrial structures were clearly visible by staining the cells with MitoTracker. Hence membrane potential is still intact in *pica* yeasts. Investigating the genomic fusion of GFP to mitochondrial proteins was carried out next. The mitochondrial membrane protein Om45 was unaffected in expression levels or cellular localization (Figure 26C). Nevertheless Cox4, a component of the respiratory chain complex, was strongly diminished in *pica* cells. This implies that specific mitochondrial proteins are affected, while the overall appearance is still intact. Conclusively a connection between polyQ toxicity and specific mitochondrial impairment becomes evident in *pica* cells, as overall energy metabolism is still functional.

5.3.8 Polyglutamine Constructs Are Processed via Autophagy

Is the heat-shock response induced by aggregation of toxic polyQ proteins or by stress of increased iron concentrations in the yeast model? Analyzing the transcriptional response it became evident that the heat-shock response is not activated in Q_{56}-YFP expressing yeasts (Figure 27). Via cluster analysis two additional connecting clusters became visible. Neither the trehalose induction nor the proteasomal system was up-regulated by polyQ constructs (Figure 27). Misfolded proteins are targeted by the ubiquitin system and subsequently degraded by the proteasome. In other model systems polyglutamines were found to interfere with the ubiquitin proteasome system (UPS) (Hipp *et al*, 2012; Verhoef *et al*, 2002). For an analysis beyond the transcriptional response, markers of the ubiquitin proteasome system fused to GFP were analyzed via fluorescence microscopy (Figure 28A). Hereby Ufd4, a ubiquitin protein ligase, which interacts with the proteasome, changed its localisation upon Q_{56}-mCherry expression (Figure 28A, Xie & Varshavsky, 2000). Furthermore, differences in the E3-ligase Pep5 and in the E1-ligase Uba1 were not detectable. Likewise, Scl1, one subunit of the core complex of the 20 S proteasome was not altered in its expression level. A slight shift in localization becomes visible in Q_{56}-mCherry expressing yeasts as more tubular structures were detected compared to Q_0-mCherry expressing cells. Hence, in agreement with the microarray data, parts of the ubiquitin proteasome system seem to react to polyglutamine constructs with localization differences but not with overall expression changes.

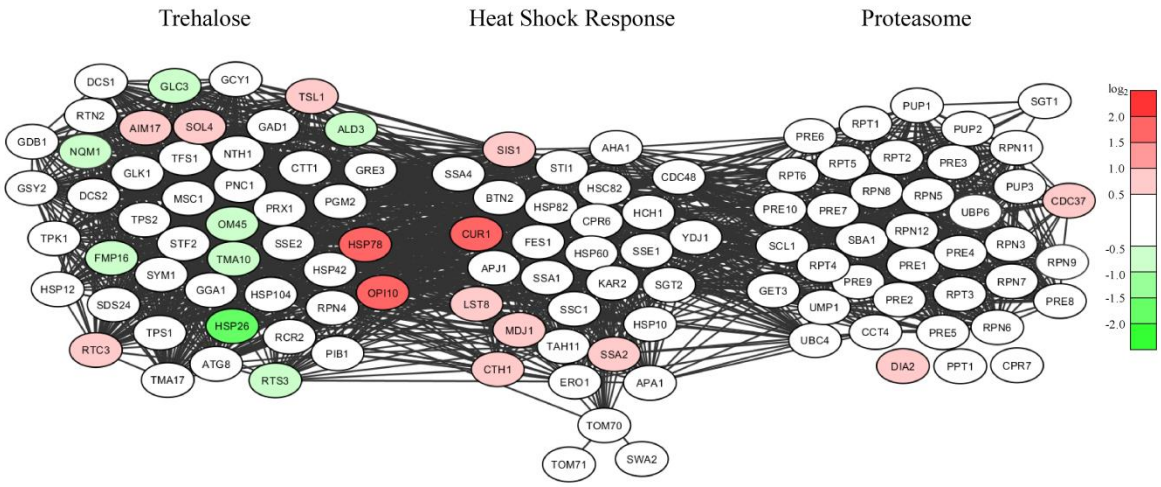

Figure 27 Network of selected genes not regulated in Q_{56}-YFP compared to Q_0 expressing yeast. Genes are colored according to their log differences (100% green: 100% green: log2>2, 75% green: 2>log2>1.5, 50% green: 1.5>log2>1, 25% green: 1>log2>0.5, white: 0.5>log2>-0.5, 25% red: -0.5>log2>-1, 50% red: -1>log2>-1.5, 75% red: -1.5>log2>-2, 100% green: -2>log2.

Beyond this pathway damaged protein aggregates and cellular organelles can be removed by an additional mechanism termed autophagy (Feng *et al*, 2014). This system is known to respond to cellular stresses such as nutrient shortage including sulfur and carbon starvation. Localization and expression levels of autophagy related proteins tagged with GFP were investigated (Figure 28). In yeast more than 30 autophagic proteins exist which regulate double membrane phagopore assembly engulfing around the target, phagopore maturation and subsequent fusion with the vacuole (Feng *et al*, 2014). Atg1 is one of the first proteins regulating phagopore assembly, the structure which maturates to the autolysosome (Feng *et al*, 2014). Upon expression of Q_{56}-mCherry the punctual localization of Atg1 was lost, its expression enhanced and the protein was transferred to the vacuole (Figure 28B). Atg2, Atg21 and Atg27 are part of a cycling system, which delivers membrane to the expanding phagopore. Overall expression changes in Atg2 or in Atg21 were not observed upon Q_{56}-mCherry expression. Nevertheless punctual localization was lost for Atg2. Instead expression of Atg27, an integral membrane protein involved in autophagy vacuole assembly was up-regulated upon polyQ expression (Figure 28B). Atg16, which is part of the ubiquitin-like conjugating system during phagopore assembly, was up-regulated in response to polyQ expression. Autophagy of bulky aggregates termed macroautophagy can be divided into selective and son-selective pathways. The two selective pathways are the cytosplasm-to-vacuole targeting pathway (CVT) and the organelle specific degradation pathways as termed mitophagy for mitochondria. Both, Atg11 and Atg19 are receptor and adaptor proteins for vesicle fusion in mitophagy and the CVT pathway. Those proteins were not altered in Q_{56} expressing yeasts (Figure 28B). Thus

mechanisms involved in phagopore assembly and expansion are altered in Q_{56}-mCherry expressing cells. Specific degradation of aggregates via the CVT pathway does not take place. In addition targeting mitochondrial degradation via mitophagy is not induced although mitochondrial functions have been shown to be diminished (5.3.6).

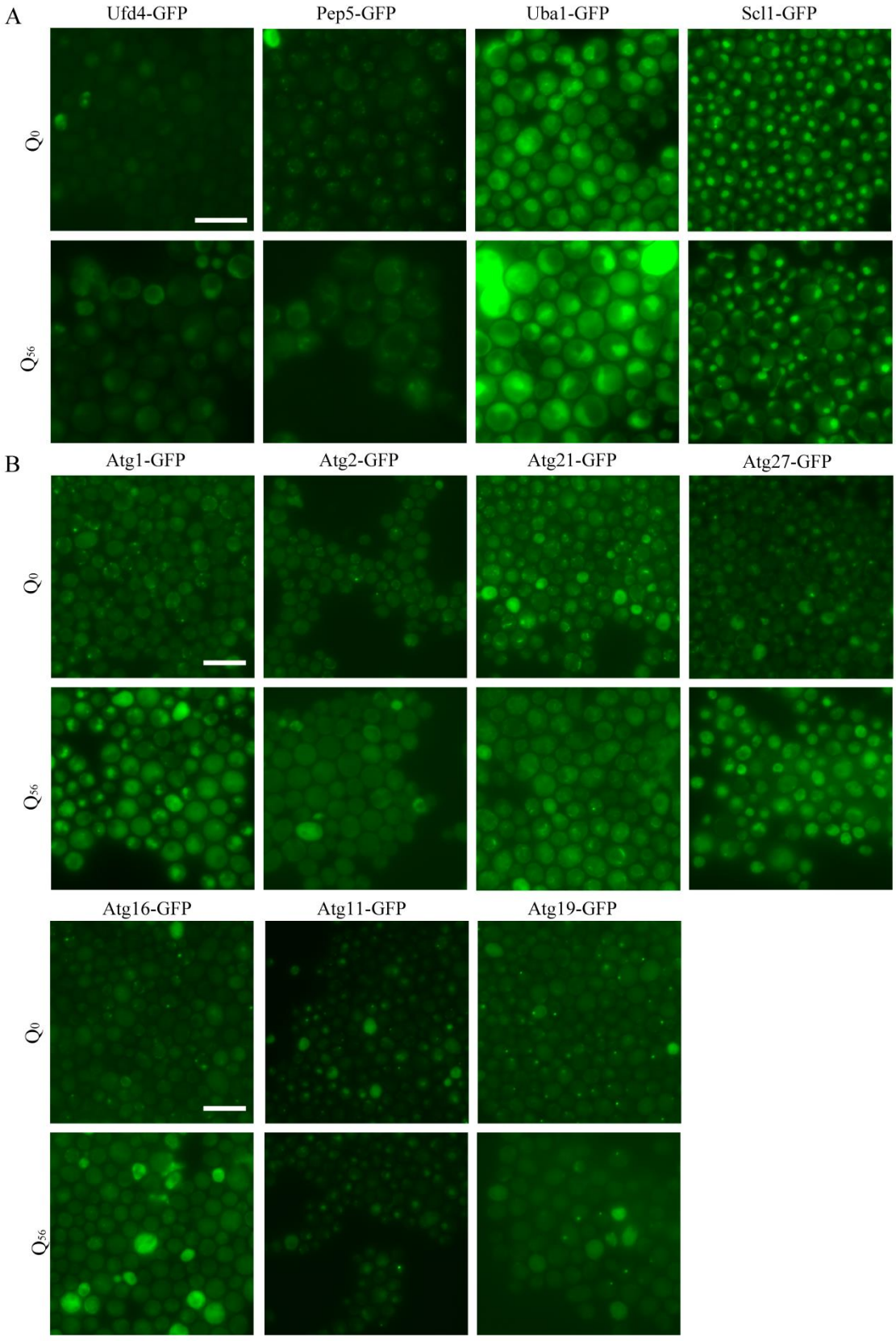

Figure 28 Expression pattern of proteins related to protein degradation systems were analyzed. A: Components of the ubiquitin proteasome system fused to GFP were observed. Rpn4, Pep5, Uba1 and Scl1 fused to GFP were analyzed in the presence of Q_0- and Q_{56}-mCherry. Exposure time was not altered between Q_0- and Q_{56}-mCherry expressing yeasts. Scale bar represents 10 µm. B: Components of the autophagy system fused to GFP were observed. Atg1, Atg2, Atg21, Atg16, Atg27, Atg11 and Atg19 fused to GFP were analyzed in the presence of Q_0- and Q_{56}-mCherry. Exposure time was not altered between Q_0- and Q_{56}-mCherry expressing yeasts. Scale bar represents 10 µm.

5.4 Investigating Similarities between Aggregation Systems

In order to dissect how toxicity is mediated, another model construct besides the polyglutamine stretch was analyzed. The viral protein precursor VP0 was investigated as a model protein with no known cellular functions in yeast. In 2014 Dr. Rehn detected that yeasts expressing the poliovirus precursor VP0 resemble the *pica* phenotype (Rehn, 2014). Mutation of the myristoylation domain glycine 2 to alanine results in a loss of toxicity in yeast (Rehn, 2014). Interestingly aggregation in this case does not correlate with toxicity as VP0 and VP0 G2A both aggregate when expressed in yeast (Rehn, 2014). It remains to be addressed how the toxicity is mediated in an organism, which is no host for the poliovirus. Mechanisms known to be induced by polyglutamine stretches are investigated whether they are activated in VP0 expressing cells.

5.4.1 Polyploidy Rescues Toxicity in other Systems

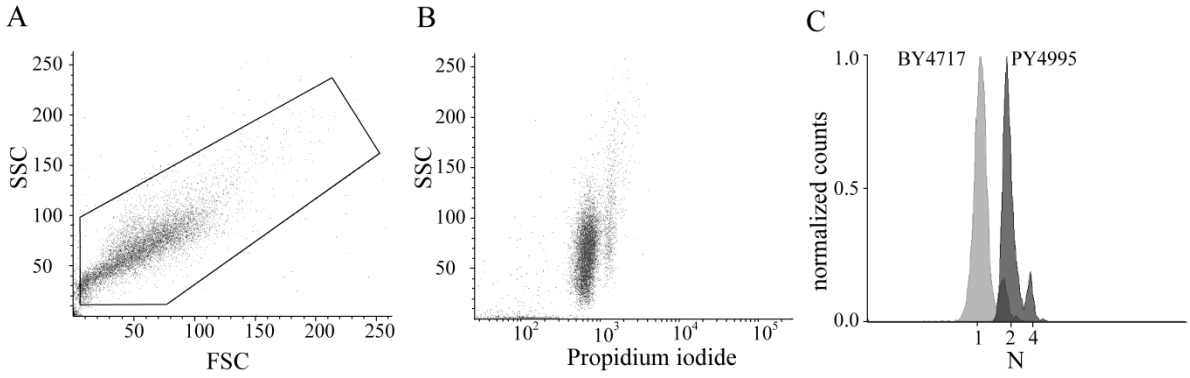

Figure 29 FACS analysis of aggregate expressing yeasts. A: Forward scatter plotted against sideward scatter show different particle size distribution within the mixture of stained BY4741 cells. Cells were gated according to the box to exclude cell debris. B: Sideward scatter plotted against logarithmic propidium iodide fluorescence of propidium iodide stained BY4741. Two distinct populations are visible. In grey: the larger peak corresponds to haploid BY4741 yeasts, the smaller one to haploid budding yeasts. In black: The larger peak corresponds to diploid PY4995 yeasts, the smaller one to diploid budding yeasts C: To create a better overview the normalized number of events is plotted against the logarithmic propidium iodide fluorescence. Peak in light grey represents BY4741 cells, the peak in dark grey represents PY4995 cells.

Dr. Kaiser screened a knockout library to identify modifiers of polyglutamine toxicity and found 32 genes to enhance toxicity in Q_{56}-YFP expressing yeasts (Kaiser, 2012). Most of the genes induce polyploidy if deleted. Polyploidy rescues polyQ toxicity and yeasts tend to alter their ploidy status in the presence of extended polyglutamine stretches. Indeed, diploid yeasts are insensitive to Q_{56}-YFP and the *pica* phenotype is impeded. Dr. Rehn

investigated these deletion mutants and could show that polyploidy rescues VP0 toxicity likewise (Rehn, 2014).

Now further effects of this system were analyzed. By means of FACS it was analyzed how yeasts respond to VP0-CFP with respect to their ploidy status. Therefore yeast cells were harvested from SD plates, fixed and stained with propidium iodide. The ploidy status was monitored via propidium iodide staining and fluorescence intensity plotted logarithmically. The cells were gated to avoid cell debris as shown in Figure 29A. In stained BY4741 cells two distinct populations can be monitored when plotting the sideward scatter to the propidium iodide fluorescence intensity (Figure 29B). Haploid BY4741 cells and diploid PY4995 cells were taken as references and all histograms were normalized to the fluorescence intensity of the 1N peak of strain BY4741 (Figure 29C). Cell populations exhibit a shoulder, monitoring the cells during budding. For VP0-CFP the *pica* like phenotype is present and the intoxicated small colonies as well as the rescuing big colonies were monitored. Here the rescuer colonies, exhibiting a faster colony growth, show a greater diploid peak (Figure 30A, grey) compared to the VP0-CFP small cells (Figure 30A, black). Nevertheless the shift in the ploidy status is not as strong as seen for Q_{56}-YFP expressing yeast (Kaiser, 2012). The non-toxic VP0 G2A-CFP mostly grew in a haploid form (Figure 30B). Thus other aggregation systems likewise are able to induce ploidy shifts.

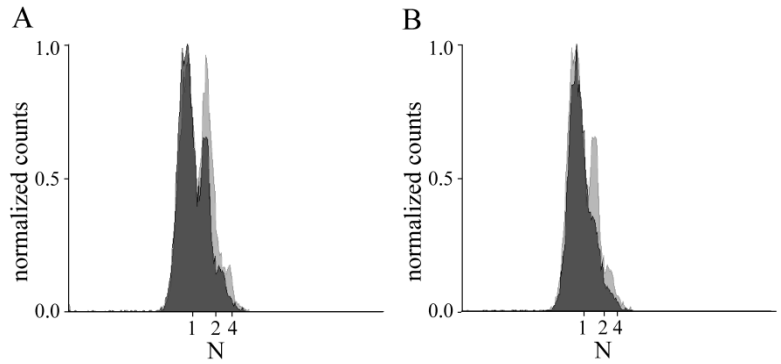

Figure 30 FACS analysis of VP0 expressing yeasts. Cells were gated as described above (Figure 29A). The normalized number of events is plotted against the normalized fluorescence intensity of the 1N peak of strain BY4741. A: Peak in grey represents cells transfected with VP0 from small, intoxicated colonies. The peak in black represents cells transfected with VP0 from big rescuer colonies. B: Peak in grey represents cells transfected with VP0 from small, intoxicated colonies. The peak in black represents cells transfected with the non-toxic VP0 G2A.

As polyploidy was seen as a rescuer of toxicity the aggregation of the constructs was analyzed via fluorescence microscopy in haploid and diploid yeast strains. No difference in VP0-CFP aggregation formation was observable comparing haploid and diploid

transfected yeasts. Aggregates were observed in both cell types. Non-toxic VP0-G2A-CFP was used as a control. In agreement with solubility data obtained by Dr. Rehn VP0 G2A-CFP also aggregated although it rescued toxicity regarding the *pica* phenotype. VP0 G2A-CFP in haploid BY4741, VP0-CFP and VP0 G2A-CFP in diploid PY4995 were expressed to a higher amount, although all constructs were expressed under the same promoter and are processed similarly. Interestingly higher expression levels seem to correlate with a loss of toxicity of the construct in the corresponding yeast strain (Figure 31).

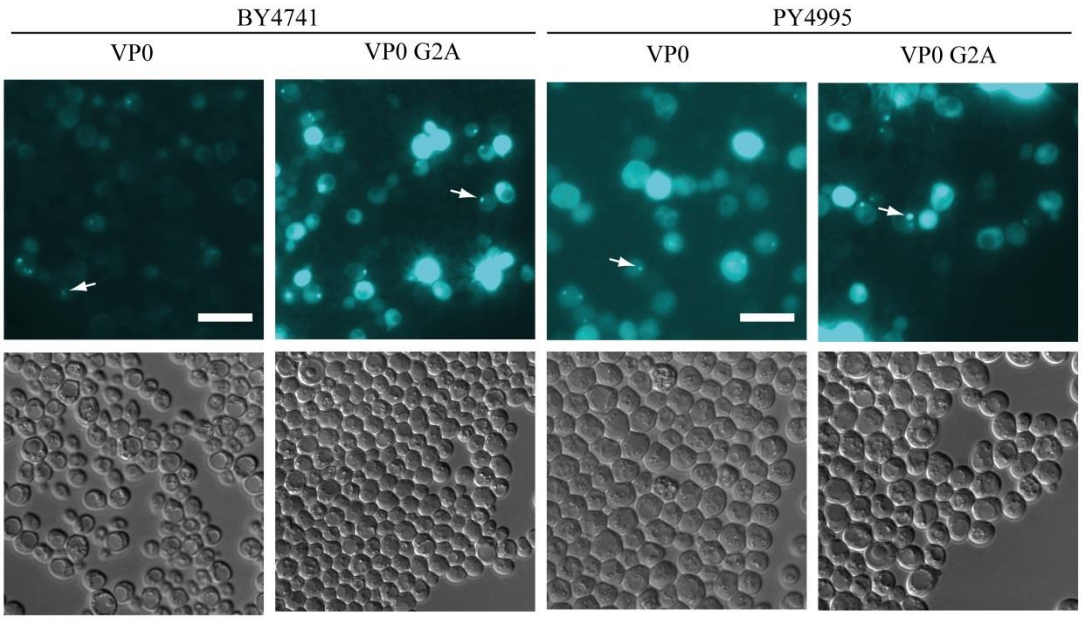

Figure 31 Aggregate morphology of the toxic poliovirus precursor protein VP0-CFP and the non-toxic VP0 G2A-CFP expressed by haploid BY4741 or diploid PY4995 cells. Exposure times are not changed between the samples. Aggregates are highlighted by an arrow. Scale bar represents 10 µm.

5.4.2 Poliovirus Precursor VP0 Induces Polyphosphate Production

To investigate if the detected mechanisms found for polyQ intoxication are part of a general aggregation response or if aggregate specific pathways exist, VP0-CFP aggregation was further elucidated. Polyphosphate enrichment was shown in Q_{56}-YFP expressing cells. Indeed, comparable to polyQ, polyphosphate induction was visible in toxic VP0-CFP expressing cells but not in the non-toxic VP0 G2A-CFP (Figure 32A). In the presence of all VP0 constructs the polyphosphate level exceeded the level of orthophosphate (Figure 32A). Interestingly heat-shock itself does not induce polyphosphate but rather orthophosphate accumulation (Figure 32B). Hence the enrichment of polyphosphate in comparison to other phosphate species is a process coupled to the presence of toxic aggregate species.

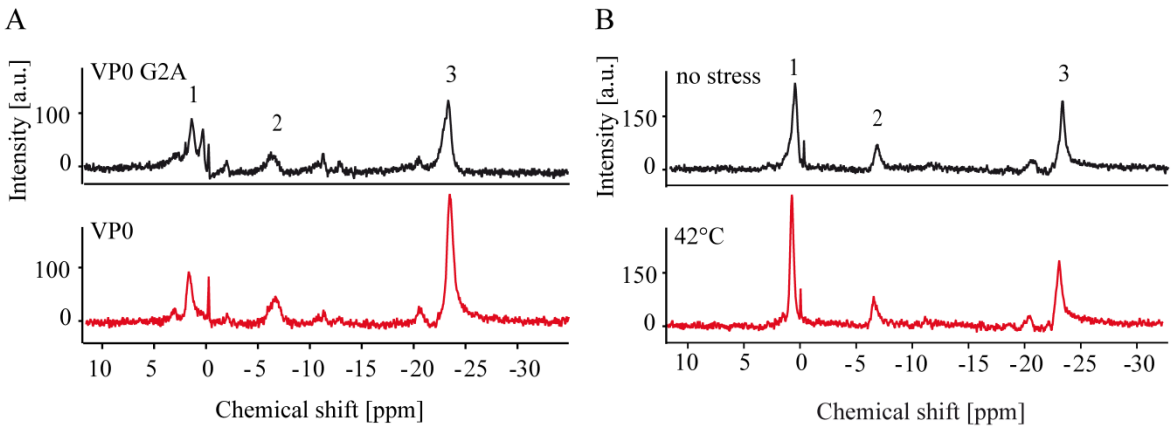

Figure 32 ^{31}P phosphate NMR spectra of yeasts expressing toxic polio virus VP0-CFP and non-toxic VP0 G2A-CFP. A: spectra of yeast cells in presence of either VP0 G2A (top) or VP0 (bottom). Aggregate production is controlled by the GPD promoter. Yeasts were resuspended in phosphate free buffer and spectra recorded immediately after harvesting. Peak assignments are listed in Table 16. 1: inorganic phosphate, 2: polyphosphate (end of chain), 3: polyphosphate (internal). B: Heat-shock does not induce polyphosphate accumulation. BY4741 cells were grown to a stationary phase in liquid YPD with and without 1 h heat-shock at 42°C. Yeasts were resuspended in phosphate free buffer and spectra recorded immediately after. Peak assignments are listed in Table 16. 1: inorganic phosphate, 2: polyphosphate (end of chain), 3: polyphosphate (internal).

5.4.3 Poliovirus Precursor Does Not Interfere with Septin Ring Assembly but Reduces Cox4 Levels

Related mechanisms seem to be activated by the presence of toxic Q_{56}-YFP and VP0-CFP expressing yeasts. Genomic GFP fusions of markers known to be involved in Q_{56}-mCherry were investigated in context of VP0-CFP intoxication. Q_{56}-mCherry was shown to interfere with the septin ring formation in budding yeasts. Additionally levels of Cox4, a protein part of the respiratory chain complex, were found decreased. Next it was tested, whether the localization of these proteins was also affected in VP0 producing yeasts. As a control the non-toxic VP0 G2A-CFP construct was used. The septin Shs1 and septin localized Cdc10 form ring-like structures, which were not disturbed by VP0-CFP (Figure 33A). VP0-CFP did not induce changes in localization of Cdc10 or Shs1-GFP. Thus the disturbance in septin ring assembly likely is a polyglutamine specific process. As mitochondrial proteins are altered in Q_{56}-mCherry expressing yeasts, these markers were also tested in the context of VP0. Indeed, VP0-CFP induces reduction of mitochondrial protein Cox4 (Figure 33B). Here VP0 G2A-CFP showed increased Cox4-GFP expression compared to VP0-CFP. In accordance with the findings regarding the polyglutamine system no alterations in the outer membrane protein Om45 were found comparing VP0-CFP and VP0 G2A-CFP (Figure 33B).

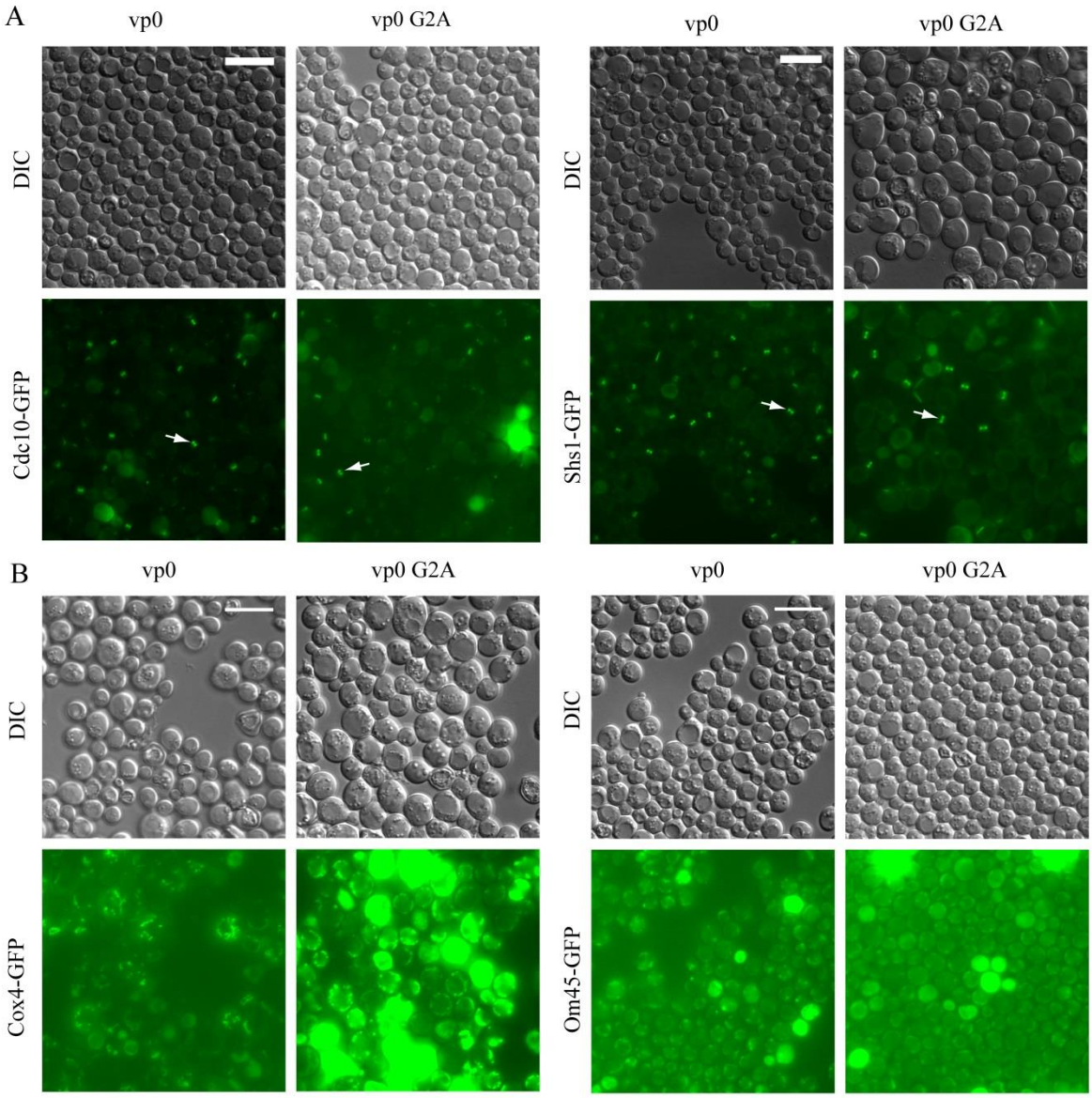

Figure 33 Morphology markers for septin assembly and mitochondrial integrity in yeasts expressing the toxic poliovirus precursor protein VP0-CFP and the non-toxic VP0 G2A-CFP. A: Cdc10 localizes to the septin ring (arrow). The septin ring can be further observed by the septin Shs1 (arrow). B: The proteins Cox4 and Om45 localize to mitochondria. Exposure times are not changed between the samples. Scale bar represents 10 µm.

6. Discussion

The cellular proteostasis network maintains the folding state of the proteome and responds to acute cellular stress and aging. Thereby the folding of unfolded proteins is promoted and misfolded protein degradation controlled. A balanced system containing chaperones, disaggregases and the degradation system is required for cellular homeostasis. A misregulated proteostasis network can lead to neurodegenerative, cardiovascular and metabolic disorders.

A tight regulation of the proteostasis network is required for tissue maintenance in all multicellular organisms. Muscular structures in the model organism *C. elegans* require the control by the Hsc70 chaperone cycle and its cochaperones. Misbalances in this system lead to a failure in muscular integrity. Here, it was addressed how the muscular integrity is regulated by Hsc70 together with UNC-23 and DNJ-13. Screening for small compounds was carried out to find modifiers of the Hsc70 chaperone cycle in isolated protein assays. Altering this cycle would be of great interest to find new therapeutic approaches. Once the proteostasis network is misbalanced due to an overload of mutant proteins as in polyglutamine diseases toxic event occur. In this thesis toxic polyglutamine stretches were investigated in *S. cerevisiae* to dissect the exact processes which drive toxicity.

6.1 The Balanced Regulation of Hsc70 by UNC-23 and DNJ-13 is Required For Muscle Functionality[3]

The Bcl-2-associated athanogene (BAG)-family proteins are nucleotide exchange factors for Hsc70 and conserved through evolution with homologs in mammals, invertebrates *(C. elegans, D. melanogaster*), plants *(A. thaliana)* and yeast (*S. cerevisiae*) (Takayama *et al*, 1999; Sondermann, 2001; Mayer & Bukau, 2005; Kabbage & Dickman, 2008). They often contribute functionality to the Hsc70 machinery. BAG proteins, including Bag1, are known to bind Hsc70 targets such as the protein kinase Raf1, ubiquitin ligases, retinoic acid receptors and growth factor receptors. Thereby nucleotide dissociation dependent delivery of Hsc70 bound clients is connected with cellular processes (Arndt, Daniel, Nastainczyk, & Alberti, 2005b; Dai et al., 2005; J Höhfeld & Jentsch, 1997; Kabbage & Dickman, 2008;

[3] This chapter is published in the *Journal of Biological Chemistry* (Papsdorf *et al*, 2014)

Liu, 1998; Song, Takeda, & Morimoto, 2001; Takayama et al., 1999). However, the exact role of Hsc70 connected to the client processing activity is unknown in these events. Here the interaction of the nematode BAG protein UNC-23 with the Hsc70 chaperone system is investigated. UNC-23 is a NEF with a rather low affinity for Hsc70. It is required to maintain muscular integrity during development and aging of *C. elegans*. UNC-23 is one of few genes known to be involved in muscle attachment, a phenotype commonly termed *mua* (Plenefisch, Zhu, & Hedgecock, 2000b).

A potential mechanism for UNC-23 function in cooperation with Hsc70 and its cofactor DNJ-13 is postulated by the characteristics of the UNC-23 protein and the *in vivo* data presented here (Figure 34). Among other cellular localizations, UNC-23 is prominent as part of the dense body structures. This could be relevant for the stability of the muscle cells or the ultrastructure of the myofilaments, which is compromised if UNC-23 is mutated or during *unc-23* RNAi (Waterston *et al*, 1980; Meissner *et al*, 2009; Rahmani, 2002). A loss of this specific localization to the dense bodies can be observed if the N-terminus is deleted. Presumably the full-length protein is required for the correct localization to the attachment sites, whereas the C-terminus regulates Hsc70 related functions.

The rescue of the *unc-23* mutant allele by the reduction of DNJ-13 levels and the mimicking of the phenotype by overexpression of CFP-Hsc70 clearly points to an involvement of the wider Hsc70 system to fulfill the important UNC-23 functions. *In vitro* DNJ-13 supports exactly the opposite conformational states of Hsc70 in terms of ATP-binding and client processing, locking Hsc70 in an ADP-client bound state, while BAG proteins facilitate client and nucleotide release. Thus, in the absence of UNC-23, DNJ-13 may indeed be harmful, hindering the discharge of nucleotides and clients. The Hsc70-system without both cofactors apparently is able to sufficiently support muscle attachment, rendering the knock-down of DNJ-13 beneficial under these conditions (Figure 34C). Besides, a competitive mechanism of cofactor directed Hsc70 localization can be envisioned for DNJ-13 and UNC-23.

Are homologous functions conserved in mammalian BAG-proteins? Human Bag2 is known to be involved in the cellular stress response and proteosomal degradation pathways, regulating the degradation of tau fragments and the cystic fibrosis transmembrane conductance regulator (CFTR) together with Hsc70 and CHIP (Arndt et al., 2005b; Dai et al., 2005). Nevertheless, muscle-related functions are not reported to date. Human Bag3 instead controls the degradation of filamin in mammalian muscle cells (Ulbricht *et al*, 2013). The wider processes are regulated by the chaperone-associated

autophagy network to maintain the filamin balance in the muscle and ensure muscular homeostasis (Ulbricht et al., 2013; Ulbricht & Höhfeld, 2013). In mice Bag3 interacts with damaged filamin, which is targeted for degradation via the Hsc70/HspB8/CHIP system (Ulbricht *et al*, 2013). Indeed, Bag3 and filamin C mutations are responsible for a large fraction of genetic myofibrillar myopathies in humans (Selcen *et al*, 2010; Vorgerd *et al*, 2005; Harms *et al*, 2013).

The homology to the mammalian system here is astonishing, in particular as UNC-23 combines sequence elements of the human Bag2, Bag3 and Bag4 proteins. Probably this involvement is also relevant for the muscular attachment functions of the BAG-domain containing UNC-23 in *C. elegans*. Dense bodies are integrin based adhesion complexes and resemble vertebrate focal adhesion complexes, which contain filamin in *C. elegans* (Tu *et al*, 2003; Hynes, 1992). Thus it is tempting to speculate that UNC-23 fulfills similar tasks in *C. elegans*, even though the direct interaction partners of UNC-23 remain to be identified (Papsdorf *et al*, 2014).

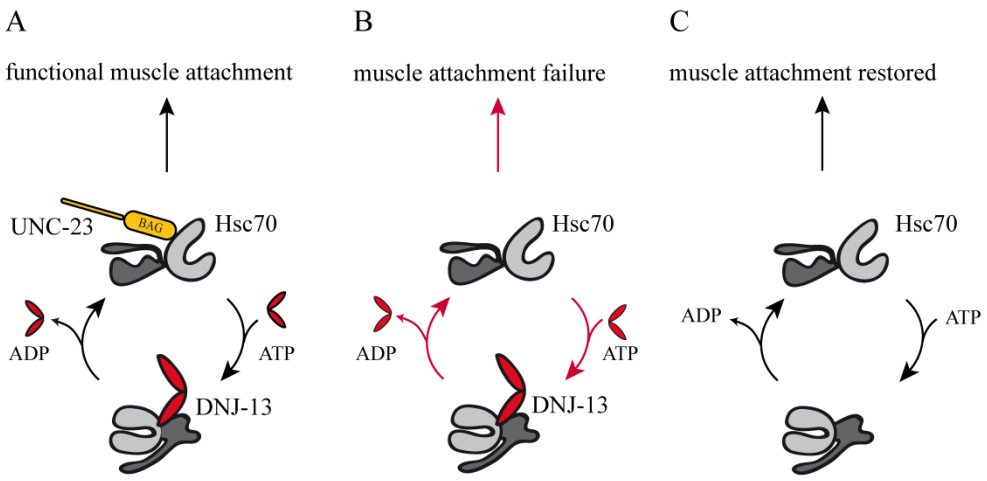

Figure 34 Role of UNC-23 in muscle maintenance. Schematic model of Hsc70 function in C. elegans muscle attachment. UNC-23 is depicted in red with the highlighted BAG-domain. Hsc70 with its substrate binding domain (dark grey), the nucleotide binding domain (light grey) and the helical lid. DNJ-13 is shown in green. A: Under physiological conditions. B: The attachment fails if UNC-23 is not present, C:If the two cofactors UNC-23 and DNJ-13 are missing the Hsc70 cycle is able to restore muscle attachment (Papsdorf *et al*, 2014).

6.2 Modulator Screen of the Hsc70/DNJ-12/BAG-1 System

The Hsc70 family is an essential protein system conserved through all kingdoms of life. It is a tightly regulated protein with cochaperones altering its cycle. It carries out its cellular functions in response to stress and during physiological conditions. Hsc70 has been shown to be involved in a wide range of processes and diseases such as cancer, neurodegenerative

diseases, immune responses and infections (Mayer & Bukau, 2005). Thus, it is of great interest to search for modifying compounds (Evans *et al*, 2010). It still is under discussion whether it is beneficial to stimulate, inhibit or redirect the activity of Hsc70.

In order to address this issue the focus was set on the detection of compounds modifying the ATPase activity of nematode Hsc70. The system with the highest ATPase activity was chosen for the modulator screen. A library consisting of 10 000 substances was screened with respect to their ability to modify the Hsc70/DNJ12/BAG1 system. Surprisingly no inhibitors were found to reduce the ATPase activity of Hsc70 potentially due to the high affinity of Hsc70 for nucleotides. Three different hits were found to activate Hsc70 ATPase 70Mod1, 70Mod2 and 70Mod3 (Figure 35).

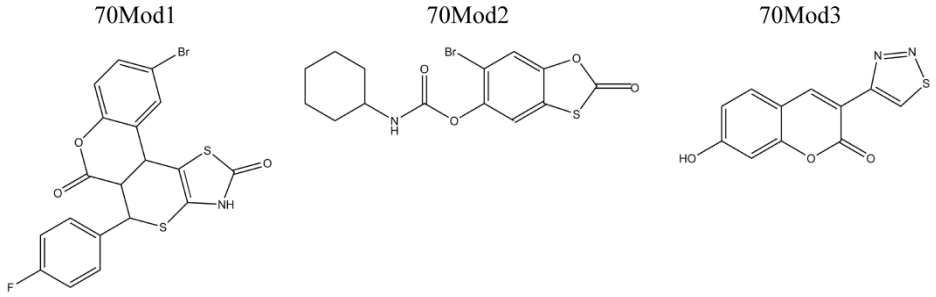

Figure 35 The nematode Hsc70 system´s ATPase modulators 70Mod1, 70Mod2 and 70 Mod3.

The compounds can be largely classified into heterocycles. The systematic name of 70Mod1 is 5(4-fluoroplhenyl)-10-methyl-3,5,5a,11b-tetrahydro2*H*,6*H*-chromeno[4´,3´:4,5]thiopyrano [2,3d]thiazole-2,6 dione, of 70Mod2 is 6-bromo-2-oxobenzo [d][1,3]oxathiol-5-yl cyclohexylcarbamate and of 70Mod3 is 7-hydroxy-3(1,2,3-thiadiazol-4-yl)2H-chromen-2-one. Here 70Mod1 and 70Mod2 both contain coumarin rings, which may hint to a possible role of this structure in interfering with the Hsc70 system. Apart from their heterocyclic structure these compounds are not similar to the reported Hsc70 inhibitors. The thiazole structure may be found in other compounds such as the rhodacyanine MKT-077, nevertheless overall large structural differences are present. The coumarin ring can also be found in other chaperone inhibitors such as the Hsp90 compound Novobiocin. Modifying Novobiocin to KU-32 resulted in a compound, which also affects Hsc70 expression (Urban *et al*, 2010). Exact studies on the mechanism were not performed yet. For the identified modulators 70Mod1-3 it remains to be addressed how the compounds bind to Hsc70, which is their affinity to the protein and which protein complex is altered by adding the modifiers. Additionally studies on the general handling

and storage will be carried out as degradation might be problematic. If specificity regarding the cochaperones exists the substances provide a great chance to further study the effects of alterations in the Hsc70 system *in vitro* and potentially *in vivo*.

6.3 Polyglutamine Toxicity in Yeast Induces Metabolic Alterations and Mitochondrial Defects[4]

Elongated polyQ stretches have been reported as genetic cause for several neurodegenerative diseases, including Huntington's disease (Kaiser *et al*, 2013; Krobitsch & Lindquist, 2000; Labbadia & Morimoto, 2013; Orr & Zoghbi, 2007). The reasons for this toxicity and the cellular pathways relevant for this process are under debate and many alterations have been reported, including DNA-fragmentation, apoptosis, spindle disorganization and involvement of the chaperone system or diverse prion proteins (Kaiser *et al*, 2013; Treusch & Lindquist, 2012; Sokolov *et al*, 2006; Manogaran *et al*, 2011). Here a toxic polyQ system composed of 0, 30 or 56 glutamine residues has been applied to expose affected cellular pathways. First evidence which processes are affected was found based on an un-biased approach starting from a genome-wide screen of the EUROSCARF deletion strain library and a genome-wide assessment of expression changes upon intoxication by Dr. Kaiser (Kaiser, 2012).

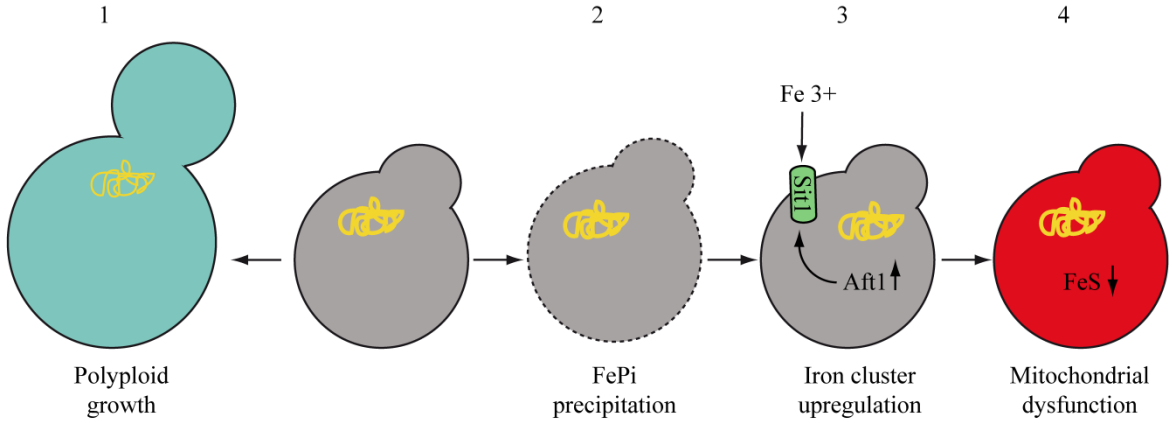

Figure 36 Hypothetical response to toxic polyglutamine stretches. Upon Q_{56}-YFP (yellow) expression the yeast can grow in a diploid form and overcome toxicity (1). The phosphate metabolism is an early event which is deregulated. Depicted in 2 is the iron shortage, which can hypothetically be explained by the precipitation with phosphate inside the vacuole (Cockrell et al., 2011). *Due to iron shortage up-regulation of iron cluster transcription factor Aft1 and subsequently the corresponding iron transporter is induced (3). Later events affect mitochondrial functionality resulting in an iron-sulfur cluster shortage and inability to grow when the mitochondrial system is challenged (4).*

[4] This chapter is submitted to BMC Genomics (Papsdorf *et al*, 2015)

Fourteen genomic deletion strains were uncovered that act synergistically with the polyQ induced phenotype, which were mostly associated with mitochondrial functions. Some of these have been associated with the *petite*-phenotype before, a small-colony formation phenotype, which can be intensified by cultivation on non-fermentable growth media (Contamine & Picard, 2000). Given the similar appearance of polyQ-intoxicated *pica* yeasts, a related cause for these phenotypes could be assumed, in particular as *pica* is similarly not able to form any colonies on non-fermentable carbon sources. This information points to a mitochondrial impairment in *pica* yeasts and led to further analysis.

The transcriptional profiling stated here also uncovers pathways with mitochondrial association and suggests the iron- and sulfur-metabolism as a potential target. Both pathways converge in the mitochondria during Fe-S cluster synthesis (Lill *et al*, 2012; Netz *et al*, 2014). The iron cluster includes the iron importers of the plasma membrane and several other proteins, which regulate the distribution and metabolism of iron ions in the cell. Generally this transcriptional cluster is activated by the lack of or shortage of Fe-S cluster proteins via the Fe-S containing sensor complex Grx (Outten & Albetel, 2013; Rutherford *et al*, 2005). This reduction becomes obvious in our system by the reduced activity of aconitase, a very prominent Fe-S cluster protein in the cytosol. Aconitase usually catalyzes the isomerization from citrate to isocitrate in the citric acid cycle (Beinert *et al*, 1996). The shortage in aconitase is not due to transcriptional down-regulation as evident from the genome-wide expression data, which show only slightly up-regulated ACO1 and slightly down-regulated ACO2 expression, but is apparently due to reduced levels of active protein (ACO1: -0.35 $\log_2$; ACO2: 0.52 $\log_2$). The increased levels of iron in the cell do not necessarily have to imply that Fe^{2+} is sufficiently present in the mitochondria for generation of Fe-S clusters. Fe^{3+} could also be present in the cytosol or even in complex with polyphosphate in the vacuole, all of which could lead to a shortage of mitochondrial iron in the presence of excessive Fe^{3+} (Seguin *et al*, 2011). Interestingly, also Cox4p, a subunit of the cytochrome C oxidase complex (Complex IV) in the mitochondria and highly sensitive to polyQ intoxication, is part of a multi subunit protein, which complexes iron ions (Maréchal *et al*, 2012). Thus proteome-wide data are necessary to confirm whether especially iron-containing proteins are affected by the presence of polyQ aggregates. It is tempting to speculate that metabolic disabilities observed by the disability to grow on non-fermentable carbon sources and the mitochondrial phenotype might be due to the lack in functional aconitase or respiratory chain complexes.

The cellular response to toxic aggregate stress is a complex chain of events in the end leading to cellular death. Nevertheless it is not fully understood which pathways are directly affected and which are activated as a consequence. The transcriptional response provided a great platform to analyze the cellular effect of toxic polyglutamine aggregates. Further dissecting the transcription factors regulating the affected genes is of great interest. Strikingly the transcription factors controlling down-regulation and up-regulation of the genes retrieved in the microarray study do overlap including Msn2, Gcn4, Spt20, Tup1 and Met32. While Tup1 and Spt20 are involved in wider transcription processes, Msn2 is a stress response specific transcription factor activated upon to multiple stresses (Courey & Jia, 2001; Roberts & Winston, 1996; Martínez-Pastor *et al*, 1996). Instead Gcn4 induces a more specific response as it is activated in response to amino acid starvation. Additionally it plays a role in organelle biosynthesis and autophagy. Again amino acid starvation is identified as a result of polyglutamine intoxication although the polyQ intoxicated yeasts do not undergo nutrient starvation. Supporting previous data, Met32 regulating sulfur metabolic genes is found (P. Blaiseau, Isnard, Surdin-kerjan, & Thomas, 1997; P. Blaiseau & Thomas, 1998; Natarajan et al., 2001). The shared regulators imply that proteins exist which mutually up- and down-regulate the genes retrieved in the microarray studies. Regulation in the clusters may connect via shared transcription factors. To address this assumption the analysis was performed for the isolated clusters. Spt10, Ixr1 and Cfb1 were found in more than one cluster supporting this hypothesis. Additionally regulators were found which specifically are detected in one cluster. In this context Aft1 is observed which controls the up-regulation of the iron cluster. In addition Met32 and Met4 transcription factors are found to regulate the sulfur cluster and Pho4 and Pho2 transcription factors the phosphate cluster. Indeed this hints to a specific response of the yeast to toxic polyQ stretches which might connect via shared transcription factors.

In contrast to the expectations, the highly responsive heat-shock and stress response network of chaperones does not react to polyQ intoxication. This could imply that this part of the proteostasis network is not directly induced and that shortage of chaperones is not related to toxicity in this yeast model. As shown for other polyglutamine systems, the degradation of the aggregated proteins is performed mainly by the autophagy system (Qin *et al*, 2003; Ravikumar *et al*, 2002). Here mechanisms involved in phagopore assembly and expansion are altered in Q_{56}-mCherry expressing yeasts. Specific degradation of aggregates via the CVT pathway does not occur. In addition mitochondrial degradation via

mitophagy is not induced although mitochondrial functions have been shown to be diminished.

Several genome-wide studies had been performed in the past on similar aggregation systems in higher eukaryotes (Lejeune *et al*, 2012; Becanovic *et al*, 2010; Kaltenbach *et al*, 2007; Miller *et al*, 2012b; Branco *et al*, 2008). These uncovered a broad range of genetic and physical interactors. As such an RNAi screen in *C. elegans* uncovered metabolic influences, but mostly in connection with the ascorbate and aldarate system (Lejeune *et al*, 2012). Transcriptional changes in mutant huntingtin expressing mice and men point to genes in signal transduction more strongly (Becanovic *et al*, 2010), likewise do studies in mammalian cell culture based on RNA interference (Kaltenbach *et al*, 2007; Miller *et al*, 2012b). Also studies in *D. melanogaster*, employing huntingtin and ataxin as model systems find mostly genes in signal transduction and cellular proteostasis (Branco *et al*, 2008).

Beyond that, the damage to the mitochondrial system has been observed in other aggregation model systems repeatedly (Zhu *et al*, 2010; Tabrizi *et al*, 2000). In subsets of patients suffering from neurodegenerative diseases the involvement of mitochondrial damage or the involvement of iron metabolism has been described (Oliveira, 2010; Núñez *et al*, 2012). In several cases the reduction in aconitase and the reduction in respiratory chain complexes have been reported (Solans *et al*, 2006; Kim *et al*, 2005). Another striking example linking the iron metabolism to neurodegenerative disease is the protein frataxin, which itself is an iron importer into mitochondria. Due to an extension in intronic GAA repeats functional protein levels are decreased and neurodegenerative ataxias occur (Klockgether & Evert, 1998). While it is speculative to assume a common mechanism in generation of neurodegenerative defects in polyQ diseases, this study suggests that alterations and damages to the mitochondrial system are highly relevant for the toxicity observable upon expression of polyQ proteins in yeast. These damages manifest themselves via stressful alterations to the Fe-S cluster generating system and reduced metabolic abilities (Papsdorf *et al*, 2015).

6.4 The Cellular Response to VP0 Aggregates

In order to dissect the specificity of the yeast´s response to aggregates the poliovirus precursor protein VP0 was investigated. Yeasts transfected with VP0-CFP exhibit a similar

growth defect as Q_{56}-YFP transformed yeasts culminating in a *pica*-like phenotype present after transformation of the construct controlled by an ubiquitously active promoter (Rehn, 2014). To analyze whether the growth phenotype is rescued via the same cellular pathways, Dr. Rehn tested polyQ resistant deletion strains with respect to their growth in response to VP0 stress (Rehn, 2014, Table 19). Interestingly, strains with enhanced ploidy are more resistant not only to Q_{56}-YFP but also to VP0-CFP aggregation stress (Rehn, 2014). Nevertheless, yeasts exposed to toxic VP0-CFP aggregates show a slight alteration in their ploidy status. Thus changes in ploidy are observable regarding toxic aggregation systems but with a diverse intensity.

Both aggregation systems, VP0-CFP and Q_{56}-YFP, induce polyphosphate production. Interestingly heat-shock itself does not generate polyphosphate but rather orthophosphate accumulation. Hence the enrichment of polyphosphate in comparison to other phosphate species and the changes in the yeasts ploidy status are processes likely coupled to the presence of toxic aggregate species.

Aggregation in this context is not coupled to toxicity, as VP0-CFP and VP0 G2A-CFP both aggregate within the cell. It could be shown that higher expression levels seem to correlate with a loss of toxicity of the construct in the corresponding yeast strain. This hints to a potential interference of toxic VP0-CFP proteins with the cellular metabolism. This hypothesis is strengthened by the diminishment of cellular Cox4-GFP levels in response to VP0-CFP. Thus metabolic processes together with mitochondrial impairment might not only lead to the *pica* phenotype in polyglutamine but also to the toxicity of the VP0-CFP aggregation system.

7. References

Ahringer J (2006) Reverse Genetics. In *WormBook* p The C. elegans Research Community, doi/10.1895/wor.

Ali JA, Jackson AP, Howells AJ & Maxwell A (1993) The 43-kilodalton N-terminal fragment of the DNA gyrase B protein hydrolyzes ATP and binds coumarin drugs. *Biochemistry* **32:** 2717–24

Anfinsen CB (1972) The formation and stabilization of protein structure. *Biochemical Journal* **128:** 737–749

Arakawa A, Handa N, Shirouzu M & Yokoyama S (2011) Biochemical and structural studies on the high affinity of Hsp70 for ADP. *Protein science : a publication of the Protein Society* **20:** 1367–79

Arndt V, Daniel C, Nastainczyk W & Alberti S (2005) BAG-2 Acts as an Inhibitor of the Chaperone-associated Ubiquitin Ligase CHIP. *Molecular biology of the cell* **16:** 5891–5900

Arrasate M, Mitra S, Schweitzer ES, Segal MR & Finkbeiner S (2004) Inclusion body formation reduces levels of mutant huntingtin and the risk of neuronal death. *Nature* **431:** 805–810

Balch WE, Morimoto RI, Dillin A & Kelly JW (2008) Adapting proteostasis for disease intervention. *Science (New York, N.Y.)* **319:** 916–9

Bardwell JC & Craig EA (1988) Ancient heat shock gene is dispensable. *Journal of bacteriology* **170:** 2977–83

Becanovic K, Pouladi M a, Lim RS, Kuhn A, Pavlidis P, Luthi-Carter R, Hayden MR & Leavitt BR (2010) Transcriptional changes in Huntington disease identified using genome-wide expression profiling and cross-platform analysis. *Human molecular genetics* **19:** 1438–52

Beinert H, Kennedy MC & Stout CD (1996) Aconitase as Iron − Sulfur Protein , Enzyme , and Iron-Regulatory Protein. *Chemical Reviews* **96:** 2335–2374

Ben-Zvi A, Miller EA & Morimoto RI (2009) Collapse of proteostasis represents an early molecular event in Caenorhabditis elegans aging. *Proceedings of the National Academy of Sciences of the United States of America* **106:** 14914–14919

Bendz H, Ruhland SC, Pandya MJ, Hainzl O, Riegelsberger S, Braüchle C, Mayer MP, Buchner J, Issels RD & Noessner E (2007) Human heat shock protein 70 enhances tumor antigen presentation through complex formation and intracellular antigen delivery without innate immune signaling. *The Journal of biological chemistry* **282:** 31688–31702

Blaiseau P, Isnard A, Surdin-kerjan Y & Thomas D (1997) Met31p and Met32p , Two Related Zinc Finger Proteins , Are Involved in Transcriptional Regulation of Yeast Sulfur Amino Acid Metabolism. **17:** 3640–3648

Blaiseau PL & Thomas D (1998) Multiple transcriptional activation complexes tether the yeast activator Met4 to DNA. *EMBO Journal* **17:** 6327–6336

Bracher A & Verghese J (2015) The Networking of Chaperones by Co-chaperones Blatch GL & Edkins AL (eds) Cham: Springer International Publishing

Brachmann CB, Davies A, Cost GJ & Caputo E (1998) Designer Deletion Strains derived from Saccharomyces cerevisiae S288C : a Useful set of Strains and Plasmids for PCR-mediated Gene Disruption and Other Applications. **132:** 115–132

Branco J, Al-Ramahi I, Ukani L, Pérez AM, Fernandez-Funez P, Rincón-Limas D & Botas J (2008) Comparative analysis of genetic modifiers in Drosophila points to common and distinct mechanisms of pathogenesis among polyglutamine diseases. *Human molecular genetics* **17:** 376–90

Braun RJ, Büttner S, Ring J, Kroemer G & Madeo F (2010) Nervous yeast: modeling neurotoxic cell death. *Trends in biochemical sciences* **35:** 135–44

Brenner S (1974) The genetics of Caenorhabditis elegans. *Genetics* **77:** 71–94

Broadley S a. & Hartl FU (2009) The role of molecular chaperones in human misfolding diseases. *FEBS Letters* **583:** 2647–2653

Brown SJ, Kellett PJ & Lippard SJ (1993) Ixr1, a yeast protein that binds to platinated DNA and confers sensitivity to cisplatin. *Science (New York, N.Y.)* **261:** 603–5

Caplan AJ (2003) What is a co-chaperone? *Cell stress & chaperones* **8:** 105–7

Cellitti J, Zhang Z, Wang S, Wu B, Yuan H, Hasegawa P, Guiney DG & Pellecchia M (2009) Small molecule dnak modulators targeting the β-domain. *Chemical Biology and Drug Design* **74:** 349–357

Chang L, Bertelsen EB, Wisén S, Larsen EM, Zuiderweg ERP & Gestwicki JE (2008) High-throughput screen for small molecules that modulate the ATPase activity of the molecular chaperone DnaK. *Analytical biochemistry* **372:** 167–76

Chen S & Smith DF (1998) Hop as an adaptor in the heat shock protein 70 (Hsp70) and hsp90 chaperone machinery. *The Journal of biological chemistry* **273:** 35194–200

Chiti F & Dobson CM (2006) Protein misfolding, functional amyloid, and human disease. *Annual review of biochemistry* **75:** 333–66

Ciocca DR & Calderwood SK (2005) Heat shock proteins in cancer: diagnostic, prognostic, predictive, and treatment implications. *Cell stress & chaperones* **10:** 86–103

Cockrell A, L, Holmes-hampton GP, Mccormick SP, Chakrabarti M & Lindahl PA (2011) Mössbauer and EPR Study of Iron in Vacuoles from Fermenting Saccharomyces cerevisiae. *Biochemistry* **50:** 10275–10283

Contamine V & Picard M (2000) Maintenance and Integrity of the Mitochondrial Genome : a Plethora of Nuclear Genes in the Budding Yeast. *Microbiology and Molecular Biology Reviews* **64:** 281–315

Courey AJ & Jia S (2001) Transcriptional repression: the long and the short of it. *Genes & development* **15:** 2786–96

Dai Q, Qian S-B, Li H-H, McDonough H, Borchers C, Huang D, Takayama S, Younger JM, Ren HY, Cyr DM & Patterson C (2005) Regulation of the cytoplasmic quality control protein degradation pathway by BAG2. *The Journal of biological chemistry* **280:** 38673–81

Dam J & Schuck P (2005) Sedimentation velocity analysis of heterogeneous protein-protein interactions: sedimentation coefficient distributions c(s) and asymptotic boundary profiles from Gilbert-Jenkins theory. *Biophysical journal* **89:** 651–66

Demeler B, Brookes E, Wang R, Schirf V & Kim C a (2010) Characterization of reversible associations by sedimentation velocity with UltraScan. *Macromolecular bioscience* **10:** 775–82

Dill KA, Maccallum JL & Folding P (2012) The Protein-Folding Problem , 50 Years On. **:** 1042–1047

Doong H, Vrailas A & Kohn EC (2002) What's in the "BAG"?--A functional domain analysis of the BAG-family proteins. *Cancer letters* **188:** 25–32

Dosztányi Z, Csizmok V, Tompa P & Simon I (2005) IUPred: web server for the prediction of intrinsically unstructured regions of proteins based on estimated energy content. *Bioinformatics (Oxford, England)* **21:** 3433–4

Douglas NR, Reissmann S, Zhang J, Chen B, Jakana J, Kumar R, Chiu W & Frydman J (2011) Dual action of ATP hydrolysis couples lid closure to substrate release into the group II chaperonin chamber. *Cell* **144:** 240–52

Eddy SR (2009) A new generation of homology search tools based on probabilistic inference. *Genome informatics. International Conference on Genome Informatics* **23:** 205–11

Elble R (1992) A simple and efficient procedure for transformation of yeasts. *BioTechniques* **13:** 18–20

Ellis JR & Minton AP (2006) Protein aggregation in crowded environments. *Biol Chem* **387:** 485–497

Evans CG, Chang L & Gestwicki JE (2010) Heat shock protein 70 (hsp70) as an emerging drug target. *Journal of medicinal chemistry* **53:** 4585–602

Fairbanks G, Steck TL & Wallachl DFH (1968) Electrophoretic Analysis of the Major Polypeptides of the Human Erythrocyte Membrane. *Biochemistry* **10:** 2606–2617

Feller SM, Ren R, Hanafusa H & Baltimore D (1994) SH2 and SH3 domains as molecular adhesives: The interactions of Crk and Abl. *Trends in Biochemical Sciences* **19:** 453–458

Feng Y, He D, Yao Z & Klionsky DJ (2014) The machinery of macroautophagy. *Cell research* **24:** 24–41

Fewell SW, Smith CM, Lyon MA, Dumitrescu TP, Wipf P, Day BW & Brodsky JL (2004) Small molecule modulators of endogenous and co-chaperone-stimulated Hsp70 ATPase activity. *The Journal of biological chemistry* **279:** 51131–40

Frumkin A, Dror S, Pokrzywa W, Bar-Lavan Y, Karady I, Hoppe T & Ben-Zvi A (2014) Challenging muscle homeostasis uncovers novel chaperone interactions in Caenorhabditis elegans. *Frontiers in Molecular Biosciences* **1:** 1–12

Gaiser AM, Kaiser CJO, Haslbeck V & Richter K (2011) Downregulation of the Hsp90 system causes defects in muscle cells of Caenorhabditis elegans. *PloS one* **6:** e25485

Gasch AP, Spellman PT, Kao CM, Carmel-Harel O, Eisen MB, Storz G, Botstein D & Brown PO (2000) Genomic expression programs in the response of yeast cells to environmental changes. *Molecular biology of the cell* **11:** 4241–57

Gasteiger E, Hoogland C, Gattiker A, Duvaud S, Wilkins MR, Appel RD & Bairoch A (2005) Protein Identification and Analysis Tools on the ExPASy Server. In *The Proteomics Protocol Handbook* pp 571–608. Humana Press

Gidalevitz T, Ben-Zvi A, Ho KH, Brignull HR & Morimoto RI (2006) Progressive Disruption of Cellular Protein Folding in Models of Polyglutamine Diseases. *Science* **347:** 1471–1475

Gidalevitz T, Prahlad V & Morimoto RI (2011) The stress of protein misfolding: From single cells to multicellular organisms. *Cold Spring Harbor Perspectives in Biology* **3:** 1–18

Gray MJ, Wholey W-Y, Wagner NO, Cremers CM, Mueller-Schickert A, Hock NT, Krieger AG, Smith EM, Bender R a, Bardwell JC a & Jakob U (2014) Polyphosphate is a primordial chaperone. *Molecular cell* **53:** 689–99

Green NS, Reisler E & Houk KN (2001) Quantitative evaluation of the lengths of homobifunctional protein cross-linking reagents used as molecular rulers. *Protein Science* **10:** 1293–1304

Guhathakurta D, Palomar L, Stormo GD, Tedesco P, Johnson TE, Walker DW, Lithgow G, Kim S & Link CD (2002) Identification of a Novel cis-Regulatory Element Involved in the Heat Shock Response in Caenorhabditis elegans Using Microarray Gene Expression and Computational Methods. **:** 701–712

Guisbert E, Czyz DM, Richter K, McMullen PD & Morimoto RI (2013) Identification of a tissue-selective heat shock response regulatory network. *PLoS genetics* **9:** e1003466

Hageman J, Rujano M a., van Waarde M a WH, Kakkar V, Dirks RP, Govorukhina N, Oosterveld-Hut HMJ, Lubsen NH & Kampinga HH (2010) A DNAJB Chaperone Subfamily with HDAC-Dependent Activities Suppresses Toxic Protein Aggregation. *Molecular Cell* **37:** 355–369

Hansson O, Nylandsted J, Castilho RF, Leist M, Jaattela M & Brundin P (2003) Overexpression of heat shock protein 70 in R6/2 Huntington ' s disease mice has only modest effects on disease progression. **970:** 47–57

Harms MB, Sommerville RB, Allred P, Ma D, Ph D, Cooper P, Lopate G, Pestronk A, Weihl CC & Baloh RH (2013) NIH Public Access. **71:** 407–416

Hartl FU, Bracher A & Hayer-Hartl M (2011) Molecular chaperones in protein folding and proteostasis. *Nature* **475:** 324–32

Haslbeck V, Eckl JM, Kaiser CJO, Papsdorf K, Hessling M & Richter K (2013) Chaperone-interacting TPR proteins in Caenorhabditis elegans. *Journal of molecular biology* **425:** 2922–39

Hibbs M a, Hess DC, Myers CL, Huttenhower C, Li K & Troyanskaya OG (2007) Exploring the functional landscape of gene expression: directed search of large microarray compendia. *Bioinformatics (Oxford, England)* **23:** 2692–9

Hiller MM, Finger A, Schweiger M & Wolf DH (1996) ER degradation of a misfolded luminal protein by the cytosolic ubiquitin-proteasome pathway. *Science (New York, N.Y.)* **273:** 1725–8

Hipp MS, Park SH & Hartl FU (2014) Proteostasis impairment in protein-misfolding and -aggregation diseases. *Trends in Cell Biology*

Hipp MS, Patel CN, Bersuker K, Riley BE, Kaiser SE, Shaler T a, Brandeis M & Kopito RR (2012) Indirect inhibition of 26S proteasome activity in a cellular model of Huntington's disease. *The Journal of cell biology* **196:** 573–87

Honig B, Ray a & Levinthal C (1976) Conformational flexibility and protein folding: rigid structural fragments connected by flexible joints in subtilisin BPN. *Proceedings of the National Academy of Sciences of the United States of America* **73:** 1974–1978

Huang S & O'Shea EK (2005) A systematic high-throughput screen of a yeast deletion collection for mutants defective in PHO5 regulation. *Genetics* **169:** 1859–71

Hughes RE, Lo RS, Davis C, Strand AD, Neal CL, Olson JM & Fields S (2001) Altered transcription in yeast expressing expanded polyglutamine. *Proceedings of the National Academy of Sciences of the United States of America* **98:** 13201–13206

Huh W, Falvo J V, Gerke LC, Carroll AS, Howson RW, Weissman JS & Shea EKO (2003) Global analysis of protein localization in budding yeast. *Nature* **425:** 686–691

Hynes RO (1992) Integrins: versatility, modulation, and signaling in cell adhesion. *Cell* **69:** 11–25

Höhfeld J, Cyr DM & Patterson C (2001) From the cradle to the grave: Molecular chaperones that may choose between folding and degradation. *EMBO Reports* **2:** 885–890

Höhfeld J & Jentsch S (1997) GrpE-like Regulation of the Hsc70 Chaperone by the Anti-Apoptotic Protein BAG-1. *The EMBO journal* **16:** 6209–16

Inoue H, Nojima H & 0kayama H (1990) High efficiency transformation of Escherichia coli with plasmids. *Gene* **96:** 23–28

Irizarry R a. (2003) Summaries of Affymetrix GeneChip probe level data. *Nucleic Acids Research* **31:** 15e–15

De Jesus NH (2007) Epidemics to eradication: the modern history of poliomyelitis. *Virology journal* **4:** 70

Jinwal UK, Miyata Y, Koren J, Jones JR, Trotter JH, Chang L, O'Leary J, Morgan D, Lee DC, Shults CL, Rousaki A, Weeber EJ, Zuiderweg ERP, Gestwicki JE & Dickey CA (2009) Chemical manipulation of hsp70 ATPase activity regulates tau stability. *The Journal of neuroscience : the official journal of the Society for Neuroscience* **29:** 12079–88

Johnson JL, Beito TG, Krco CJ & Toft DO (1994) Characterization of a novel 23-kilodalton protein of unactive progesterone receptor complexes. *Molecular and cellular biology* **14:** 1956–63

Kabbage M & Dickman MB (2008) The BAG proteins: a ubiquitous family of chaperone regulators. *Cellular and Molecular Life Sciences* **65:** 1390–1402

Kaganovich D, Kopito R & Frydman J (2008) Misfolded proteins partition between two distinct quality control compartments. *Nature* **454:** 1088–1095

Kaiser CJO (2012) Studying Cellular Protein Folding in Nematodes and Baker ' s Yeast.

Kaiser CJO, Grötzinger SW, Eckl JM, Papsdorf K, Jordan S & Richter K (2013) A network of genes connects polyglutamine toxicity to ploidy control in yeast. *Nature communications* **4:** 1571

Kaltenbach LS, Romero E, Becklin RR, Chettier R, Bell R, Phansalkar A, Strand A, Torcassi C, Savage J, Hurlburt A, Cha G-H, Ukani L, Chepanoske C Lou, Zhen Y, Sahasrabudhe S, Olson J, Kurschner C, Ellerby LM, Peltier JM, Botas J, *et al* (2007) Huntingtin interacting proteins are genetic modifiers of neurodegeneration. *PLoS genetics* **3:** e82

Kamath RS, Fraser AG, Dong Y, Poulin G, Durbin R, Gotta M, Kanapin A, Le Bot N, Moreno S, Sohrmann M, Welchman DP, Zipperlen P & Ahringer J (2003) Systematic functional analysis of the Caenorhabditis elegans genome using RNAi. *Nature* **421:** 231–7

Kampinga HH & Craig E a (2010) The HSP70 chaperone machinery: J proteins as drivers of functional specificity. *Nature reviews. Molecular cell biology* **11:** 579–92

Kang J, Lemaire H-G, Unterbeck A, Salbaum JM, Masters CL, Grzeschik K-H, Multhaup G, Beyreuther K & Müller-Hill B (1987) The prescursor of Alzheimer's disease amyloid A4 protein resembles a cell-surface receptor. *Nature* **325:** 733–736

Kelly SM, Jess TJ & Price NC (2005) How to study proteins by circular dichroism. *Biochimica et biophysica acta* **1751:** 119–39

Kettern N, Dreiseidler M, Tawo R & Höhfeld J (2010) Chaperone-assisted degradation: Multiple paths to destruction. *Biological Chemistry* **391:** 481–489

Kiefhaber T, Rudolph R, Kohler H & Buchner J (1991) Protein aggregation in vitro and in vivo: a quantitative model of the kinetic competition between folding and aggregation. *Biotechnology* **9:** 825–829

Kim S-Y, Marekov L, Bubber P, Browne SE, Stavrovskaya I, Lee J, Steinert PM, Blass JP, Beal MF, Gibson GE & Cooper AJL (2005) Mitochondrial aconitase is a transglutaminase 2 substrate: transglutamination is a probable mechanism contributing to high-molecular-weight aggregates of aconitase and loss of aconitase activity in Huntington disease brain. *Neurochemical research* **30:** 1245–55

Kirkwood TB (1977) Evolution of ageing. *Nature* **270:** 301–4

Kitamura N, Semler BL, Rothberg PG, Larsen GR, Adler CJ, Dorner AJ, Emini EA, Hanecak R, Lee JJ, van der Werf S, Anderson CW & Wimmer E (1981) Primary structure, gene organization and polypeptide expression of poliovirus RNA. *Nature* **291:** 547–53

Klockgether T & Evert B (1998) Genes involved in hereditary ataxias. *Trends in neurosciences* **21:** 413–8

Koya K, Li Y, Wang H, Ukai T, Tatsuta N, Kawakami M, Shishido & Chen LB (1996) MKT-077, a novel rhodacyanine dye in clinical trials, exhibits anticarcinoma activity in preclinical studies based on selective mitochondrial accumulation. *Cancer research* **56:** 538–43

Krobitsch S & Lindquist S (2000) Aggregation of huntingtin in yeast varies with the length of the polyglutamine expansion and the expression of chaperone proteins. *Proceedings of the National Academy of Sciences of the United States of America* **97:** 1589–1594

Labbadia J & Morimoto RI (2013) Huntington's disease: underlying molecular mechanisms and emerging concepts. *Trends in biochemical sciences* **38:** 378–85

Laemmli UK (1970) Cleavage of Structural Proteins during the Assembly of the Head of Bacteriophage T4. *Nature* **227:** 680–685

Lashuel H a & Lansbury PT (2006) Are amyloid diseases caused by protein aggregates that mimic bacterial pore-forming toxins? *Quarterly reviews of biophysics* **39:** 167–201

Laufen T, Mayer MP, Beisel C, Klostermeier D, Mogk A, Reinstein J & Bukau B (1999) Mechanism of Regulation of Hsp70 Chaperones by DnaJ Cochaperones. *Proceedings of the National Academy of Sciences of the United States of America* **96:** 5452–7

Lee C-H, Saksela K, Mirza U a., Chait BT & Kuriyan J (1996) Crystal structure of the conserved core of HIV-1 Nef complexed with a Src family SH3 domain. *Cell* **85:** 931–942

Lejeune F-X, Mesrob L, Parmentier F, Bicep C, Vazquez-Manrique RP, Parker JA, Vert J-P, Tourette C & Neri C (2012) Large-scale functional RNAi screen in C. elegans identifies genes that regulate the dysfunction of mutant polyglutamine neurons. *BMC genomics* **13:** 91

Leu JI, Pimkina J, Frank A, Murphy ME & Donna L (2009) A Small Molecule Inhibitor of Inducible Heat Shock Protein 70 (HSP70). *Molecular Cell* **36:** 15–27

Li S, Armstrong CM, Bertin N, Ge H, Milstein S, Boxem M, Vidalain P-O, Han J-DJ, Chesneau A, Hao T, Goldberg DS, Li N, Martinez M, Rual J-F, Lamesch P, Xu L, Tewari M, Wong SL, Zhang L V, Berriz GF, *et al* (2004) A map of the interactome network of the metazoan C. elegans. *Science (New York, N.Y.)* **303:** 540–3

Li X, Srinivasan SR, Connarn J, Ahmad A, Young ZT, Kabza AM, Zuiderweg ERP, Sun D & Gestwicki JE (2013) Analogues of the allosteric heat shock protein 70 (Hsp70) inhibitor, MKT-077, as anti-cancer agents. *ACS Medicinal Chemistry Letters* **4:** 1042–1047

Lill R, Hoffmann B, Molik S, Pierik AJ, Rietzschel N, Stehling O, Uzarska M a, Webert H, Wilbrecht C & Mühlenhoff U (2012) The role of mitochondria in cellular iron-sulfur protein biogenesis and iron metabolism. *Biochimica et biophysica acta* **1823:** 1491–508

Liu R (1998) Interaction of BAG-1 with Retinoic Acid Receptor and Its Inhibition of Retinoic Acid-induced Apoptosis in Cancer Cells. *Journal of Biological Chemistry* **273:** 16985–16992

Mamelak D, Mylvaganam M, Whetstone H, Hartmann E, Lennarz W, Wyrick PB, Raulston J, Han H, Hoffman P & Lingwood C a. (2001) Hsp70s contain a specific sulfogalactolipid binding site. Differential aglycone influence on sulfogalactosyl ceramide binding by recombinant prokaryotic and eukaryotic Hsp70 family members. *Biochemistry* **40:** 3572–3582

Manogaran AL, Hong JY, Hufana J, Tyedmers J, Lindquist S & Liebman SW (2011) Prion formation and polyglutamine aggregation are controlled by two classes of genes. *PLoS genetics* **7:** e1001386

Martínez-Pastor MT, Marchler G, Schüller C, Marchler-Bauer A, Ruis H & Estruch F (1996) The Saccharomyces cerevisiae zinc finger proteins Msn2p and Msn4p are required for transcriptional induction through the stress response element (STRE). *The EMBO journal* **15:** 2227–35

Maréchal A, Meunier B, Lee D, Orengo C & Rich PR (2012) Yeast cytochrome c oxidase: a model system to study mitochondrial forms of the haem-copper oxidase superfamily. *Biochimica et biophysica acta* **1817:** 620–8

Mayer MP & Bukau B (2005) Hsp70 chaperones: Cellular functions and molecular mechanism. *Cellular and Molecular Life Sciences* **62:** 670–684

Meimaridou E, Gooljar SB & Chapple JP (2009) From hatching to dispatching: The multiple cellular roles of the Hsp70 molecular chaperone machinery. *Journal of Molecular Endocrinology* **42:** 1–9

Meissner B, Warner A, Wong K, Dube N, Lorch A, McKay SJ, Khattra J, Rogalski T, Somasiri A, Chaudhry I, Fox RM, Miller DM, Baillie DL, Holt R a, Jones SJM, Marra M a & Moerman DG (2009) An integrated strategy to study muscle development and myofilament structure in Caenorhabditis elegans. *PLoS genetics* **5:** e1000537

Mello CC, Kramer JM, Stinchcomb D & Ambros V (1991) Efficient gene transfer in C.elegans: extrachromosomal maintenance and integration of transforming sequences. *The EMBO journal* **10:** 3959–3970

Miller J, Arrasate M, Brooks E, Libeu CP, Legleiter J, Hatters D, Curtis J, Cheung K, Krishnan P, Mitra S, Widjaja K, Shaby BA, Lotz GP, Newhouse Y, Mitchell EJ, Osmand A, Gray M, Thulasiramin V, Saudou F, Segal M, *et al* (2012a) Identifying polyglutamine protein species in situ that best predict neurodegeneration. *Nature Chemical Biology* **8:** 318–318

Miller JP, Yates BE, Al-Ramahi I, Berman AE, Sanhueza M, Kim E, de Haro M, DeGiacomo F, Torcassi C, Holcomb J, Gafni J, Mooney SD, Botas J, Ellerby LM & Hughes RE (2012b) A genome-scale RNA-interference screen identifies RRAS signaling as a pathologic feature of Huntington's disease. *PLoS genetics* **8:** e1003042

Miller SBM, Mogk A & Bukau B (2015) Spatially organized aggregation of misfolded proteins as cellular stress defense strategy. *Journal of molecular biology*

Montgomery DL, Morimoto RI & Gierasch LM (1999) Mutations in the substrate binding domain of the Escherichia coli 70 kDa molecular chaperone, DnaK, which alter substrate affinity or interdomain coupling. *Journal of molecular biology* **286:** 915–32

Morimoto RI & Cuervo AM (2009) Protein homeostasis and aging: Taking care of proteins from the cradle to the grave. *Journals of Gerontology - Series A Biological Sciences and Medical Sciences* **64:** 167–170

Morimoto RI & Cuervo AM (2014) Proteostasis and the aging proteome in health and disease. *Journals of Gerontology - Series A Biological Sciences and Medical Sciences* **69:** 33–38

Morimoto RI, Driessen AJM, Hegde RS & Langer T (2011) The life of proteins: the good, the mostly good and the ugly. *Nature structural & molecular biology* **18:** 1–4

Mosser DD & Morimoto RI (2004) Molecular chaperones and the stress of oncogenesis. *Oncogene* **23:** 2907–2918

Muchowski PJ, Schaffar G, Sittler A, Wanker EE, Hayer-hartl MK & Hartl FU (2000) Hsp70 and Hsp40 chaperones can inhibit self-assembly of polyglutamine proteins into amyloid-like fibrils. *Proceedings of the National Academy of Sciences of the United States of America* **97:** 7841–7846

Nadler SG, Dischino DD, Malacko AR, Cleaveland JS, Fujihara SM & Marquardt H (1998) Identification of a binding site on Hsc70 for the immunosuppressant 15-deoxyspergualin. *Biochemical and biophysical research communications* **253:** 176–80

Natarajan K, Meyer MR, Jackson BM, Slade D, Roberts C, Hinnebusch AG & Marton MJ (2001) Transcriptional Profiling Shows that Gcn4p Is a Master Regulator of Gene Expression during Amino Acid Starvation in Yeast. **21:** 4347–4368

Netz DJ a, Mascarenhas J, Stehling O, Pierik AJ & Lill R (2014) Maturation of cytosolic and nuclear iron-sulfur proteins. *Trends in cell biology* **24:** 303–12

Nollen E a a, Garcia SM, van Haaften G, Kim S, Chavez A, Morimoto RI & Plasterk RH a (2004) Genome-wide RNA interference screen identifies previously undescribed regulators of polyglutamine aggregation. *Proceedings of the National Academy of Sciences of the United States of America* **101:** 6403–8

Núñez MT, Urrutia P, Mena N, Aguirre P, Tapia V & Salazar J (2012) Iron toxicity in neurodegeneration. *Biometals* **25:** 761–76

Oh HJ, Easton D, Murawski M, Kaneko Y & Subjeck JR (1999) The chaperoning activity of hsp110. Identification of functional domains by use of targeted deletions. *The Journal of biological chemistry* **274:** 15712–8

Oliveira JM a (2010) Nature and cause of mitochondrial dysfunction in Huntington's disease: focusing on huntingtin and the striatum. *Journal of neurochemistry* **114:** 1–12

Olzscha H, Schermann SM, Woerner AC, Pinkert S, Hecht MH, Tartaglia GG, Vendruscolo M, Hayer-Hartl M, Hartl FU & Vabulas RM (2011) Amyloid-like aggregates sequester numerous metastable proteins with essential cellular functions. *Cell* **144:** 67–78

Orr HT, Chung M, Banfi S, Kwiatkowski TJ, Servadio A, Beaudet AL, McCall AA, Duvick LA, Ranum LPW & Zoghbi HY (1993) Expansion of an unstable trinucleotide CAG repeat in spinocerebellar ataxia type 1. *Nature genetics*

Orr HT & Zoghbi HY (2007) Trinucleotide repeat disorders. *Annual review of neuroscience* **30:** 575–621

Otvos L, O I, Rogers ME, Consolvo PJ, Condie BA, Lovas S, Bulet P & Blaszczyk-Thurin M (2000) Interaction between heat shock proteins and antimicrobial peptides. *Biochemistry* **39:** 14150–9

Outten CE & Albetel A-N (2013) Iron sensing and regulation in Saccharomyces cerevisiae: Ironing out the mechanistic details. *Current opinion in microbiology* **16:** 662–8

Papsdorf K, Kaiser CJO, Drazic A, Grötzinger SW, Haeßner C, Eisenreich W & Richter K (2015) Polyglutamine Toxitcy in Yeast Induces Metabolic Alterations and Mitochondrial Defects. *BMC genomics***:** manuscript submitted

Papsdorf K & Richter K (2014) Protein folding, misfolding and quality control: the role of molecular chaperones. *Essays in Biochemistry* **56:** 53–68

Papsdorf K, Sacherl J & Richter K (2014) The balanced regulation of Hsc70 by DNJ-13 and UNC-23 is required for muscle functionality. *The Journal of biological chemistry* **289:** 25250–61

Park SH, Kukushkin Y, Gupta R, Chen T, Konagai A, Hipp MS, Hayer-Hartl M & Hartl FU (2013) PolyQ proteins interfere with nuclear degradation of cytosolic proteins by sequestering the Sis1p chaperone. *Cell* **154:** 134–145

Parker JA, Connolly JB, Wellington C, Hayden M, Dausset J & Neri C (2001) Expanded polyglutamines in Caenorhabditis elegans cause axonal abnormalities and severe dysfunction of PLM mechanosensory neurons without cell death. *Proceedings of the National Academy of Sciences of the United States of America* **98:** 13318–23

Paul VD & Lill R (2015) Biogenesis of cytosolic and nuclear iron-sulfur proteins and their role in genome stability. *Biochimica et biophysica acta*

Pepper SD, Saunders EK, Edwards LE, Wilson CL & Miller CJ (2007) The utility of MAS5 expression summary and detection call algorithms. *BMC bioinformatics* **8:** 273

Philpott CC, Protchenko O, Kim YW, Y B & Shakoury-Elizeh M (2002) The response to iron deprivation in Saccharomyces cerevisiae : expression of siderophore-based systems of iron uptake Interactions of siderophores with the Fit family of cell-wall proteins. *Biochemical Society Transactions* **30:** 698–702

Plenefisch JD, Zhu X & Hedgecock EM (2000) Fragile skeletal muscle attachments in dystrophic mutants of Caenorhabditis elegans: isolation and characterization of the mua genes. *Development (Cambridge, England)* **127:** 1197–207

Polier S, Dragovic Z, Hartl FU & Bracher A (2008) Structural basis for the cooperation of Hsp70 and Hsp110 chaperones in protein folding. *Cell* **133:** 1068–79

Preissler S & Deuerling E (2012) Ribosome-associated chaperones as key players in proteostasis. *Trends in Biochemical Sciences* **37:** 274–283

Qin Z-H, Wang Y, Kegel KB, Kazantsev A, Apostol BL, Thompson LM, Yoder J, Aronin N & DiFiglia M (2003) Autophagy regulates the processing of amino terminal huntingtin fragments. *Human molecular genetics* **12:** 3231–44

Rahmani P (2002) Characterization of the unc-23 gene, an HSP-1 chaperone regulator, in Caenorhabditis elegans. *PhD Thesis, Laboratory of Prof. Donald Moerman, Department of Zoology, University of British Columbia, Vancouver, B.C., Canada***:** 1–117

Rahmani P, Rogalski T & Moerman DG (2015) The C. elegans UNC-23 protein, a member of the BCL-2-associated athanogene (BAG) family of chaperone regulators, interacts with HSP-1 to regulate cell attachment and maintain hypodermal integrity. *Worm*

Ravikumar B, Duden R & Rubinsztein DC (2002) Aggregate-prone proteins with polyglutamine and polyalanine expansions are degraded by autophagy. *Human molecular genetics* **11:** 1107–17

Rehn AB (2014) Mechanistic Analysis of the Hsp90 Machinery: Effects of Cochaperones, Posttranslational Modifications and Clients.

Richter K, Haslbeck M & Buchner J (2010) The Heat Shock Response: Life on the Verge of Death. *Molecular Cell* **40:** 253–266

Roberts SM & Winston F (1996) SPT20/ADA5 encodes a novel protein functionally related to the TATA-binding protein and important for transcription in Saccharomyces cerevisiae. *Molecular and cellular biology* **16:** 3206–13

Rohde M, Daugaard M, Jensen MH, Helin K & Nylandsted J (2005) growth by distinct mechanisms Members of the heat-shock protein 70 family promote cancer cell growth by distinct mechanisms. *Genes & Development* **70:** 570–582

Rosen D, Siddique T, Patterson D, Figlewicz D, Sapp P, Henati A, Donaldson D, Goto J, O'Regan J, Deng X, Rahmani Z, Krizus A, McKenna-Yasek D, Cayabyab A, Gaston S, Berger R, Tanzi R, Halperin J, Herzfeldt B, Van den Bergh R, *et al* (1993) Mutations in Cu/Zn superoxide dismutase are associated with familiar amyotrophic lateral sclerosis. *Nature* **362:** 59–62

Rubinsztein DC, Barton D, Davison B & Ferguson-Smith M (1993) Analysis of the huntingtin gene reveals a trinucleotide-length polymorphism in the region of the gene that contains two CCG-rich stretches and a correlation between decreased age of onset of Huntington's disease and CAG repeat number. *Hum Mol Genet.* **2:** 1713–5

Rujano M a, Kampinga HH & Salomons F a (2007) Modulation of polyglutamine inclusion formation by the Hsp70 chaperone machine. *Experimental cell research* **313:** 3568–78

Rujano MA, Bosveld F, Salomons FA, Dijk F, Van Waarde MAWH, Van Der Want JJL, De Vos RAI, Brunt ER, Sibon OCM & Kampinga HH (2006) Polarised asymmetric inheritance of accumulated protein damage in higher eukaryotes. *PLoS Biology* **4:** 2325–2335

Rutherford JC, Ojeda L, Balk J, Mühlenhoff U, Lill R & Winge DR (2005) Activation of the iron regulon by the yeast Aft1/Aft2 transcription factors depends on mitochondrial but not cytosolic iron-sulfur protein biogenesis. *The Journal of biological chemistry* **280:** 10135–40

Rutherford SL & Lindquist S (1998) Hsp90 as a capacitor for morphological evolution. *Nature* **396:** 336–42

Saito R, Smoot ME, Ono K, Ruscheinski J, Wang P-L, Lotia S, Pico AR, Bader GD & Ideker T (2012) A travel guide to Cytoscape plugins. *Nature methods* **9:** 1069–76

Schilling B, Row RH, Gibson BW, Guo X & Young MM (2003) MS2Assign, automated assignment and nomenclature of tandem mass spectra of chemically crosslinked peptides. *Journal of the American Society for Mass Spectrometry* **14:** 834–50

Schindelin J, Arganda-Carreras I, Frise E, Kaynig V, Longair M, Pietzsch T, Preibisch S, Rueden C, Saalfeld S, Schmid B, Tinevez J-Y, White DJ, Hartenstein V, Eliceiri K, Tomancak P & Cardona A (2012) Fiji: an open-source platform for biological-image analysis. *Nature methods* **9:** 676–82

Seebacher J, Mallick P, Zhang N, Eddes JS, Aebersold R & Gelb MH (2006) Protein Cross-Linking Analysis Using Mass Spectrometry , Isotope-Coded Cross-Linkers , and Integrated Computational Data Processing research articles. **:** 2270–2282

Seguin A, Santos R, Pain D, Dancis A, Camadro J-M & Lesuisse E (2011) Co-precipitation of phosphate and iron limits mitochondrial phosphate availability in Saccharomyces cerevisiae lacking the yeast frataxin homologue (YFH1). *The Journal of biological chemistry* **286:** 6071–9

Selcen D, Muntoni F, Burton BK, Pegoraro E, Sewry C, Bite A V & Engel AG (2010) NIH Public Access. **65:** 83–89

Smith DF, Sullivan WP, Marion TN, Zaitsu K, Madden B, McCormick DJ & Toft DO (1993) Identification of a 60-kilodalton stress-related protein, p60, which interacts with hsp90 and hsp70. *Molecular and cellular biology* **13:** 869–76

Sokolov S, Pozniakovsky A, Bocharova N, Knorre D & Severin F (2006) Expression of an expanded polyglutamine domain in yeast causes death with apoptotic markers. *Biochimica et biophysica acta* **1757:** 660–6

Solans A, Zambrano A, Rodríguez M & Barrientos A (2006) Cytotoxicity of a mutant huntingtin fragment in yeast involves early alterations in mitochondrial OXPHOS complexes II and III. *Human molecular genetics* **15:** 3063–81

Sondermann H (2001) Structure of a Bag/Hsc70 Complex: Convergent Functional Evolution of Hsp70 Nucleotide Exchange Factors. *Science* **291:** 1553–1557

Song J, Takeda M & Morimoto RI (2001) Bag1-Hsp70 mediates a physiological stress signalling pathway that regulates Raf-1/ERK and cell growth. *Nature cell biology* **3:** 276–82

La Spada AR, Wilson EM, Lubahn DB, Harding A & Fischbeck KH (1991) Androgen receptor gene mutations in X-linked in spinal and bulbar muscular atrophy. *Nature* **352:** 77–79

Speed TP, Bolstad BM, Irizarry RA & Astrand M (2003) A comparison of normalization methods for high density oligonucleotide array data based on variance and bias. **19:** 185–193

Stafford WFI (1994) Modern Analytical Ultracentrifugation Emerging Biochemical and Biophysical Techniques Birkhäuser Boston

Storchová Z, Breneman A, Cande J, Dunn J, Burbank K, O'Toole E & Pellman D (2006) Genome-wide genetic analysis of polyploidy in yeast. *Nature* **443:** 541–7

Sun L, Edelmann FT, Kaiser CJO, Papsdorf K, Gaiser AM & Richter K (2012) The lid domain of Caenorhabditis elegans Hsc70 influences ATP turnover, cofactor binding and protein folding activity. *PloS one* **7:** e33980

Tabrizi S, Workman J, Hart P, Mangiarini L, Mahal A, Bates G, Cooper J & Schapira A (2000) Mitochondrial dysfunction and free radical damage in the Huntington R6/2 transgenic mouse. *Ann Neurol* **47:** 80–86

Taipale M, Krykbaeva I, Koeva M, Kayatekin C, Westover KD, Karras GI & Lindquist S (2012) Quantitative analysis of HSP90-client interactions reveals principles of substrate recognition. *Cell* **150:** 987–1001

Taipale M, Tucker G, Peng J, Krykbaeva I, Lin Z-Y, Larsen B, Choi H, Berger B, Gingras A-C & Lindquist S (2014) A quantitative chaperone interaction network reveals the architecture of cellular protein homeostasis pathways. *Cell* **158:** 434–48

Takahashi T, Katada S & Onodera O (2010) Polyglutamine diseases: where does toxicity come from? what is toxicity? where are we going? *Journal of molecular cell biology* **2:** 180–91

Takahashi T, Kikuchi S, Katada S, Nagai Y, Nishizawa M & Onodera O (2008) Soluble polyglutamine oligomers formed prior to inclusion body formation are cytotoxic. *Human Molecular Genetics* **17:** 345–356

Takayama S, Bimston DN, Matsuzawa S, Freeman BC, Aime-Sempe C, Xie Z, Morimoto RI & Reed JC (1997) BAG-1 modulates the chaperone activity of Hsp70/Hsc70. *The EMBO journal* **16:** 4887–96

Takayama S & Reed J (2001) Molecular chaperone targeting and regulation by BAG family proteins. *Nature cell biology* **3:** 237–41

Takayama S, Xie Z & Reed JC (1999) An Evolutionarily Conserved Family of Hsp70/Hsc70 Molecular Chaperone Regulators. *The Journal of biological chemistry* **274:** 781–6

Tilly K, McKittrick N, Zylicz M & Georgopoulos C (1983) The DnaK protein modulates the heat-shock response of Escherichia coli. *Cell* **34:** 641–6

Timmons L & Fire A (1998) Specific interference by ingested dsRNA. *Nature* **395:** 854

Todd TW & Lim J (2013) Aggregation formation in the polyglutamine diseases: Protection at a cost? *Molecules and Cells* **36:** 185–194

Treusch S & Lindquist S (2012) An intrinsically disordered yeast prion arrests the cell cycle by sequestering a spindle pole body component. *The Journal of cell biology* **197:** 369–79

Tu Y, Wu S, Shi X, Chen K & Wu C (2003) Migfilin and Mig-2 link focal adhesions to filamin and the actin cytoskeleton and function in cell shape modulation. *Cell* **113:** 37–47

Ulbricht A, Eppler FJ, Tapia VE, van der Ven PFM, Hampe N, Hersch N, Vakeel P, Stadel D, Haas A, Saftig P, Behrends C, Fürst DO, Volkmer R, Hoffmann B, Kolanus W & Höhfeld J (2013) Cellular mechanotransduction relies on tension-induced and chaperone-assisted autophagy. *Current biology : CB* **23:** 430–5

Ulbricht A & Höhfeld J (2013) Tension-induced autophagy. *Autophagy* **9:** 920–922

Urban MJ, Li C, Yu C, Lu Y, Krise JM, McIntosh MP, Rajewski RA, Blagg BSJ & Dobrowsky RT (2010) Inhibiting heat-shock protein 90 reverses sensory hypoalgesia in diabetic mice. *ASN neuro* **2:** e00040

Varshavsky A (2012) The Ubiquitin System, an Immense Realm. *Annual Review of Biochemistry* **81:** 167–176

Verhoef LGGC, Lindsten K, Masucci MG & Dantuma NP (2002) Aggregate formation inhibits proteasomal degradation of polyglutamine proteins. *Human molecular genetics* **11:** 2689–700

Vorgerd M, van der Ven PFM, Bruchertseifer V, Löwe T, Kley R a, Schröder R, Lochmüller H, Himmel M, Koehler K, Fürst DO & Huebner A (2005) A mutation in the dimerization

domain of filamin c causes a novel type of autosomal dominant myofibrillar myopathy. *American journal of human genetics* **77:** 297–304

Wadhwa R, Sugihara T, Yoshida A, Maruta H & Kaul SC (2000) Selective Toxicity of MKT-077 to Cancer Cells Is Mediated by Its Binding to the hsp70 Family Protein mot-2 and Reactivation of p53 Function Advances in Brief Selective Toxicity of MKT-077 to Cancer Cells Is Mediated by Its Binding to the hsp70 Family Prot. **:** 6818–6821

Waelter S, Boeddrich A, Lurz R, Scherzinger E, Lueder G, Lehrach H & Wanker EE (2001) Accumulation of mutant huntingtin fragments in aggresome-like inclusion bodies as a result of insufficient protein degradation. *Molecular biology of the cell* **12:** 1393–1407

Wang S, Sakai H & Wiedmann M (1995) NAC covers ribosome-associated nascent chains thereby forming a protective environment for regions of nascent chains just emerging from the peptidyl transferase center. *The Journal of cell biology* **130:** 519–28

Waterston RH, Thomson JN & Brenner S (1980) Mutants with Altered Muscle Structure in Caenorhabditis elegans. *Developmental Biology* **77:** 271–302

Williamson DS, Borgognoni J, Clay A, Daniels Z, Dokurno P, Drysdale MJ, Foloppe N, Francis GL, Graham CJ, Howes R, Macias AT, Murray JB, Parsons R, Shaw T, Surgenor AE, Terry L, Wang Y, Wood M & Massey AJ (2009) Novel adenosine-derived inhibitors of 70 kDa heat shock protein, discovered through structure-based design. *Journal of Medicinal Chemistry* **52:** 1510–1513

Willmund F, Alamo M, Pechmann S, Chen T, Dammer EB, Peng J & Frydman J (2013) The cotranslational function of ribosome-associated Hsp70 in eukaryotic protein homeostasis. *Cell* **152:** 196–209

Winzeler EA, Shoemaker DD, Astromoff A, Liang H, Anderson K, Andre B, Bangham R, Benito R, Boeke JD, Bussey H, Chu AM, Connelly C, Davis K, Dietrich F, Dow SW, Bakkoury M El, Friend SH, Gentalen E, Giaever G, Hegemann JH, *et al* (1999) Functional Characterization of the S . cerevisiae Genome by Gene Deletion and Parallel Analysis. *Science* **285:** 901–906

Wisén S & Gestwicki JE (2008) Identification of small molecules that modify the protein folding activity of heat shock protein 70. *Analytical biochemistry* **374:** 371–7

Woodmansee AN & Imlay JA (2002) Quantitation of Intracellular Free Iron by Electron Paramagnetic Resonance Spectroscopy. *Methods in Enzymology* **349:** 3–9

Xie Y & Varshavsky A (2000) Physical association of ubiquitin ligases and the 26S proteasome. *Proceedings of the National Academy of Sciences of the United States of America* **97:** 2497–502

Xie Y & Varshavsky A (2001) RPN4 is a ligand, substrate, and transcriptional regulator of the 26S proteasome: a negative feedback circuit. *Proceedings of the National Academy of Sciences of the United States of America* **98:** 3056–61

Yam AY, Xia Y, Lin H-TJ, Burlingame A, Gerstein M & Frydman J (2008) Defining the TRiC/CCT interactome links chaperonin function to stabilization of newly made proteins with complex topologies. *Nature structural & molecular biology* **15:** 1255–62

Yamanaka T, Miyazaki H, Oyama F, Kurosawa M, Washizu C, Doi H & Nukina N (2008) Mutant Huntingtin reduces HSP70 expression through the sequestration of NF-Y transcription factor. *The EMBO journal* **27:** 827–839

Yang N-C, Ho W-M, Chen Y-H & Hu M-L (2002) A Convenient One-Step Extraction of Cellular ATP Using Boiling Water for the Luciferin–Luciferase Assay of ATP. *Analytical Biochemistry* **306:** 323–327

Youker RT, Walsh P, Beilharz T, Lithgow T & Brodsky JL (2004) Distinct Roles for the Hsp40 and Hsp90 Molecular Chaperones during Cystic Fibrosis Transmembrane Conductance Regulator Degradation in Yeast. *Molecular biology of the cell* **15:** 4787–4797

Young JC, Barral JM & Ulrich Hartl F (2003) More than folding: localized functions of cytosolic chaperones. *Trends in biochemical sciences* **28:** 541–7

Zhu X, Beal MF, Wang X, Perry G & Smith MA (2010) Mitochondria and Neurodegenerative Diseases. *Journal of Alzheimers´s Disease* **20:** 3233

Zhuravleva A, Clerico EM & Gierasch LM (2012) An interdomain energetic tug-of-war creates the allosterically active state in Hsp70 molecular chaperones. *Cell* **151:** 1296–307

8. Abbreviations

CGC	Caenorhabditis Genetics Center
Amp	Ampicillin
OD	Optical density
PCR	Polymerase chain reaction
SMM	standard minimal medium
SOB	super optimal broth medium
h	hours
RT	room temperature
NEF	Nucleotide exchange factor
FACS	fluorescence activated cell sorting
NMR	nuclear magnetic resonance
EPR	electron spin resonance
DFO	Desferrioxamine
DETAPAC	diethylenediamine pent acetic acid
TCA cycle	tricarboxylic acid cycle
w/o	without
pica	polyglutamine induced colony growth arrest
polQ	polyglutamine
^{31}P	^{31}Phosphate
SBD	substrate binding domain
NBD	nucleotide binding domain
ATP	Adenosintriphosphat
ADP	Adenosindiphosphat

NEF	Nucleotide exchange factor
DIC microscopy	differential interference contrast microscopy
INQ	intranuclear quality control compartments
IPOD	intracellular protein deposits
Q-bodies	cytosolic quality control bodies
GdnHCl	Guanidine hydrochloride
CTD	C-terminal domain
LDH	lactate dehydrogenase
PK	pyruvate kinase
NADH	Nicotinamide adenine dinucleotide
ND	not determined
Fe-S	iron-sulfur
Proteostasis	Protein homeostasis
aUC	analytical ultracentrifugation

9. Danksagung

Ich möchte mich zuerst bei Prof. Johannes Buchner bedanken, der mir die Möglichkeit gegeben hat meine Arbeit an seinem Lehrstuhl anzufertigen, an dem ich durch seine Vielfalt und Kooperationen allen wissenschaftlichen Fragen nachgehen konnte.

Mein großer Dank gilt meinem Doktorvater Klaus Richter. Vielen Dank für die spannenden Themen, die ich bearbeiten durfte und die Freiheit, mit der ich eigene Ideen verfolgen konnte. Es war hervorragend das weite Methodenspektrum *in vitro* und *in vivo* nutzen zu können, fachlich unterstützt zu werden und gleichzeitig produktiv wie kreativ zu arbeiten.

Vielen Dank an die Gruppen mit denen ich effektiv zusammen arbeiten durfte und die mir die Möglichkeit gaben verschiedenste Fragestellungen zu beantworten. Danke an Wolfgang Eisenreich für die Möglichkeit NMR zu messen, Christine Schwarz für die Hilfe dabei, Prof. Bausch für den Zugang zu den konfokalen Mikroskopen, Carina Pelzl für die Unterstützung und die Hilfe bei Fragestellungen rund um die konfokale Mikroskopie, Carmen Haeßner für die Untersuchungen am EPR, Matthias Weiwad für die Unterstützung in Halle und Katharina Gründler für die Hilfe mit dem FACS.

Zudem danke ich allen Bacheloranten und Praktikankten, die mich während der Doktorarbeit unterstützt haben. Ein riesen Dankeschön gilt an alle meine lieben Kollegen. Julia, Danke für fachliche und nicht fachliche Unterstützung und den Beistand im Büro. Christoph, Danke für deine tausend Ideen, deine Motivation und das Übergeben deines Themas in meine Hände. Vroni und Alina, Danke für die sportlichen Aktivitäten und die schöne Zeit. Danke an Sandrine und Franzi, für die lustigen Kaffeepausen, Mittagessen und Radtouren in die Uni. Vielen Dank an alle Kollegen, die das Arbeiten so angenehm, entspannt und produktiv gemacht haben. Ein enormes Dankeschön an meine Freunde Kitty und Kathi, ihr seid die Besten! Betti, Danke für die schöne gemeinsame Zeit. Viele Dank an die Crew aus Studienzeiten und an meine Bouldergang. Vielen Dank Chris. Danke für deine Geduld, dein Verständnis, deine Unterstützung, das Kontrolllesen und die ganzen unzähligen Kaffees mit denen du mich immer wieder motiviert hast. Du bist der Beste.

Zuletzt möchte ich mich bei meinen Eltern, ihren Partnern und meinen Geschwistern bedanken. Ohne euch hätte ich das nie geschafft! Danke für das bedingungslose und uneingeschränkte Vertrauen.

10. Eidesstattliche Erklärung

Hiermit erkläre ich, dass ich die vorliegende Arbeit selbstständig verfasst habe und keine anderen als die angegebenen Quellen und Hilfsmittel verwendet habe. Diese Arbeit wurde bisher keiner Prüfungskommission vorgelegt. Teile dieser Arbeit wurden oder werden in wissenschaftlichen Journalen veröffentlicht.

München,

_____

Katharina Papsdorf